Published by Institute of Physics Publishing for SISSA

Received: *June 19, 2008*
Accepted: *June 23, 2008*
Published: *July 11, 2008*

One-loop Riemann surfaces in Schnabl gauge

Michael Kiermaier and Barton Zwiebach

Center for Theoretical Physics, Massachusetts Institute of Technology, Cambridge, MA 02139, U.S.A.
E-mail: mkiermai@mit.edu, zwiebach@mit.edu

Abstract: Due to a peculiar behavior at the open string midpoint, loop diagrams in Schnabl gauge were expected to fail to produce the relevant closed string moduli. We find that closed string moduli are generated because the Riemann surfaces are built with *slanted* wedges: semi-infinite strips whose edges have parameterizations related by scaling. We examine in detail one-loop string diagrams and find that the closed string modulus is always produced. Moreover, the conformal maps simplify so greatly that both closed and open moduli become simple calculable functions of the Schwinger parameters, a simplification that occurs neither in Siegel gauge nor in light-cone gauge.

Keywords: Bosonic Strings, String Field Theory.

Contents

JHEP07(2008)063

1. Introduction

The string field Φ that represents the tachyon vacuum in Schnabl's solution [1] of open string field theory [2] satisfies a novel gauge condition. The solution is not in Siegel gauge [3]: Φ is not annihilated by the zero mode b_0 of the antighost field in the canonical open string frame. Rather, Φ is annihilated by the zero mode B of the antighost field in the conformal frame of the sliver projector of the star algebra of open string fields. The sliver frame is central to the construction and analysis of classical solutions [4]–[30] but, as any projector frame, it is singular at the open string midpoint. One can wonder if the Schnabl gauge condition $B\Phi = 0$ defines a consistent open string perturbation theory. In this question, the singular behavior of the open string midpoint has brought interesting advantages but has also introduced some new subtleties.

At tree level, the sliver frame makes all conformal maps from the string diagrams to the upper-half plane very simple [31, 32]. This is remarkable, if we recall that in Siegel gauge these maps are extremely complicated and no closed form expressions are known except for four-string amplitudes [33]. The subtleties arise because there are delicate contributions whose origin can be traced to the singular behavior at the open string midpoint [32]. These contributions affect the off-shell part of four-string amplitudes and could affect higher-point functions on-shell. No Feynman rules are known that deal with these complications in general tree-level amplitudes.

This state of affairs prompted [34] to introduce a class of *regular linear b-gauges* that produce correct on-shell amplitudes. In this class, a propagator insertion with Schwinger parameter approaching infinity induces an open string degeneration of the Riemann surface associated with the string diagram– the desired behavior. Schnabl gauge does not belong to the class of regular b-gauges, but there is a simple one-parameter family of regular linear b-gauges that interpolates between Siegel and Schnabl gauge as its parameter λ goes from infinity to zero. This suggests that Schnabl gauge amplitudes can be obtained by taking the limit $\lambda \to 0$ of the well-behaved amplitudes in this λ-family.

While it is not yet proven that moduli space is covered for general tree amplitudes in Schnabl gauge, it is no mystery how the relevant Riemann surfaces –disks with boundary punctures — carry the moduli and how degenerations can be generated. Naive arguments, however, suggest that Schnabl gauge at loop level only produces surfaces with degenerate closed string moduli, thus making it impossible to reproduce the correct on-shell amplitudes. In a one-loop amplitude, for example, the line traced by the open string midpoint is a nontrivial closed curve. In the Schnabl propagator the open string midpoint does not move, thus naively suggesting a diagram with a zero-length closed curve that signals closed string degeneration.

It is the main purpose of this paper to discuss the one-loop string diagrams in Schnabl gauge. Our results are quite encouraging. We find that the anticipated problems with closed string moduli are not present. Our main tool is the regulation provided by the λ-family of regular linear b-gauges that yield Schnabl gauge in the limit. Not only are closed string moduli produced but they are easily calculated, something that does not happen in Siegel gauge. Our work focuses only on the moduli problem; we do not attempt to fully

JHEP07(2008)063

compute any loop-amplitude. Such a computation, of course, would be quite interesting.

The analysis shows that closed string moduli arise because vertical lines in the sliver frame that are identified horizontally in tree diagrams, require slanted identifications in the case of loops. We recall that wedge surfaces [35, 36] are semi-infinite strips of fixed width whose vertical edges carry identical parameterizations. We are led to introduce *slanted* wedges, semi-infinite strips of fixed width whose vertical edges have parameterizations related by a scale factor. These slanted wedges are new, interesting objects in their own right. One can glue them and they are a natural ingredient in the construction of loop-diagrams. As opposed to the familiar wedges, however, there are no states associated to them. With the help of slanted wedges we develop a formalism that allows us to calculate the moduli (both open and closed) of arbitrary tree and one-loop amplitudes. Our analysis also shows that the BPZ-even gauge condition $B^+\Phi = (B + B^\star)\Phi = 0$, where $\star$ denotes BPZ conjugation, fails to generate the closed string modulus in one-loop diagrams because in this gauge the identifications in the sliver frame are not slanted. Unlike Schnabl gauge, the gauge $B^+\Phi = 0$ appears to be genuinely inadequate for loop calculations.

This paper is organized as follows. In section 2, we will begin our analysis with the one-loop vacuum graph in general regular linear b-gauges, focusing on the Riemann surfaces generated by varying one of the two Schwinger parameters of the propagator. We see that the modulus of the annulus is an exactly calculable function of the Schwinger parameter and is, in fact, independent of the gauge choice. We then study the vacuum graph in Schnabl gauge as a limit in the family of regular interpolating gauges. The role of slanted identifications in Schnabl gauge first becomes apparent and the error in the presumption that diagrams are closed string degenerate is identified.

The situation becomes more nontrivial and challenging for the one-loop tadpole, i.e. the one-loop one-point function. We study this diagram in section 3 for the family of interpolating gauges parameterized by λ. The diagram only has a closed string modulus; the position of the open string puncture can be adjusted using rotations. For any fixed λ, we can use extremal length methods to show that the full moduli space of annuli is produced as the Schwinger parameter is varied over its allowed range. In Siegel gauge the modulus of the annulus is a complicated function of the Schwinger parameter (defined implicitly by certain elliptic integrals, see, for example [37]). In the limit that we reach Schnabl gauge the modulus becomes a simple function of the Schwinger parameter. In this example one can glean the main geometrical insight that shows how the two components of the annulus, each one with its own open string boundary, are glued across a *hidden boundary* at infinity! The existence of such a hidden boundary leads us to conclude that the operator L (the Virasoro zero mode in the sliver frame) has an anomalous left/right decomposition, i.e. $[L_L, L_R] \neq 0$.

In section 4, we will introduce slanted wedges and show how to glue them together, as suggested by star multiplication, to produce a closed algebra. We discuss how the operators L_L and L_R and their BPZ conjugates act on slanted wedges and derive the action of the full Schnabl propagator. This formalism simplifies tremendously the construction of string diagrams, as we discuss for the case of trees in section 5. The moduli for tree diagrams are the positions of open string punctures and these can be calculated efficiently,

JHEP07(2008)063

as is demonstrated for the case of the 5-point diagram. We present the generalization to arbitrary tree diagrams, which is surprisingly straightforward using the algebra of slanted wedges.

In section 6 we discuss the Riemann surfaces for general one-loop string diagrams in Schnabl gauge. We show how to construct such a surface by gluing the hidden boundaries of the surfaces associated with each of the boundaries of the annulus. Both of these surfaces are naturally built with slanted wedges. We determine the closed string modulus and all open string moduli as simple functions of the Schwinger parameters. In particular, we find that the closed string modulus only depends on the Schwinger parameters of the propagators running in the loop. The computations are illustrated in section 7 where we work out the one-loop diagram with two external states. If both external states are placed on the same boundary component there are two string diagrams, and we discuss how they generate together the relevant open and closed string moduli.

In section 8 we use the family of λ-regularized gauges to justify our prescription for the calculation of one-loop moduli. There are three types of gluing operations that need to be justified in the Schnabl limit $\lambda \to 0$: (i) the star multiplication of slanted wedges corresponding to external states and propagator surfaces, (ii) the gluing along hidden boundaries that forms a single strip from the two slanted wedges each of which contains one boundary component of the one-loop diagram, and (iii) the identification of the edges of the resulting strip that creates the annulus. We show that all three types of operations can be justified rigorously in the Schnabl limit. We end in section 9 with some concluding remarks.

2. The vacuum graph

In this section we discuss the geometry of the vacuum graph. Our objectives are to set up notation and to calculate the modulus of the vacuum graph as a function of the Schwinger parameter for general regular linear b-gauges.

2.1 Gauges, coordinate frames and the surface $\mathcal{R}(s)$

Reference [34] studied open string perturbation theory in a class of gauges called linear b-gauges. In these gauges, a linear combination of even moded antighost oscillators annihilates the classical string field $|\psi_{cl}\rangle$:

$$B[v]\,|\psi_{cl}\rangle = 0\,. \tag{2.1}$$

Here $B[v]$ is determined by a vector field $v(\xi)$ via

$$B[v] = \sum_{k\in\mathbb{Z}} v_{2k} b_{2k} = \oint \frac{d\xi}{2\pi i} v(\xi) b(\xi)\,, \qquad \text{with} \quad v(\xi) = \sum_{k\in\mathbb{Z}} v_{2k}\xi^{2k+1}\,, \quad v_{2k}\in\mathbb{R}\,. \tag{2.2}$$

A subset of linear b-gauges in which string perturbation is guaranteed to produce the correct on-shell amplitudes was identified in [34]. In this subset the vector field $v(\xi)$ is analytic in a neighborhood of the unit circle $|\xi| = 1$, and satisfies the condition

$$\Re\left(\bar{\xi} v(\xi)\right) > 0 \qquad \text{for} \quad |\xi| = 1\,. \tag{2.3}$$

These gauges were called *regular linear b-gauges*. One also defines

$$L[v] \equiv \{Q, B[v]\} = \oint \frac{d\xi}{2\pi i} v(\xi) T(\xi) = \sum_{k\in\mathbb{Z}} v_{2k} L_{2k} \,. \tag{2.4}$$

In a certain frame $w = g(\xi)$ the operator $L[v]$ generates translations [34, 11]. The map $g(\xi)$ is related to the vector field $v(\xi)$ through

$$\frac{dg}{d\xi} = -\frac{1}{v(\xi)} \,. \tag{2.5}$$

Normalizing $v(\xi)$ appropriately, we can impose on $g(\xi)$ the convenient boundary conditions

$$g(-1) = 0 \,, \quad g(1) = i\pi \,. \tag{2.6}$$

We also use the frame $z = f(\xi)$ where the operator $L[v]$ is the zero mode Virasoro operator and thus generates scaling. This frame is only determined up to an overall factor. We choose the normalization

$$f(\pm 1) = \pm \frac{1}{2} \,. \tag{2.7}$$

Given such a frame $z = f(\xi)$, one can determine the associated vector field $v(\xi)$ as

$$v(\xi) = \frac{f(\xi)}{f'(\xi)} \,. \tag{2.8}$$

The defining property of this vector field is that the operators $L[v]$ and $B[v]$ are, respectively, the zero modes of the Virasoro and antighost operators in the z frame. Use of (2.5) and (2.8) immediately shows that the w and z frames are related by $g = -\ln f + c$, where c is a constant. This constant is determined by our boundary conditions on $g(\xi)$ and $f(\xi)$ in (2.6) and (2.7). We obtain

$$w = g(\xi) = -\ln(2f(\xi)) + i\pi = -\ln(2z) + i\pi \,. \tag{2.9}$$

In this map z is always in the upper-half plane and the branch of the logarithm is taken using $0 \le \mathrm{Arg}\, z \le \pi$. Inverting (2.9) we get

$$z = f(\xi) = -\frac{1}{2}\, e^{-w} \,. \tag{2.10}$$

Picking a gauge condition (2.1) for the classical string field $|\psi_{cl}\rangle$ of ghost number one is only the first step in the gauge fixing procedure [38 – 40, 34]. Appropriate vector fields $v(\xi)$ must be chosen for each ghost number and the gauge condition is that the corresponding $B[v]$ operator must annihilate the string field at the given ghost number. We will return to this issue when we address general one-loop amplitudes in section 6.

We noted above that the operator $L[v]$ generates rescalings in the z frame and translations in the w frame. As a differential operator we thus have

$$L[v] = -z\frac{d}{dz} = \frac{d}{dw} \,. \tag{2.11}$$

The operator $e^{-sL[v]}$ creates a strip $\mathcal{R}(s)$ of length s in the w frame with two horizontal open string boundaries [34], as depicted in figure 1(a). The boundary conditions (2.6) ensure that the width of the strip is normalized to π. Furthermore, the strip domain $\mathcal{R}(s)$ has as right boundary the curve $w = g(\xi = e^{i\theta})$ with $0 \leq \theta \leq \pi$; this is just the w-plane image of the coordinate curve. It is clear from (2.11) that $e^{-sL[v]}$ translates by a distance s to the left. It follows that the left boundary of $\mathcal{R}(s)$ is the right boundary copied a distance s to the left.[1]

Using the relation (2.10), we can map the strip $\mathcal{R}(s)$ to the z frame. The right boundary of $\mathcal{R}(s)$ in the w frame becomes the *coordinate curve* $z = f(e^{i\theta})$ with $0 \leq \theta \leq \pi$ in the z frame. As $L[v]$ generates rescalings in this frame, the surface $\mathcal{R}(s)$ is swept out by rescalings of the coordinate curve with scale factors ranging from one to e^s. As we can decompose the operator $L[v]$ into left and right pieces,

$$L[v] = L[v]_L + L[v]_R \,, \tag{2.12}$$

we can similarly divide $\mathcal{R}(s)$ into two components, one associated with the action of $e^{-sL[v]_L}$ and the other associated with the action of $e^{-sL[v]_R}$. The component associated with $e^{-sL[v]_R}$ is the part of $\mathcal{R}(s)$ in the region $\Re(z) > 0$ and is shaded in light grey in figure 1(b). It is swept out by rescalings of the right part of the coordinate curve, which we parameterize as

$$\frac{1}{2} + \gamma_R(\theta) \equiv f\big(e^{i\theta}\big) \,, \qquad\qquad 0 \leq \theta \leq \tfrac{\pi}{2} \,. \tag{2.13}$$

Similarly, the component of $\mathcal{R}(s)$ associated with $e^{-sL[v]_L}$, shaded in dark grey in the figure, is located in the region $\Re(z) < 0$, and is swept out by rescalings of the left part of the coordinate line, which we parameterize as

$$-\frac{1}{2} + \gamma_L(\theta) \equiv f\big(e^{i(\pi-\theta)}\big) \,, \qquad 0 \leq \theta \leq \tfrac{\pi}{2} \,. \tag{2.14}$$

Note that the curves $\gamma_R(\theta)$ and $\gamma_L(\theta)$ introduced above are, respectively, the right and left parts of the coordinate curve, displaced horizontally so that for $\theta = 0$ they are at the origin (figure 1(c)). The left component of $\mathcal{R}(s)$ is simply a reflection of the right component around the axis $\Re(z) = 0$, because the general form (2.2) of the vector field $v(\xi)$ implies

$$\gamma_L(\theta) = -\overline{\gamma_R(\theta)} \,. \tag{2.15}$$

The left and right components of $\mathcal{R}(s)$ need to be glued on the imaginary axis along the line QQ', which stretches from $f(i)$ to $e^s f(i)$. For regular linear b-gauges $f(i)$ is finite, resulting in a finite boundary QQ' generated by $e^{-sL[v]_L}$ and $e^{-sL[v]_R}$. Thus, $e^{-sL[v]_L}$ and $e^{-sL[v]_R}$ do not give the surface associated with $e^{-sL[v]}$ until they are glued along QQ'. This can be traced to the non-commutativity of $L[v]_L$ and $L[v]_R$,

$$\big[\, L[v]_L \,,\, L[v]_R \,\big] \neq 0 \,, \tag{2.16}$$

which in turn implies $e^{-sL[v]} \neq e^{-sL[v]_R} e^{-sL[v]_L}$ for regular linear b-gauges. The operators in (2.16) fail to commute because the vector field v does not vanish at the open string midpoint (see [7]).

[1] This representation of $\mathcal{R}(s)$ differs from the representation in [34] by a rescaling of $\frac{1}{2}e^s$ in the z frame and by a translation of $-s$ in the w frame.

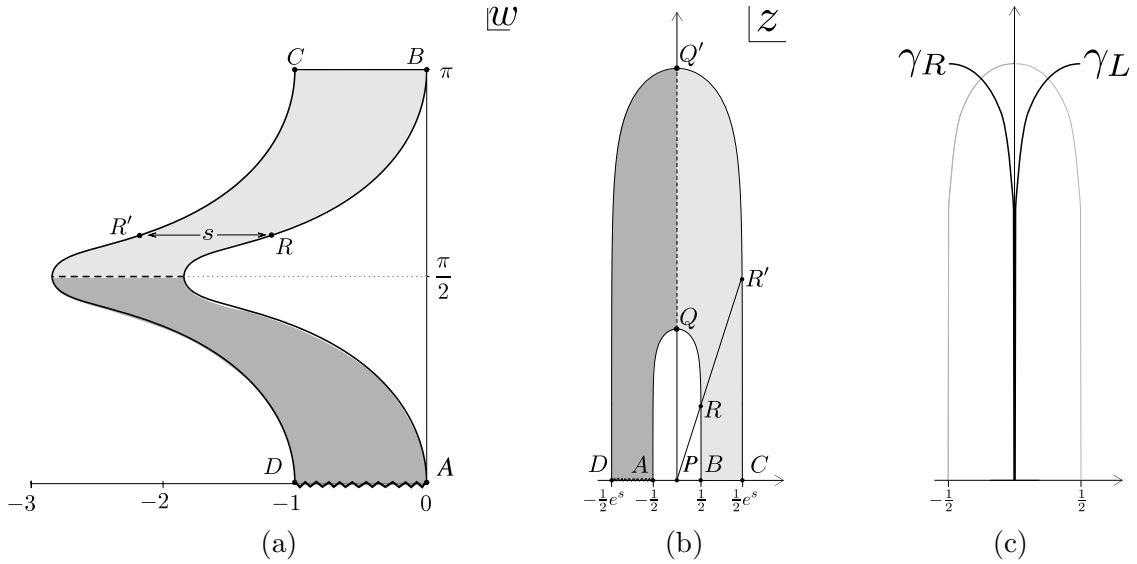

Figure 1: The surface $\mathcal{R}(s)$ created by $e^{-sL[v]}$ in the w frame (a) and in the z frame (b). Points R and R' related by horizontal translation $w \to w - s$ in the w frame are related by scaling $z \to e^s z$ in the z frame. The surface $\mathcal{R}(s)$ is displayed for $L[v] = L^\lambda$ with $\lambda = 10^{-4}$ and $s = 1$. The curves γ_L and γ_R arise from the coordinate curve $f(e^{i\theta})$, as illustrated in (c).

In this paper the family of λ-regulated gauges introduced in [34] plays an important role. This family is defined through the one-parameter family of vector fields

$$v^\lambda(\xi) = e^\lambda(1 + e^{-2\lambda}\xi^2)\tan^{-1}(e^{-\lambda}\xi)\,, \quad \text{with} \quad \lambda > 0\,. \tag{2.17}$$

The surface $\mathcal{R}(s)$ in this gauge is then generated by the operator

$$L^\lambda \equiv L[v^\lambda] = L_0 + 2\sum_{k=1}^{\infty} \frac{(-1)^{k+1}}{4k^2 - 1}\, e^{-2k\lambda}\, L_{2k}\,. \tag{2.18}$$

This family interpolates from Siegel gauge as $\lambda \to \infty$ to Schnabl gauge which arises in the limit $\lambda \to 0$. In fact, these gauges are regular linear b-gauges for all values $\lambda > 0$. Schnabl gauge is not regular – this is why there is no proof yet that amplitudes arise correctly.

For the λ-regulated z frames we have the λ-regulated functions

$$f^\lambda(\xi) = \frac{1}{2}\,\frac{\tan^{-1}(e^{-\lambda}\xi)}{\tan^{-1}(e^{-\lambda})}\,, \quad \text{with} \quad \lambda > 0\,. \tag{2.19}$$

While in general regular linear b-gauges the functions $f(\xi)$, just like $v(\xi)$, need only be analytic in a neighborhood of $|\xi| = 1$, the functions (2.19) have the nice property that they are analytic on the entire unit disk $|\xi| \le 1$. They map the real axis between $\xi = -1$ and $\xi = 1$ to the real axis between $z = -\frac{1}{2}$ and $z = \frac{1}{2}$, and map $\xi = 0$ to $z = 0$. The region in the z frame between the real axis and the curve $z = f(e^{i\theta})$ with $0 \le \theta \le \pi$ can thus be interpreted as a canonical coordinate patch that glues nicely to the boundary of $\mathcal{R}(s)$.

JHEP07(2008)063

The maps $f^\lambda(\xi)$ are thus *coordinate functions*. In the Schnabl limit $\lambda \to 0$, we obtain

$$f(\xi) \equiv \lim_{\lambda\to 0} f^\lambda(\xi) = \frac{2}{\pi}\,\tan^{-1}\xi\,. \tag{2.20}$$

This is the familiar coordinate function of the sliver frame which is well defined for all $|\xi| \le 1$ except for $\xi = i$. The open string midpoint $\xi = i$ is mapped to $i\infty$.

The behavior of the coordinate function $f^\lambda(\xi)$ for very small λ (near Schnabl gauge) will be of interest. We focus on the coordinate curve $f^\lambda(\xi = e^{i\theta})$ with $0 \le \theta \le \pi$. It is convenient to use the angular variable $\hat\theta$ that measures angles with respect to the imaginary axis

$$\hat\theta = \frac{\pi}{2} - \theta\,. \tag{2.21}$$

The coordinate function (2.19) admits a simple expansion when both λ and $\hat\theta$ are small, regardless of their ratio. One then finds[2]

$$f^\lambda(e^{i\theta}) = -\frac{i}{\pi}\ln\Big(\frac{\lambda + i\hat\theta}{2}\Big) \,+\, \mathcal{O}(\lambda) \,+\, \mathcal{O}(\hat\theta)\,. \tag{2.22}$$

We define $i\Lambda(\lambda)$ as the value of the coordinate function at $\xi = i$:

$$i\Lambda \equiv f^\lambda(i) = -\frac{i}{\pi}\ln\frac{\lambda}{2} \,+\, \mathcal{O}(\lambda)\,. \tag{2.23}$$

Happily, the regularized curve $f^\lambda(e^{i\theta})$ only differs appreciably from the sliver curve $f(e^{i\theta})$ for $\hat\theta = \mathcal{O}(\lambda)$. For $\lambda \ll 1$, the part of the curve $f^\lambda(e^{i\theta})$ which deviates significantly from $f(e^{i\theta})$ is thus entirely captured by (2.22). We can write the leading dependence as

$$f^\lambda(e^{i\theta}) \;\simeq\; i\Lambda(\lambda) - \frac{i}{2\pi}\ln\Big[1 + \Big(\frac{\hat\theta}{\lambda}\Big)^2\Big] + \frac{1}{\pi}\tan^{-1}\Big(\frac{\hat\theta}{\lambda}\Big)\,. \tag{2.24}$$

The nature of the curve $f^\lambda(e^{i\theta})$ is quite interesting. As illustrated in figure 2, for any $\lambda \ll 1$ the coordinate curve near the top takes the *same* shape. This is so because, apart from the $i\Lambda(\lambda)$ term that sets the height, the rest of f^λ depends only on the ratio $\hat\theta/\lambda$, which spans the same values as $\hat\theta$ grows from zero to some multiple of λ. For $\hat\theta = \lambda$ the coordinate curve has come down about 0.11 from the top and is 50% of the way to the maximum real value of 1/2 (top dashed lines). For $\hat\theta = 64\lambda$ the coordinate curve has come down about 1.32 from the top and is 99% of the way to the maximum real value (lower dashed lines). Clearly, for sufficiently small λ, the coordinate curve deviates from the vertical lines that define the sliver frame only for $\hat\theta \ll 1$.

The curves γ_R^λ and γ_L^λ which parameterize the coordinate curve $f^\lambda(e^{i\theta})$ for λ-regulated gauges will play an important role in our analysis. They are defined by

$$\frac{1}{2} + \gamma_R^\lambda(\theta) \equiv f^\lambda\big(e^{i\theta}\big)\,, \qquad -\frac{1}{2} + \gamma_L^\lambda(\theta) \equiv f^\lambda\big(e^{i(\pi-\theta)}\big)\,, \tag{2.25}$$

[2]We follow the convention that terms of order $\lambda\ln\lambda$ are written as $\mathcal{O}(\lambda)$.

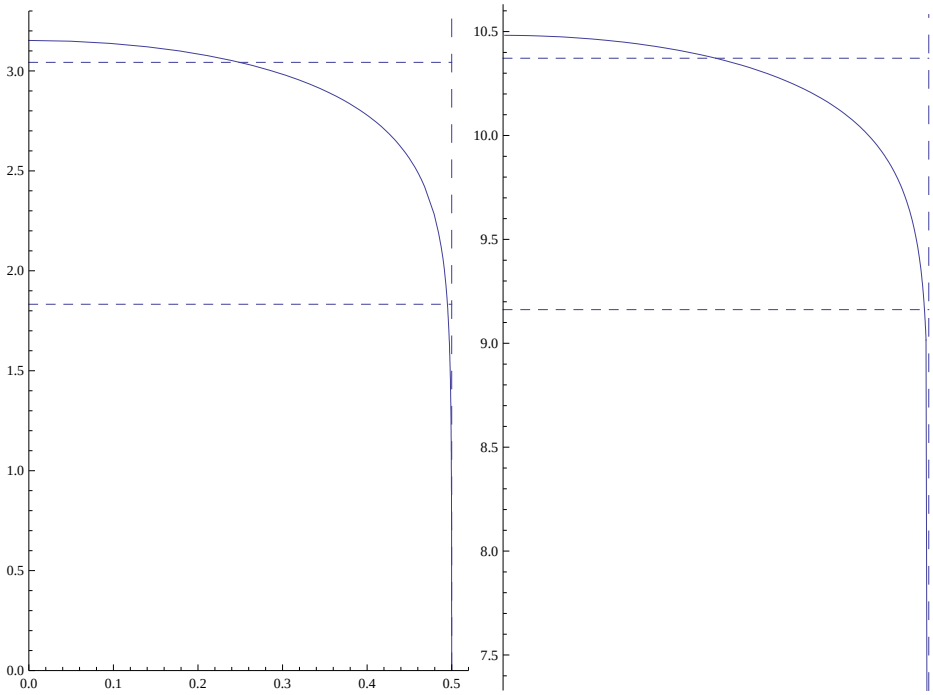

Figure 2: Left: The coordinate curve $f^\lambda(e^{i\theta})$ for $\theta \in [0, \pi/2]$ and $\lambda = 10^{-4}$. The intersection with the bottom dashed line indicates that by the time the curve has dropped about 1.32 from the top, it is within 1% of the vertical line $\Re(z) = 1/2$ that defines the sliver frame. Right: the same portion of the coordinate curve for $\lambda = 10^{-14}$. The top part of the coordinate curve is quite accurately the same as the one shown to the left, but is displaced upwards.

a particular example of the general definitions (2.13) and (2.14). In the Schnabl limit $\lambda \to 0$, γ_R^λ and γ_L^λ coincide, and we therefore define

$$\gamma(\theta) \equiv \lim_{\lambda\to 0} \gamma_R^\lambda(\theta) = \lim_{\lambda\to 0} \gamma_L^\lambda(\theta) = i\,\frac{2}{\pi}\tanh^{-1}\Big(\tan\frac{\theta}{2}\Big)\,. \tag{2.26}$$

As expected, this is the parameterized vertical line that defines the left and right parts $\frac{1}{2} - \gamma$ and $\frac{1}{2} + \gamma$ of the coordinate curve of the sliver projector. Notice, however, that the limit (2.26) is not uniform in θ. In fact, for all $\lambda > 0$ we have

$$\lim_{\theta\to\frac{\pi}{2}} \Re\big(\gamma_{L/R}^\lambda(\theta)\big) = \pm\frac{1}{2}\,, \tag{2.27}$$

while $\Re(\gamma(\theta)) = 0$, independent of θ.

We now ask how much the coordinate curve of λ-regulated gauges still deviates from the vertical line that defines the sliver by the time its imaginary part has been reduced to $\Lambda/2$, that is, half the value it has at the top. To leading order in λ, the angle corresponding to this point on the curve is given by

$$\hat\theta_{\frac{1}{2}} = \sqrt{2\lambda} \quad \to \quad \theta_{\frac{1}{2}} = \tfrac{\pi}{2} - \sqrt{2\lambda}\,. \tag{2.28}$$

JHEP07(2008)063

A short calculation then shows

$$\gamma_R^\lambda\big(\theta_{\frac{1}{2}}\big) = -\frac{1}{2\pi}\sqrt{2\lambda} + i\,\frac{\Lambda}{2} + \mathcal{O}(\lambda)\,. \tag{2.29}$$

As we can see, $\gamma_R^\lambda(\theta)$ only deviates by $\mathcal{O}(\sqrt{\lambda})$ from the imaginary axis by the time its height has dropped by half.

2.2 The annulus and its modulus

The surfaces associated with the one-loop vacuum graph are obtained by gluing the two parameterized edges of the propagator to itself. The propagator associated with regular linear b-gauges is in general a complicated object. Its geometric interpretation depends on the ghost number of the state it acts on. In alternating gauge [34] the surface of the propagator is built by gluing the strips associated with $e^{-sL[v]}$ and $e^{-s^\star L^\star[v]}$ in some order (that depends on ghost number) and by including the action of the BRST operator Q, that acts as a total derivative on moduli. The details of this construction will be important for our general analysis in section 6. For now, we focus on one term that arises from the propagator: it can be described by setting $s^\star = 0$ and gives the strip $\mathcal{R}(s)$ associated with $e^{-sL[v]}$. The generalization to the full propagator will not introduce further conceptual problems in our Riemann surface analysis. We restrict ourselves to the simplified propagator in the discussion of the vacuum and the tadpole diagrams because it suffices to demonstrate the main features of loop diagrams in Schnabl gauge.

For any regular linear b-gauge, the gluing of the simplified propagator $\mathcal{R}(s)$ to itself is implemented in the w frame by the identification $w \sim w - s$. The result, for each value of s, is an annulus. In this annulus the boundaries are the horizontal segments BC and AD, shown in figure 1(a) for λ-regularized gauges. The map from this annulus to a canonically presented annulus in the ζ frame is

$$\zeta = \exp\Big(-\frac{2\pi i}{s}(w - i\pi)\Big) = \exp\Big(-\frac{2\pi^2}{s}\Big)\exp\Big(-\frac{2\pi i w}{s}\Big)\,. \tag{2.30}$$

See figure 3(a). We can also write, using (2.9),

$$\zeta = \exp\Big(\frac{2\pi i}{s}\ln 2z\Big)\,. \tag{2.31}$$

The map (2.30) takes BC into the unit circle $|\zeta| = 1$ and AD into the inner circle $|\zeta| = \exp(-2\pi^2/s)$. Since the strip $\mathcal{R}(s)$ is foliated in the w frame by horizontal lines of length s at heights that go from zero to π it is clear that the map (2.30) takes the interior of the strip to the region between the two ζ circles mentioned above. The shape of the edges of $\mathcal{R}(s)$ is irrelevant to the map; their image under the map is a cutting curve for the annulus. Shown to the right in figure 3(b) is the w-frame picture of $\mathcal{R}(s)$ rolled up into a cylinder of height π and circumference s. The cutting curve is shown in both presentations.

The modulus M of an annulus with radii $r_{\rm in}$ and $r_{\rm out}$ with $r_{\rm in} < r_{\rm out}$ is usually defined by

$$M \equiv \frac{1}{2\pi}\ln\frac{r_{\rm out}}{r_{\rm in}}\,. \tag{2.32}$$

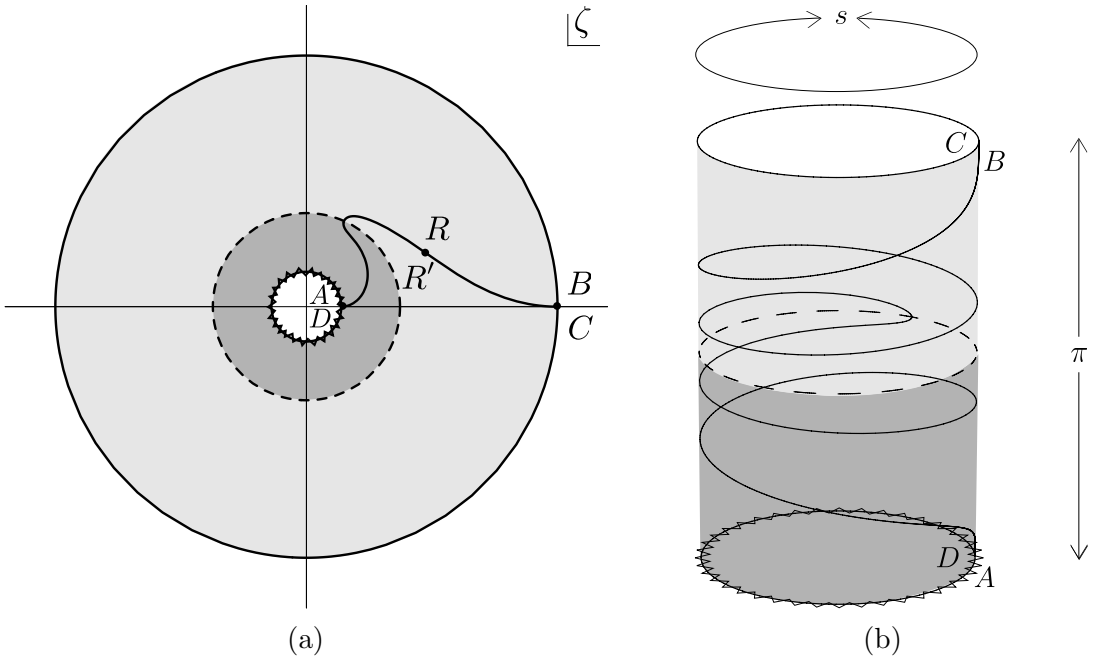

Figure 3: The vacuum graph obtained from gluing the edges of $\mathcal{R}(s)$, illustrated for $L[v] = L^\lambda$ with $\lambda = 10^{-4}$. In (a) the surface is displayed as a canonical annulus in the ζ frame for $s = 10$. The cutting curve is shown explicitly. In (b) the surface is displayed as a cylinder obtained from the identification $w \sim w - s$ in the w frame for $s = 1$. This should be compared to figure 1(a).

The moduli space of annuli is the set

$$0 \leq M \leq \infty \,. \tag{2.33}$$

For our annulus the modulus is

$$M = \frac{\pi}{s} \,. \tag{2.34}$$

This result for the annulus modulus is valid for any regular linear b-gauge. In particular, the modulus M of the annulus produced by the gluing of the edges of $\mathcal{R}(s)$ is the same for all values of λ in the λ-regularized gauges and depends only on s. As $s \to 0$, $M \to \infty$, the inner circle goes to zero size, and we approach closed string degeneration. As $s \to \infty$ the inner circle approaches the outer circle, M goes to zero, and we approach open string degeneration. The full moduli space (2.33) is therefore covered. It thus follows that in the Schnabl limit $\lambda \to 0$ the gluing of $\mathcal{R}(s)$ also gives an annulus of $M = \pi/s$ and that moduli space is covered in this case as well. The limit $\lambda \to 0$ of figure 1 is shown in figure 4. Moreover, figure 5 shows the map to the ζ plane and the cylinder view of the w-presentation. Note that we could have calculated the annulus modulus in Schnabl gauge using any other family of regular linear b-gauges which approaches Schnabl gauge when the regulator is removed. The result for M would have been the same.

A few remarks about this construction in the Schnabl limit are in order.

JHEP07(2008)063

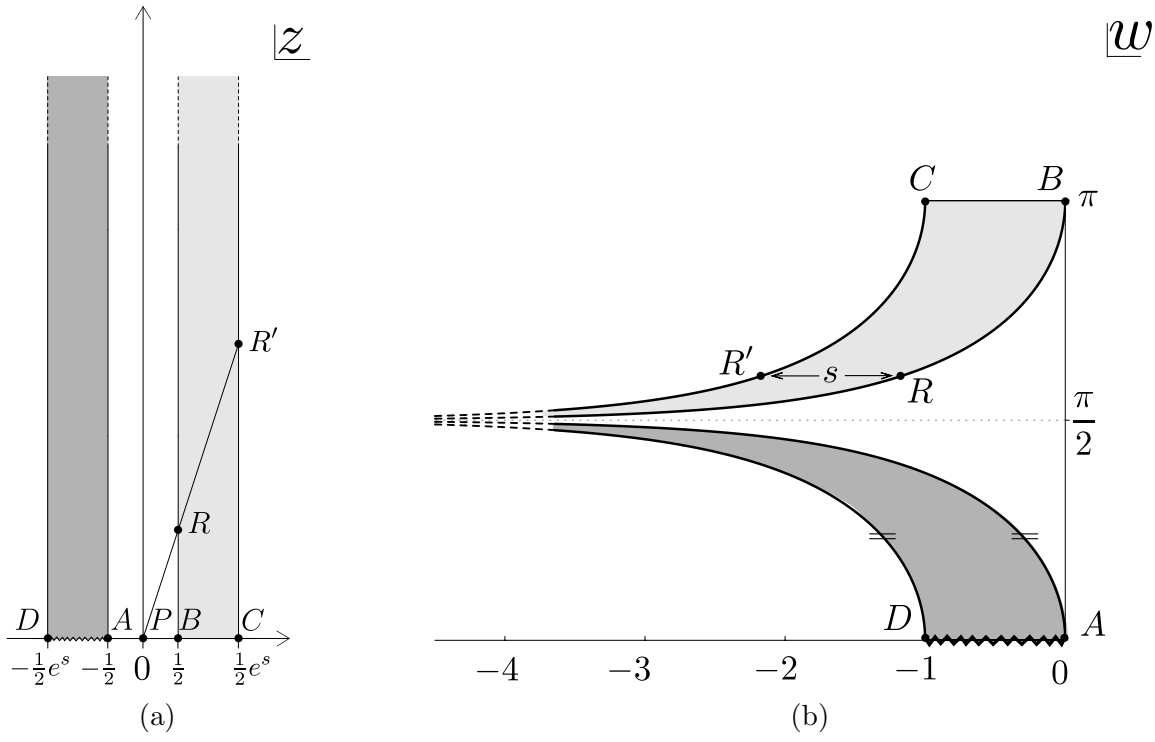

Figure 4: The $\mathcal{R}(s)$ strip in the Schnabl limit $\lambda = 0$ both in the w and in the z frames, displayed for $s = 1$. The gluing of the free edges of the strip gives rise to an annulus of finite modulus (see figure 5). The gluing identification in the z frame is that induced by radial lines emerging from the origin.

- The map (2.30) still takes the shaded domain in the w plane to the circular annulus because the identification $w \sim w - s$ still holds. The cutting curve is infinitely long (figure 5).

- In the z plane the vertical strip to the right produces the upper half of the annulus (the upper half of the vertical cylinder of height π and circumference s). The vertical strip to the left produces the lower half of the annulus. The two halves are glued.

- The identifications $w \sim w - s$ become *slanted* identifications $z \sim e^s z$ of the vertical lines through B and C, and of the vertical lines through A and D. If the identifications had been horizontal ($z \sim z - \frac{1}{2} + \frac{1}{2}e^s$) both the right and left strips would have each given rise to a (closed string) degenerate annulus. In fact, such a problematic horizontal identification happens for the gauge condition $B^+\Phi = 0$ in the sliver frame. It is the slanted identification that makes the z frame picture in Schnabl gauge consistent with a finite modulus annulus.

In the previous section we remarked that the propagator strip $\mathcal{R}(s)$ for regular linear b-gauges can be decomposed into two components associated with $e^{-sL[v]_L}$ and $e^{-sL[v]_R}$, respectively. These components are glued along the boundary QQ' in figure 1(b). $L[v]_L$

JHEP07(2008)063

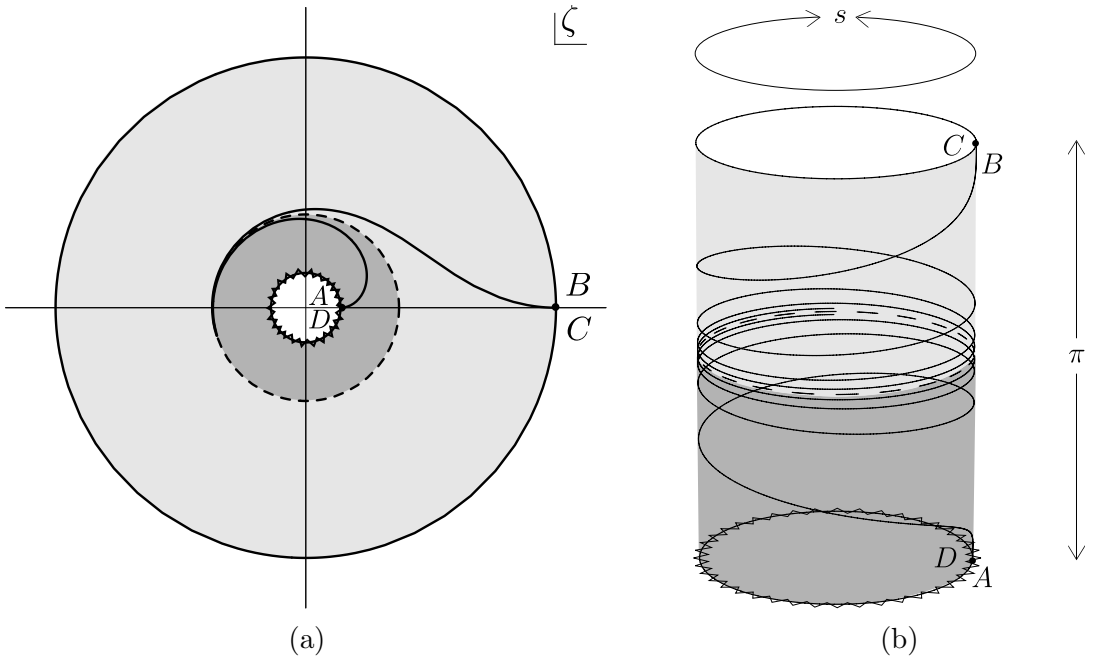

Figure 5: The vacuum graph obtained from gluing the edges of $\mathcal{R}(s)$ in the Schnabl limit $\lambda \to 0$. In (a) the surface is displayed as a canonical annulus in the ζ frame for $s = 10$. In (b) the surface is displayed as a cylinder obtained from the identification $w \sim w - s$ in the w frame for $s = 1$. These surfaces differ from the corresponding finite-λ surfaces in figure 3 only through the shape of the cutting curve.

and $L[v]_R$ generate this unmatched boundary that needs to be glued by hand because they do not commute. The operators L and $L^\star$ in Schnabl gauge can also be decomposed into left and right parts. We write $L = L_L + L_R$, $L^\star = L^\star_L + L^\star_R$. In the Schnabl limit, the unmatched boundary is hidden at $i\infty$ in the z- frame, but arises in the annulus frame ζ as the circle $|\zeta| = \exp(-\pi^2/s)$, shown dashed in figure 5(a). We are led to conclude that while both L and $L^\star$ arise from vector fields that vanish at the open string midpoint, they do not vanish fast enough to ensure that L_L and L_R commute and that $L^\star_L$ and $L^\star_R$ commute:[3]

$$[L_L, L_R] \neq 0\,, \qquad [L^\star_L, L^\star_R] \neq 0\,. \tag{2.35}$$

We conclude this subsection by recalling the relation of the modulus M with the conformal invariant known as the extremal length [41]. The extremal length is an invariant associated to a given set of curves Γ on a Riemann surface. Let ρ denote a conformal metric (a metric for which $ds = \rho(z,\bar{z})|dz|$) on the Riemann surface. The length $\ell(\gamma,\rho)$ of a curve $\gamma \in \Gamma$ and the area $A(\Omega,\rho)$ of the Riemann surface Ω are given by:

$$\ell(\gamma,\rho) = \int_\gamma \rho|dz|\,, \quad A(\Omega,\rho) = \iint_\Omega \rho^2\, dxdy\,. \tag{2.36}$$

[3]In fact the linear combination $L^+ = L + L^*$ arises from a vector that, as we approach the midpoint, vanishes sufficiently fast to ensure that L^+_L and L^+_R commute.

JHEP07(2008)063

We define $\ell(\Gamma,\rho)$ as the length of the shortest curve in Γ with respect to the metric ρ:

$$\ell(\Gamma,\rho) = \inf_{\gamma\in\Gamma} \ell(\gamma,\rho)\,. \tag{2.37}$$

The extremal length λ_Γ is defined as [41]

$$\lambda_\Gamma = \sup_\rho \left(\frac{\ell^2(\Gamma,\rho)}{A(\Omega,\rho)}\right). \tag{2.38}$$

To evaluate λ_Γ one must search over metrics until the quantity inside parenthesis on the right-hand side is maximized. The extremal metric ρ for which the maximum is attained is a minimal area metric: it is the metric with least area consistent with all curves in the set having a length greater than or equal to a certain prescribed value. From the definition (2.38) it is clear that the extremal length λ_Γ is a conformal invariant.

Let us now return to the vacuum graph of regular linear b-gauges. Imagine the domain $\mathcal{R}(s)$, glued to itself to form the vacuum graph, as a cylinder of circumference s and height π. This is, in fact, the w frame picture in figure 3(b). There are two types of curves on this cylinder (or annulus): open curves that stretch from one boundary to the other and closed curves that go around the cylinder. We thus have an extremal length $\lambda_{\rm open}$ associated with the set of open curves and an extremal length $\lambda_{\rm closed}$ associated with the set of closed curves. It is a familiar result that in the w frame the *same* metric $\rho = 1$ is extremal for *both* open and closed curves [42]. It is clear that in this flat metric the shortest open curves have length π and the shortest closed curves have length s. The area, moreover, is πs. It follows that the extremal lengths are

$$\lambda_{\rm open} = \frac{\pi^2}{\pi s} = \frac{\pi}{s}\,, \qquad \lambda_{\rm closed} = \frac{s^2}{\pi s} = \frac{s}{\pi}\,. \tag{2.39}$$

It is interesting to note that

$$\lambda_{\rm open}\lambda_{\rm closed} = 1\,, \quad \text{and} \quad M = \lambda_{\rm open} = \frac{1}{\lambda_{\rm closed}}\,. \tag{2.40}$$

The relations (2.40) are general and valid for any annulus. Note that degeneration of a given type means vanishing extremal length for the curves of associated type. Thus closed string degeneration ($s \to 0$) happens for $\lambda_{\rm closed} \to 0$ and open string degeneration ($s \to \infty$) happens for $\lambda_{\rm open} \to 0$.

3. One-loop tadpole graph

In this section we discuss the one-loop tadpole graph. The underlying Riemann surface is an annulus with an open string puncture, that is, a puncture on one of the boundary components of the annulus. The puncture, which represents the external state, introduces significant complications in the geometry. Indeed, it is well known that in Siegel gauge the map of the string diagram to the round annulus is nontrivial and the modulus of the annulus cannot be calculated in simple closed form.

JHEP07(2008)063

As in the previous section we restrict ourselves to the contribution from the propagator surface $\mathcal{R}(s)$ generated by $e^{-sL[v]}$. We discuss the graph for the family of interpolating gauges. We first show that for any value of the regulator λ the moduli space of annuli is generated when the Schwinger parameter s covers the range from zero to infinity. We then study the geometry as the regulator parameter λ goes to zero and we approach Schnabl gauge. We present a construction which allows us to exactly map the tadpole string diagram to the round annulus in the limit $\lambda \to 0$. The modulus of the annulus becomes exactly calculable in Schnabl gauge.

3.1 Covering moduli space in the λ-regulated gauges

Let us consider the one-loop tadpole graph with propagator $e^{-sL[v]}$. It is useful to first examine the surface obtained in the λ-regulated gauges. The way to assemble the surface is illustrated using figure 6. We need the part of the surface associated with the external state and the propagator strip $\mathcal{R}(s)$.

As we can see in figure 6(b), the placement of $\mathcal{R}(s)$ in the z frame is the same one used for the vacuum graph in the last section (figure 1(b)). As discussed above equation (2.35), it is convenient to view the surface $\mathcal{R}(s)$ as built by gluing together two pieces — one associated with $e^{-sL^\lambda_R}$ and one associated with $e^{-sL^\lambda_L}$. These two pieces are glued along the dashed line QQ' to form the complete surface $\mathcal{R}(s)$.

The two curved boundaries of $e^{-sL^\lambda_L}$ are identified, just as for the vacuum graph. This time, however, the two curved boundaries of $e^{-sL^\lambda_R}$ are not glued to each other. To form the tadpole, we need to glue these two boundaries to the left and right boundaries of the external state. As the functions $f^\lambda(\xi)$ are coordinate functions and thus well defined for all $|\xi| \le 1$, we can conveniently place this external state in the region between the real axis and the coordinate curve $f^\lambda(e^{i\theta})$. The operator insertion is then located at $z = f(0) = 0$ (see figure 6(b)).

The gluing patterns both in the z and w frames are readily obtained from the graph in figure 6(a). The only slightly nontrivial gluing operation is that identifying the curves AQ and CQ' in the z plane (the lines with triple arrows). We can express these two curves using $\gamma^\lambda_{L/R}$ defined in (2.25):

$$AQ = -\frac{1}{2} + \gamma^\lambda_L\,, \qquad CQ' = e^s(\frac{1}{2} + \gamma^\lambda_R)\,. \tag{3.1}$$

It then follows that the identification between AQ and CQ' is given by the map

$$z = -\frac{1}{2} + \gamma^\lambda_L(\theta) \;\to\; z' = e^s\big(\frac{1}{2} + \gamma^\lambda_R(\theta)\big)\,. \tag{3.2}$$

Recalling $\gamma_L(\theta) = -\overline{\gamma_R(\theta)}$, we find that a point $z \in AQ$ is identified with the point $z' \in CQ'$, where z' is obtained by first reflecting z across the vertical axis $z \to -\bar{z}$, and then applying the expansion factor e^s:

$$z \to z' = -e^s\,\bar{z}\,. \tag{3.3}$$

There should be no concern that z' appears to be a non-analytic function of z. The above relation is not a *sewing* relation, but just a relation valid on the curve (for example, the

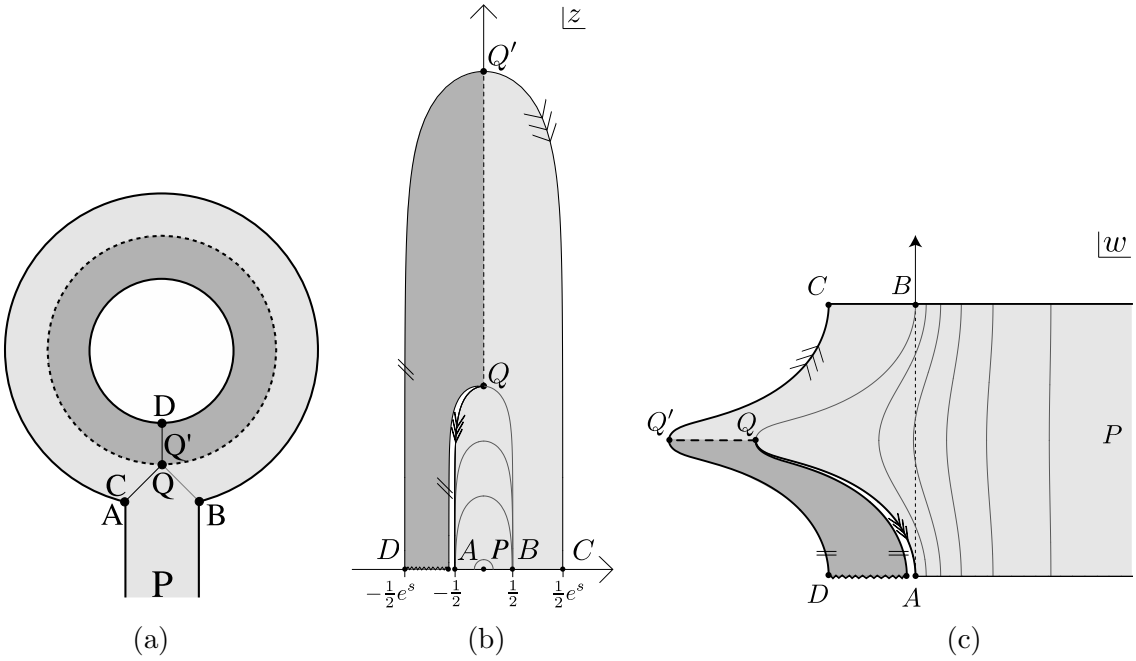

Figure 6: (a) The topology of the one-loop tadpole diagram obtained by gluing the external strip for the Fock space state to the propagator strip. (b) The tadpole diagram for a λ-regulated gauge in the z frame, displayed for $\lambda = 10^{-4}$ and $s = 1$. Note the cut from Q to A that separates the two boundary components. (c) The tadpole diagram in the w frame.

analytic relation $\xi\xi' = -1$ becomes $\xi' = -\bar{\xi}$ on the unit circle). The analytic gluing relation is determined by the sequence of conformal maps $z \to f^{-1}(z)$ back to the coordinate circle, $\xi \to -1/\xi$, followed by the action of f and, finally, multiplication by e^s. The analytic gluing relation corresponding to the identification (3.3) is thus

$$z \sim e^s f\Big(-\frac{1}{f^{-1}(z)}\Big)\,. \tag{3.4}$$

Since there is no simple closed form expression for the modulus $M(s)$ of the annulus in Siegel gauge, we cannot hope to calculate explicitly $M(s)$ for arbitrary finite λ. Extremal length, however, gives a very simple proof that moduli space will be covered. Consider the w-frame picture in figure 6(c). The extremal metric cannot be found, but let us use the metric $\rho = 1$ on the lower half of the strip $\mathcal{R}(s)$ (below $Q'Q$) and $\rho = 0$ elsewhere. In other words, we are setting $\rho = 1$ only on the part of the surface corresponding to $e^{-sL_L^\lambda}$ (shaded in dark grey in the figure). The area of the surface in this metric is $A = \frac{1}{2}\pi s$. In this metric the shortest open curves have length $\frac{\pi}{2}$. This gives the following inequality for the open string extremal length

$$\lambda_{\rm open} \geq \frac{\left(\frac{\pi}{2}\right)^2}{\frac{\pi s}{2}} = \frac{\pi}{2s}\,. \tag{3.5}$$

For closed curves we take $\rho = 1$ all over the propagator strip $\mathcal{R}(s)$ *and* over the portion of the external state strip that lies to the left of the vertical line AB in figure 6(c). In other

JHEP07(2008)063

words, we set $\rho = 1$ in the region $\Re(w) < 0$. We set $\rho = 0$ elsewhere. A little thought shows that in this metric the shortest closed curve has length s. The area is $\pi s + A(\lambda)$, where $A(\lambda)$ is the area of the external state strip in the chosen metric. We thus get

$$\lambda_{\rm closed} \geq \frac{s^2}{\pi s + A(\lambda)} \quad \rightarrow \quad \lambda_{\rm open} \leq \frac{\pi}{s} + \frac{A(\lambda)}{s^2}\,. \tag{3.6}$$

In the Siegel limit $\lambda \to \infty$, the vertical line AB in the w frame coincides with the right boundary of $\mathcal{R}(s)$ so that the area $A(\infty) = 0$. It is easy to see that the area $A(\lambda)$ grows as λ decreases, but it stays finite even in the limit $\lambda \to 0$. In fact, the relevant integral can be exactly calculated and one finds that

$$A_0 \equiv \lim_{\lambda\to 0} A(\lambda) = \pi \ln 2\,. \tag{3.7}$$

Back in (3.6), we use $A(\lambda) \leq A_0$ and find

$$\lambda_{\rm open} \leq \frac{\pi}{s} + \frac{A_0}{s^2} = \frac{\pi}{s} + \frac{\pi \ln 2}{s^2}\,. \tag{3.8}$$

Combining (3.5) and (3.8) and recalling that $M = \lambda_{\rm open}$ we get

$$\frac{\pi}{2s} \leq M(s) \leq \frac{\pi}{s}\Big(1 + \frac{\ln 2}{s}\Big)\,. \tag{3.9}$$

The above inequalities imply that $M(s) \to 0$ as $s \to \infty$ and $M(s) \to \infty$ as $s \to 0$, so the full moduli space will be covered for $s \in [0, \infty)$. This is consistent with the results of [34] which showed that regular linear b-gauges, such as the λ-regulated gauges, give correct on-shell string amplitudes. The inequalities (3.9) hold for all $\lambda > 0$. We thus conclude that moduli space is covered in the Schnabl limit $\lambda \to 0$.

3.2 Modulus in Schnabl gauge

The estimates done in the previous subsection bound $M(s)$ and allow us to confirm that moduli space is covered for any value of the deformation parameter λ. We now claim that the value of the modulus $M(s)$ becomes calculable in simple closed form in the Schnabl limit $\lambda \to 0$. The derivation requires careful analysis of a conformal map in the limit $\lambda \to 0$. Since the final result is simple, we will present it here, without proof. In the following subsection we justify our claim.

We begin with figure 7(a), where we see that the surface of the tadpole diagram appears as two *disconnected* vertical strips in the z frame. The strip above the real segment $[-\frac{1}{2}e^s, -\frac{1}{2}]$ represents e^{-sL_L} and the strip above the real segment $[-\frac{1}{2}, \frac{1}{2}e^s]$ represents the external state and e^{-sL_R}. These real segments are the boundaries of the annulus. On the left strip the identification of the edges is $z \sim e^s z$. On the right strip the identification is more nontrivial. Its left boundary carries the ordinary sliver parameterization and is given by $-\frac{1}{2} + \gamma(\theta)$, with $\gamma(\theta)$ defined in (2.26). The right boundary of the right strip is given by $e^s(\frac{1}{2} + \gamma(\theta))$ and thus carries a parameterization which is rescaled by e^s. It follows that a point R on the line above $z = -\frac{1}{2}$ and a point R' on the line above $z = \frac{1}{2}e^s$ are identified if the copy S of R on the line above $z = \frac{1}{2}$ is related to R' via the scaling

JHEP07(2008)063

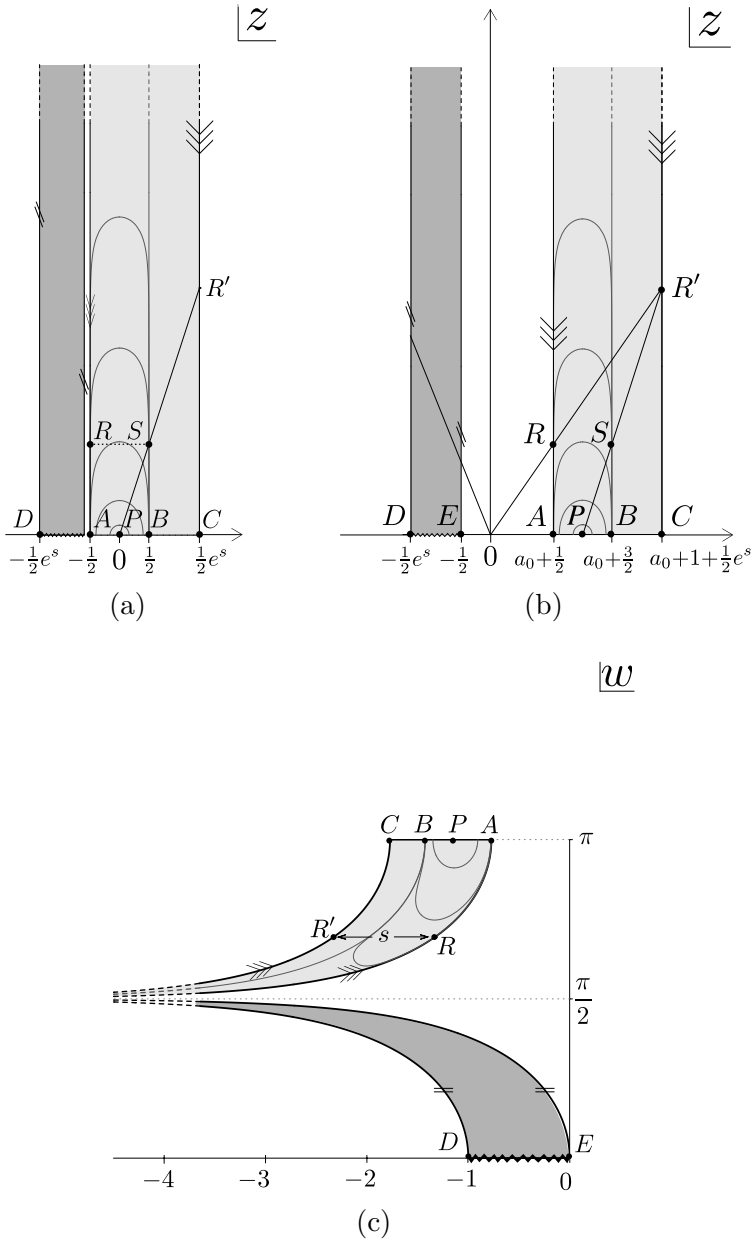

Figure 7: (a) The one-loop tadpole in the z frame. The surface is composed of two separate strips: one above $z \in [-\frac{1}{2}e^s, -\frac{1}{2}]$ and the other above $z \in [-\frac{1}{2}, \frac{1}{2}e^s]$. These two strips are joined at $i\infty$. The figure is displayed for $s = 1$. (b) The same surface with the right strip translated to the right by a distance $a_0 + 1$, which depends on s and makes the identifications of the left and right boundaries work with rays through the origin. (c) The middle figure mapped to the w frame with $w = -\ln 2z + i\pi$.

$z \sim e^s z$. This is, in fact, the gluing prescription discussed around equation (3.3). The two separate strips are supposed to be glued together at $i\infty$ but it is not obvious how to glue

JHEP07(2008)063

these hidden boundaries.

We could proceed as we did in the previous section and map this configuration of surfaces directly to the w frame via (2.9). Just like in figure 6(c)), the external state would be represented in the w frame by an infinite strip of height π. In Schnabl gauge, however, we can construct a different map of the tadpole diagram to the w frame, one in which the whole surface is foliated by horizontal lines of length s. It is then possible to use the map $\zeta(w)$ in (2.30) to get a round annulus. We will now show how this is done.

In the z frame we translate the right strip towards the right by a distance that makes the line through the identified points R and R' go through the origin. Since the heights of R and R' are related by e^s it follows, by similar triangles, that $R \sim R'$ are related by $z \sim e^s z$ (see figure 7(b)). The requisite displacement, called $a_0 + 1$ for later convenience, is determined from the similar triangles:

$$e^s = \frac{CR'}{AR} = \frac{a_0 + 1 + \frac{1}{2}e^s}{a_0 + \frac{1}{2}}\,. \tag{3.10}$$

One readily finds that

$$a_0 = \frac{1}{e^s - 1}\,, \quad a_0 + 1 = \frac{1}{1 - e^{-s}}\,. \tag{3.11}$$

With this result one can check that the two vertical lines for the right strip are located at

$$\Re(z) = a_0 + \frac{1}{2} = \frac{1}{2}\coth\left(\frac{s}{2}\right)\,, \quad \text{and} \quad \Re(z) = a_0 + 1 + \frac{1}{2}e^s = e^s \cdot \frac{1}{2}\coth\left(\frac{s}{2}\right)\,. \tag{3.12}$$

The map $w = -\ln(2z) + i\pi$ in (2.9) takes the full left and right strips to the w-frame picture in figure 7(c). This picture is similar to that in figure 4(b), which refers to the vacuum graph. There is only one minor difference: the image of the right strip in figure 7(c) is displaced some distance to the left. This happens because the coordinate $z(A)$ of the point A satisfies

$$z(A) = a_0 + \frac{1}{2} > \frac{1}{2} \quad \to \quad \Re\big(w(A)\big) < 0\,. \tag{3.13}$$

Since both strips in figure 7(b) work with identification $z \sim e^s z$, the w plane figure 7(c) has the identification $w \sim w - s$. This w presentation is different from the earlier w presentation in which the coordinate half-disk for the external state appears as a semi-infinite strip (figure 6(c)); the coordinate half-disk has been pushed up! The identification $w \sim w - s$ ensures that the map (2.30) takes the w-plane region to the annulus with modulus

$$M = \frac{\pi}{s}\,. \tag{3.14}$$

Inserting an external state to form the tadpole graph therefore did not affect the modulus of the annulus — the modulus (3.14) coincides with our result (2.34) for the modulus of the vacuum graph. The only evidence of the external state is that the top boundary of the annulus is split between the boundary AB of the coordinate half-disk with the puncture and the boundary BC generated by e^{-sL_R}. The surprisingly simple form of the modulus will turn out to be generic for one-loop diagrams in Schnabl gauge. In fact, we will find that the annulus modulus of a general one-loop diagram is a simple function that depends only on the Schwinger parameters of the propagators running in the loop; the Schwinger parameters of trees attached to the loop do not affect the modulus of the annulus.

JHEP07(2008)063

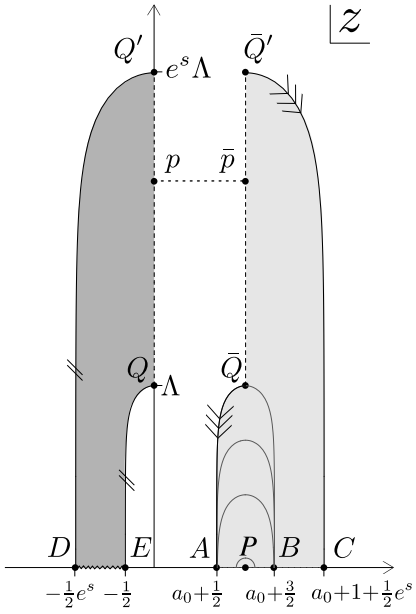

Figure 8: The z-frame λ-regulated one-loop tadpole of figure 6 cut along QQ' and with the right piece translated to the right a distance $a_0 + 1$ so that the identification of A and C is through scaling by e^s. The figure is displayed for $\lambda = 10^{-4}$ and $s = 1$.

3.3 Taking the $\lambda \to 0$ limit

We will now justify our construction of the map of the Schnabl tadpole diagram to the round annulus. Let us consider the λ-regulated version of the one-loop tadpole graph, first shown in figure 6(b). We cut the diagram along the QQ' line to produce two disconnected pieces. Just like we did for the Schnabl tadpole, we displace the right part of the figure to the right a distance $a_0 + 1$. The identifications on the left part of the surface still work with $z \sim e^s z$, but on the right they do not anymore. Choosing a_0 as before (see (3.11)) we ensure that the points A and C are still identified with $z \sim e^s z$, but this identification is only approximate for the other points on the curves $A\bar{Q}$ and $C\bar{Q}'$.

As before, the map $w = -\ln(2z) + i\pi$ takes the left part of figure 8 (the surface associated with $e^{-sL_L^\lambda}$) to the familiar annular domain with identifications exactly given by $w \sim w - s$ (see figure 9). Since $z(Q) = i\Lambda$ (see (2.23)) the image of QQ' in the w frame is shifted $\ln 2\Lambda$ to the left with respect to the image of the inner boundary DE.

For the map of the right part of figure 8 we have to be a bit more careful. We will use the same map $w = -\ln(2z) + i\pi$, which results in a surface whose identification is not quite $w \sim w - s$ and thus cannot be interpreted as an annular region for general λ. Furthermore, the image of $\bar{Q}\bar{Q}'$ in the w frame does not quite coincide with the image of QQ'. What we are going to show is that in the limit as $\lambda \to 0$ (and consequently $\Lambda \to \infty$) the identifications needed to form the full annulus become exact. More precisely, as $\lambda \to 0$ two things should happen:

1. All points $p \in QQ'$ and $\bar{p} \in \bar{Q}\bar{Q}'$ that are at the same height (and should therefore be

identified), are mapped to points on the w frame that approach each other as $\lambda \to 0$. This convergence is uniform on QQ' ensuring that the top and bottom parts of the annulus glue well.

2. Points $q \in A\bar{Q}$ and $q' \in A\bar{Q}'$ that must be identified will map to coordinates w that satisfy $w(q) - w(q') = s$ in the limit $\lambda \to 0$. This convergence is uniform on $A\bar{Q}$, ensuring that the top part of the annulus works with the same identification $w \sim w - s$ as the bottom part.

If these two claims hold, it justifies the prescription given in the previous subsection for the Schnabl limit. In the remainder of this subsection we will prove (1) and (2).

Consider first claim (1) regarding the gluing of QQ' to $\bar{Q}\bar{Q}'$. Let $ix\Lambda$, with x a real number, denote the imaginary part of a point $p \in QQ'$ that must be identified with a point $\bar{p} \in \bar{Q}\bar{Q}'$ with the same imaginary part. Since the imaginary part of any point p (or $\bar{p}$) ranges between Λ and $e^s\Lambda$ we have

$$1 \le x \le e^s \quad \to \quad \Lambda \le x\Lambda \le e^s\Lambda\,. \tag{3.15}$$

We then have

$$z(p) = i\,x\Lambda\,, \quad z(\bar{p}) = a_0 + 1 + i\,x\Lambda = \frac{1}{1-e^{-s}} + i\,x\Lambda\,, \tag{3.16}$$

where we made use of (3.11). Using (2.9) we get

$$w(\bar{p}) - w(p) = -\ln\left[\frac{z(\bar{p})}{z(p)}\right] = -\ln\left[1 + \frac{1}{ix\Lambda(1-e^{-s})}\right] \tag{3.17}$$

As $\lambda \to 0$ we have $\Lambda \to \infty$. It is then clear that for any fixed value of $s > 0$ and any $x \in [1, e^s]$ the above gives $w(\bar{p}) - w(p) \to 0$. Furthermore, it follows from (3.17) and $x \ge 1$ that the convergence of $\bar{Q}\bar{Q}'$ to QQ' is uniform. This proves claim (1).

It is interesting to discuss the above result in more detail. We show in figure 9 two examples of the w plane surface, both for $s = 1$. The top figure uses $\lambda = 10^{-4}$ and the bottom one uses $\lambda = 10^{-14}$. One can see the image of $\bar{Q}\bar{Q}'$ as the sloping edge that approaches (as we go from the top figure to the bottom figure) the horizontal image of QQ'. Expanding the logarithm in (3.17) we get

$$w(\bar{p}) - w(p) = i\,\frac{1}{x\Lambda(1-e^{-s})} - \frac{1}{2}\,\frac{1}{x^2\Lambda^2(1-e^{-s})^2} + \mathcal{O}(\Lambda^{-3})\,. \tag{3.18}$$

The vertical distance between the images of p and $\bar{p}$ vanishes as Λ^{-1}. The horizontal distance vanishes faster, as fast as Λ^{-2}. These features are clearly seen in the figure for the pair $\bar{Q}$, Q, and for the pair $\bar{Q}'$, Q'. Furthermore, the vertical convergence of Q' to $\bar{Q}'$ in the w frame is faster by a factor of e^s than the vertical convergence of Q to Q'. This is due to the suppression factor $\frac{1}{x}$ in the imaginary part of (3.18), and is clearly visible in the figure.

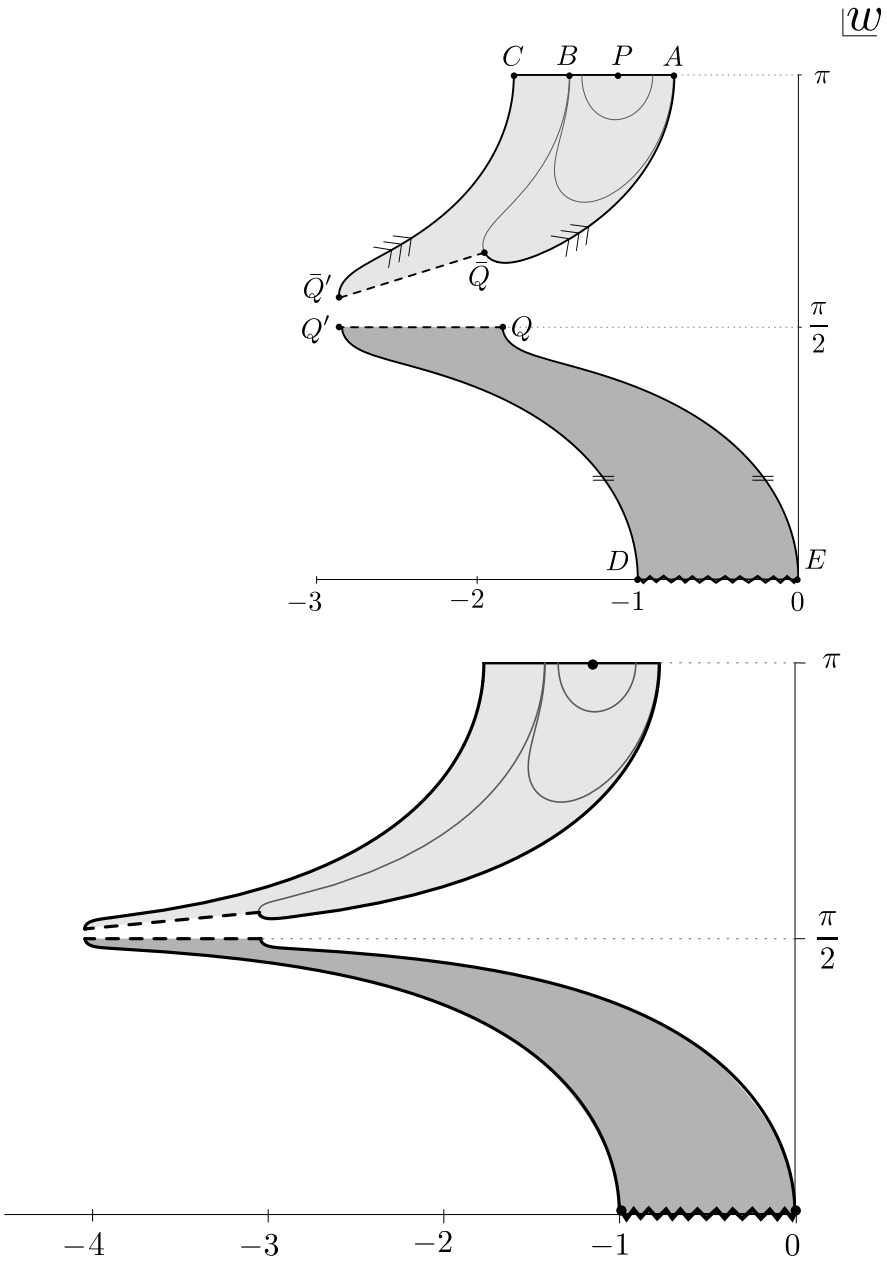

Figure 9: The λ-regulated one-loop tadpole in the plane $w = -\ln(2z) + i\pi$. The top figure arises for $\lambda = 10^{-4}$ and the bottom figure arises for $\lambda = 10^{-14}$. Both figures use $s = 1$.

Let us now address claim (2). Before the translation is performed (see figure 6(b)), the identified curves AQ and CQ' are parameterized as shown in (3.1). After the translation by $a_0 + 1$, we obtain figure 8 with the curves $A\bar{Q}$ and $C\bar{Q}'$ given by

$$A\bar{Q} = a_0 + \frac{1}{2} + \gamma_L^\lambda\,, \qquad C\bar{Q}' = a_0 + 1 + e^s\left(\frac{1}{2} + \gamma_R^\lambda\right). \tag{3.19}$$

These parameterized curves are identified. The (complex) ratio $r(\theta)$ between identified

points on the curves is given by

$$r(\theta) = \frac{a_0 + 1 + e^s\big(\frac{1}{2} + \gamma_R^\lambda(\theta)\big)}{a_0 + \frac{1}{2} + \gamma_L^\lambda(\theta)} = e^s \cdot \frac{\gamma_R(\theta) + \frac{1}{2}\coth\frac{s}{2}}{\gamma_L(\theta) + \frac{1}{2}\coth\frac{s}{2}}\,, \tag{3.20}$$

where we used the definition (3.11) of the shift $a_0 + 1$ as well as (3.12). We must show that this ratio has the limit

$$r(\theta) \to e^s \qquad \text{for} \quad \lambda \to 0\,, \quad 0 \le \theta \le \frac{\pi}{2}\,. \tag{3.21}$$

If this is so, the map to the w plane (via the logarithm) will imply that the points corresponding to θ are separated by a horizontal translation by s. To make the map to the annulus well defined in the limit $\lambda \to 0$, we need this horizontal separation by s to hold to arbitrary precision for all points on the identified curves, i.e. we need the limit (3.21) to hold *uniformly* on $0 \le \theta \le \frac{\pi}{2}$.

One finds $r(\theta = 0) = e^s$, exactly, as expected for the ratio of the base points A and C of the two curves. Indeed, the translation was designed to make the identification $z \sim e^s z$ work on the real axis. For general θ, a short calculation gives

$$r(\theta) = e^s \cdot \frac{1 + \delta(\theta)}{1 - \delta(\theta)}\,, \quad \text{with} \quad \delta = \frac{\gamma_R - \gamma_L}{\gamma_R + \gamma_L + \coth\frac{s}{2}} = \frac{\Re\big(\gamma_R\big)}{i\Im\big(\gamma_R\big) + \frac{1}{2}\coth\frac{s}{2}}\,, \tag{3.22}$$

where we used $\gamma_L = -\overline{\gamma_R}$ in the last step. As we map the two points in question to the w plane, their separation is given by $\ln r$. We obtain

$$\ln r = s + \ln\Big(\frac{1-\delta}{1+\delta}\Big)\,. \tag{3.23}$$

We want to show that δ goes to zero uniformly on $0 \le \theta \le \frac{\pi}{2}$ when $\lambda \to 0$. We are going to break the curve γ_R into two parts: (i) the top part for which $\Im(\gamma_R) \in [\Lambda/2, \Lambda]$ and (ii) the bottom part for which $\Im(\gamma_R) \in [0, \Lambda/2]$. We recall from (2.29), that this corresponds to splitting the range of θ at $\theta = \theta_{\frac{1}{2}}$. Consider the top part (i). In this region we estimate

$$\big|\delta\big| = \left|\frac{\Re\big(\gamma_R\big)}{i\Im\big(\gamma_R\big) + \frac{1}{2}\coth\frac{s}{2}}\right| \le \frac{\operatorname{Max}\Re\big(\gamma_R\big)}{\operatorname{Min}\Im\big(\gamma_R\big)} = \frac{\frac{1}{2}}{\frac{\Lambda}{2}} = \frac{1}{\Lambda} \tag{3.24}$$

so that

$$\big|\delta(\theta)\big| \le \frac{1}{\Lambda} \qquad \text{for} \quad \theta \in \left[\theta_{\frac{1}{2}}, \frac{\pi}{2}\right]. \tag{3.25}$$

Now consider region (ii), i.e. $0 \le \theta \le \theta_{\frac{1}{2}}$. Recall our earlier estimate (2.29) that at $\theta = \theta_{\frac{1}{2}}$ the coordinate curve has indeed risen to a height of $\Lambda/2$ and that

$$\Re\Big(\gamma_R\big(\theta_{\frac{1}{2}}\big)\Big) = -\frac{1}{2\pi}\sqrt{2\lambda}\,. \tag{3.26}$$

In this region $\Im(\gamma_R)$ can be arbitrarily small, and $|\Re(\gamma_R)|$ reaches its maximal value at $\theta = \theta_{\frac{1}{2}}$. We thus estimate

$$|\delta| = \left|\frac{\Re(\gamma_R)}{i\Im(\gamma_R) + \frac{1}{2}\coth\frac{s}{2}}\right| \le \left|\frac{\Re(\gamma_R)}{\frac{1}{2}\coth\frac{s}{2}}\right| \le \frac{\frac{1}{2\pi}\sqrt{2\lambda}}{\frac{1}{2}} = \frac{1}{\pi}\sqrt{2\lambda} \tag{3.27}$$

for region (ii), so that

$$\big|\delta(\theta)\big| \le \frac{1}{\pi}\sqrt{2\lambda} \qquad \text{for} \quad \theta \in \big[0, \theta_{\frac{1}{2}}\big]\,. \tag{3.28}$$

We now have upper bounds on δ valid for the regions (i) and (ii). For any $\lambda < 1$ the upper bound in (3.25) for region (i) is larger than that in (3.28) for region (ii). Therefore we obtain the uniform upper bound

$$\big|\delta(\theta)\big| \le \frac{1}{\Lambda} \quad \text{for all} \quad \theta \in \left[0, \frac{\pi}{2}\right], \quad \lambda < 1\,. \tag{3.29}$$

This means that $\delta(\theta)$ will vanish uniformly on $0 \le \theta \le \frac{\pi}{2}$ as $\lambda \to 0$, as we wanted to prove. This establishes the second claim, and thus completes the argument that shows that regulation leads to the claimed simple map in Schnabl gauge.

We conclude with a comment concerning the Schnabl gauge limit. In the unregulated case, shown in figure 7(b), we see that the left and right cylinders are supposed to be glued at $i\infty$. It may seem as if the gluing involves both the coordinate patch strip of the external state and the strip to the right of it. The regulation shows that this is not quite the way things work. The coordinate frame for the external state tapers out and does not glue to the bottom part of the diagram, which arises from the left cylinder. The tip $\bar{Q}$ of the local coordinate frame (the string midpoint) lies at the end of the gluing line. As can be seen in figure 9, at $\bar{Q}$ the coordinate curve goes both up towards B and down to eventually reach A. The behavior at $\bar{Q}$ follows from conformality to the z frame, as shown in figure 8.

4. Slanted wedges: a family of surfaces

Loop amplitudes in Schnabl gauge use surfaces that do not feature in tree amplitudes. As we have seen in the previous sections, we sometimes deal with semi-infinite strips that look like the familiar wedge surfaces, except that the vertical edges are subject to identifications that are slanted. For wedge surfaces, presented as vertical semi-infinite strips, the natural identification of the vertical edges is a horizontal translation by the width a of the wedge.

It turns out to be convenient to introduce a set of surfaces that generalize the wedge surfaces. They will be called *slanted* wedges and are characterized by two parameters: the width a of the underlying wedge and the slant b, to be defined below. There is one important difference between wedges and slanted wedges. Associated with wedges there are wedge states but there are no surface states associated with slanted wedges.

For wedge surfaces, the surface states are based on once-punctured disks. The disk is formed by attaching the left edge of the wedge surface to the right edge of a unit-width wedge coordinate frame (with a marked point, or puncture) and gluing the two remaining vertical edges with a horizontal identification. The resulting surface is a semi-infinite cylinder with a puncture on the boundary at the real axis. This surface can be conformally mapped to a disk. More precisely, the disk has an inner puncture because it misses one point, the image of $i\infty$ on the wedges. This missing point can be ignored. The situation is far more serious for slanted wedges. As we have seen in the construction of the one-loop tadpole, a wedge with a slanted identification has a hidden boundary at $i\infty$, a boundary

JHEP07(2008)063

that must be glued to another surface. Instead of having a vanishingly small additional boundary associated with a missing point, as in the case for wedges, slanted wedges have an additional boundary that cannot be ignored. As a result there are no canonical surface states associated with slanted wedges. The hidden boundaries of slanted wedges can be brought into the open by λ-regularization.

Even without associated states, we can define a kind of star algebra of slanted wedges. While not strictly needed for tree diagrams, slanted wedges simplify significantly the construction of the associated Riemann surfaces. For loop diagrams slanted wedges are key to the construction of the relevant Riemann surfaces.

4.1 Definition and examples

The slanted wedge $[a;b]$, with $a, b \geq 0$, is defined on the upper-half plane z as the semi-infinite strip between $\Re(z) = \frac{1}{2}$ and $\Re(z) = \frac{1}{2} + a$:

$$[a;b] \equiv \left\{ z \,\middle|\, \frac{1}{2} \leq \Re(z) \leq \frac{1}{2} + a\,,\ \Im(z) \geq 0 \right\}. \tag{4.1}$$

The above states that, as a region, $[a;b]$ is the wedge of width a, positioned so that the left boundary is $\Re(z) = \frac{1}{2}$. By definition, the left boundary $\Re(z) = \frac{1}{2}$ carries the parameterization induced by the sliver map $z = \frac{2}{\pi}\tan^{-1}\xi$. More explicitly, the point $\xi = e^{i\theta}$ is mapped to

$$\text{Left Boundary:} \quad e^{i\theta} \to \frac{1}{2} + \gamma(\theta) \qquad \text{with} \quad 0 \leq \theta \leq \frac{\pi}{2}\,, \tag{4.2}$$

where the curve $\gamma(\theta)$ was defined in (2.26). It follows that the left boundary of $[a;b]$ glues naturally to a coordinate patch $-\frac{1}{2} \leq \Re(z) \leq \frac{1}{2}$ of the sliver frame. The slant parameter $b > 0$ is a scaling factor for the parameterization of the right boundary $\Re(z) = \frac{1}{2} + a$ of $[a;b]$. We have

$$\text{Right Boundary:} \quad e^{i\theta} \to \frac{1}{2} + a + b \cdot \gamma(\theta) \quad \text{with} \quad 0 \leq \theta \leq \frac{\pi}{2}\,. \tag{4.3}$$

This implies that the parameterization of the right boundary is obtained by stretching that of the left boundary by the factor b. See figure 10(a) for a representation of the slanted wedge $[a;b]$. For $b = 1$ both boundaries of the slanted wedge carry the same parameterization and are thus horizontal translations of each other. Thus $[a;1]$ is just the familiar ordinary wedge surface of width a:

$$[a;1] = W_a\,. \tag{4.4}$$

Fock space states are described as $[1;1]$ with a local operator insertion at $z = 1$ between the two boundaries. The Fock space state insertion is mapped from $\xi = 0$ to $[1;1]$ via $z = 1 + \frac{2}{\pi}\tan^{-1}\xi$. In general, slanted wedges can carry operator insertions or line integrals.

Since slanted wedges are Riemann surfaces we have some equivalence relations that must be noted. First, the position of the slanted wedge can be altered. While $[a;b]$ is

JHEP07(2008)063

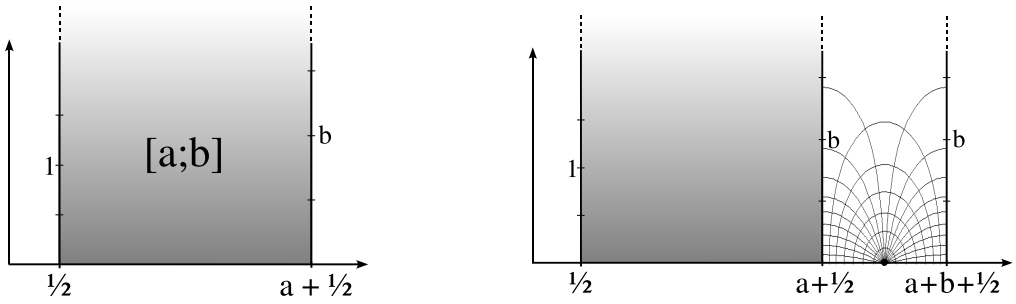

Figure 10: (a) The slanted wedge $[a;b]$ in the sliver frame z. (b) Illustration of the star multiplication of a slanted wedge $[a;b]$ with a Fock space state $[1;1]$. The result is a slanted wedge $[a+b;b]$.

always assumed to have a left boundary $\Re(z) = \frac{1}{2}$, a translation by a real constant can be used to position the slanted wedge elsewhere. This is useful to form star products, for example. Sometimes we have to deal with wedge regions where both edges carry scaled parameterizations. We could call such surfaces $[b_L; a; b_R]$ with b_L and b_R denoting the scaling factors for the left and the right edges, respectively. Explicitly, this means that the parameterizations of the left and right boundaries in (4.2) and (4.3) are replaced by $\frac{1}{2} + b_L\gamma(\theta)$ and $\frac{1}{2} + a + b_R\gamma(\theta)$, respectively. This surface, under the map $z \to z/b_L$ and a possible translation, gives us the conformal identification

$$[b_L; a; b_R] \;\sim\; [a/b_L\,; b_R/b_L]\,. \tag{4.5}$$

We obtain a wedge of width a/b_L with unit scaling on the left boundary and scaling b_R/b_L on the right boundary. The above shows that we do not have to define slanted wedges with scaled parameterizations on both edges.

4.2 Operations on slanted wedges

In order to create the surfaces relevant to the Feynman rules we need to introduce the "star-multiplication" of slanted wedges. For plain wedges the star multiplication is homomorphic to the star multiplication of the corresponding wedge states. Since we have no states associated with slanted wedges, their star multiplication is only a device to construct interesting surfaces.

As for surface states, we define star multiplication as the gluing of the right boundary of the first surface to the left boundary of the second surface. This gluing, however, requires identical parameterizations. For two slanted wedges $[a_1; b_1]$ and $[a_2; b_2]$, we define

$$[a_1; b_1] * [a_2; b_2] \equiv [\, a_1 + b_1 a_2\,;\, b_1 b_2\,]\,. \tag{4.6}$$

The logic behind this is clear: since the right boundary of the first slanted wedge carries a scaling b_1, the second slanted wedge must be fully scaled by b_1 so that its left boundary carries the same scaling. In this process its width becomes $b_1 a_2$ and the scaling of its right

boundary $b_1 b_2$. Once the surfaces are glued, we get a total width of $a_1 + b_1 a_2$ and a scaling factor $b_1 b_2$, which applies to the right boundary.

Clearly, slanted wedges form a closed algebra under the star multiplication and plain wedges form a commutative subalgebra. The algebra (4.6) of slanted wedges $[a;b]$ can also be represented as the algebra of matrices of the form

$$[a;b] \leftrightarrow \begin{pmatrix} b & a \\ 0 & 1 \end{pmatrix} . \tag{4.7}$$

Indeed, in agreement with (4.6) we then have

$$\begin{pmatrix} b_1 & a_1 \\ 0 & 1 \end{pmatrix} \begin{pmatrix} b_2 & a_2 \\ 0 & 1 \end{pmatrix} = \begin{pmatrix} b_1 b_2 & a_1 + b_1 a_2 \\ 0 & 1 \end{pmatrix} . \tag{4.8}$$

A simple and useful particular case of (4.6) involves a Fock space state and a slanted wedge:

$$[a;b] * [1;1] = [a+b\,;b\,] . \tag{4.9}$$

This example is illustrated in figure 10(b). Note that in the final surface the puncture lies at $z = \frac{1}{2} + a + \frac{1}{2}b$, the first $\frac{1}{2}$ for the conventional offset, the a due to the first surface and $\frac{1}{2}b$ because the slanting required scaling the unit width of the Fock state surface by b.

We now consider the Schnabl gauge propagator. As we will see, its various ingredients act naturally on slanted wedges and can be themselves represented by slanted wedges. The classical propagator is given by

$$\mathcal{P} = \int ds ds^\star \, e^{-sL} \, B \, Q \, B^\star e^{-s^\star L^\star} = \int ds ds^\star \; B \, Q \, e^{-sL} e^{-s^\star L^\star} B^\star . \tag{4.10}$$

We will focus solely on the Riemann surface interpretation of this propagator, namely the action of $e^{-sL} e^{-s^\star L^\star}$ on surfaces. The presence of line integral insertions from B, Q, and $B^\star$ will not play a role in the following analysis.

We will construct the action of the propagator step by step, treating the operators e^{-sL_R}, e^{-sL_L}, $e^{-s^\star L^\star_R}$, and $e^{-s^\star L^\star_L}$ separately. As discussed in section 2.2 these operators generate hidden boundaries, which will now be associated with slanted wedges. For loop diagrams these boundaries require special attention.

Let us first consider the action of e^{-sL_R} on a general Fock space state $|F\rangle$. We represent $|F\rangle$ in the sliver frame z as the semi-infinite strip between $\Re(z) = -\frac{1}{2}$ and $\Re(z) = \frac{1}{2}$. The operator insertion of the Fock space state is mapped to $z = 0$ in the sliver frame via the map $z = \frac{2}{\pi} \tan^{-1} \xi$. Recalling the discussion of $\mathcal{R}(s)$ in section 3, we see that $e^{-sL_R}|F\rangle$ is represented in the z frame by gluing a strip of width $\frac{1}{2}(e^s - 1)$ to the right boundary of $|F\rangle$ (figure 4). The parametrization of the right boundary on the resulting surface, however, has a scaling factor e^s. We conclude that e^{-sL_R} attaches to the right of $|F\rangle$ the slanted wedge $[\frac{1}{2}(e^s - 1); e^s]$ (see figure 11(a)). Having determined that e^{-sL_R} is represented by the right attachment of the slanted wedge $[\frac{1}{2}(e^s - 1); e^s]$, it follows that, more generally,

$$e^{-sL_R} \, [a;b] = [a;b] * [\tfrac{1}{2}(e^s - 1); e^s] . \tag{4.11}$$

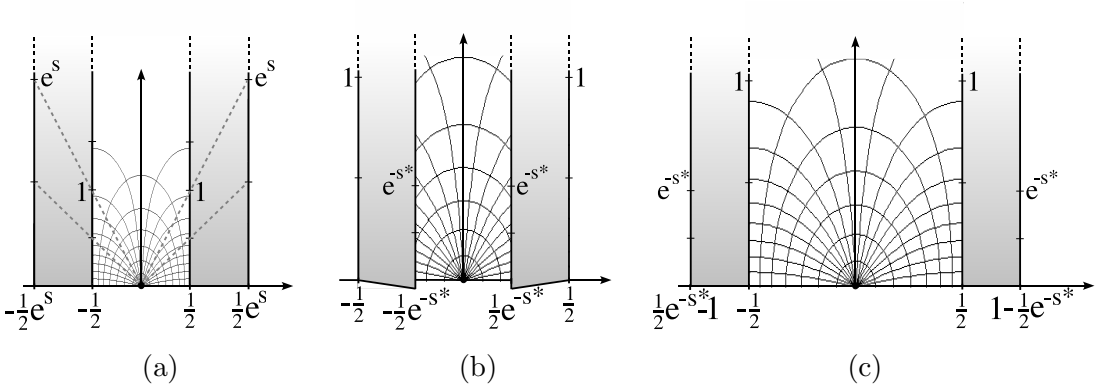

Figure 11: (a) The action of e^{-sL} on a Fock space state adds the shaded strips on both sides of the Fock space state. The shaded strip on the right represents e^{-sL_R}, the shaded strip on the left represents e^{-sL_L}. The dashed grey lines illustrate the rescaling of the parameterizations from the inner to the outer boundaries. (b) The action of $e^{-s^\star L^\star}$ on a Fock space state creates the shaded strips which lie on top of the Fock space state surface. (c) The action of $e^{-s^\star L^\star}$ on a Fock space state after flipping the strips of the propagator.

The slanted wedge $[a;b]$ has hidden boundaries and the action of e^{-sL_R} introduces an additional one that stems from cutting the propagator surface $\mathcal{R}(s)$. We have seen this hidden boundary emerge through λ-regularization as the line $\bar{Q}\bar{Q}'$ displayed in figure 8.

Similarly, e^{-sL_L} glues a strip of width $\frac{1}{2}(e^s-1)$ to the left boundary of $|F\rangle$. Now the *left* boundary of the resulting surface has a parametrization which is scaled by e^s (see figure 11(a)). To interpret this added piece of strip as a slanted wedge, we need to rescale it by a factor e^{-s} so that its left boundary has canonical parameterization. We conclude that the action e^{-sL_L} on $|F\rangle$ glues the slanted wedge $[\frac{1}{2}(1-e^{-s});e^{-s}]$ to the left boundary of $|F\rangle$. This generalizes to

$$e^{-sL_L}\,[a;b] = [\tfrac{1}{2}(1-e^{-s});e^{-s}] * [a;b]\,. \tag{4.12}$$

It follows from (4.11) and (4.12) that

$$e^{-s_R L_R} e^{-s_L L_L}[a;b] = e^{-s_L L_L} e^{-s_R L_R}[a;b]\,, \tag{4.13}$$

for all values of s_L and s_R. We thus conclude that acting on slanted wedges the operators L_L and L_R commute. The action of e^{-sL} on a given slanted wedge can be calculated as follows

$$\begin{aligned} e^{-sL}[a;b] &= e^{-s(L_L+L_R)}[a;b] = e^{-sL_L}e^{-sL_R}[a;b] \\ &= [\tfrac{1}{2}(1-e^{-s});e^{-s}] * [a;b] * [\tfrac{1}{2}(e^s-1);e^s]\,, \end{aligned} \tag{4.14}$$

and therefore

$$e^{-sL}[a;b] = [\tfrac{1}{2}(1+b)(1-e^{-s}) + ae^{-s}\,;b]\,. \tag{4.15}$$

For the particularly important case of $b=1$, the above reduces to

$$e^{-sL}\,[a;1] = [1+(a-1)e^{-s}\,;\,1]\,. \tag{4.16}$$

Since $[a;1]$ is a wedge state, this identity can be readily confirmed by familiar methods (see eq. (A.27) of [32]).

The geometric interpretation of $e^{-s^\star L^\star}|F\rangle$ is somewhat more intricate. In the construction of $e^{-sL}|F\rangle$ we glue the *right* boundary of the w-frame strip $\mathcal{R}(s)$ to the coordinate curve of $|F\rangle$. This boundary of $\mathcal{R}(s)$ is mapped by (2.10) to the coordinate curve $\Re(z) = \pm\frac{1}{2}$ and the gluing to the Fock space state works out naturally, as shown in figure 11(a). It follows from the discussion in §4.3 of [34] that the surface corresponding to $e^{-s^\star L^\star}$ can be obtained by gluing the *left* boundary of the w-frame $\mathcal{R}(s^\star)$ to the coordinate curve of $|F\rangle$. This left boundary of $\mathcal{R}(s^\star)$ is mapped by (2.10) to $\Re(z) = \pm\frac{1}{2}e^{s^\star}$ and the strip develops inwards up to $\Re(z) = \pm\frac{1}{2}$. To glue the chosen boundary of $\mathcal{R}(s^\star)$ to the coordinate curve at $\Re(z) = \pm\frac{1}{2}$, we rescale $\mathcal{R}(s^\star)$ by $z \to e^{-s^\star}z$. The result, illustrated in figure 11(b), is that $e^{-s^\star L^\star_R}$ acting on the sliver-frame $|F\rangle$ introduces a strip between $\frac{1}{2}e^{-s^\star}$ and $\frac{1}{2}$, which is glued to the Fock space state at $\Re(z) = \frac{1}{2}$. In this presentation the surface added by $e^{-s^\star L^\star_R}$ lies on top of the Fock state surface. The parameterization of the left boundary of this added strip is shrunk by a factor of $e^{-s^\star}$. We can flip the surface of $e^{-s^\star L^\star_R}$ around the axis $\Re(z) = \frac{1}{2}$ to obtain the result shown in figure 11(c). We have thus found that $e^{-s^\star L^\star_R}$ attaches the left boundary of the slanted wedge $[\frac{1}{2}(1-e^{-s^\star}); e^{-s^\star}]$ to the right boundary of $|F\rangle$. On general slanted wedges

$$e^{-s^\star L^\star_R}\,[a;b] = [a;b] * [\tfrac{1}{2}(1-e^{-s^\star}); e^{-s^\star}]\,. \tag{4.17}$$

Similarly, we obtain

$$e^{-s^\star L^\star_L}\,[a;b] = [\tfrac{1}{2}(e^{s^\star}-1); e^{s^\star}] * [a;b]\,. \tag{4.18}$$

We notice from (4.11), (4.12), (4.17), and (4.18) that the slanted wedges associated with $e^{-s^\star L^\star_L}$ and $e^{-s^\star L^\star_R}$ can be obtained from those associated with e^{-sL_R} and e^{-sL_L}, respectively, by letting $s \to s^\star$. This is not a peculiarity of Schnabl gauge; it follows because the surface $\mathcal{R}^\star(s^\star)$ generated $e^{-s^\star L[v]^\star}$ can be obtained from the surface $\mathcal{R}(s)$ generated by $e^{-sL[v]}$ from a reflection in the w frame [34].

The action of $e^{-s^\star L^\star}$ on a given slanted wedge can be calculated from

$$e^{-s^\star L^\star}[a;b] \equiv e^{-s^\star L^\star_L} e^{-s^\star L^\star_R}[a;b] = [\tfrac{1}{2}(e^{s^\star}-1); e^{s^\star}] * [a;b] * [\tfrac{1}{2}(1-e^{-s^\star}); e^{-s^\star}] \tag{4.19}$$

and gives

$$e^{-s^\star L^\star}[a;b] = [\tfrac{1}{2}(1+b)(e^{s^\star}-1) + ae^{s^\star}\,; b]\,. \tag{4.20}$$

For the case of surface states the above reduces to the identity

$$e^{-s^\star L^\star}\,[a;1] = [(1+a)e^{s^\star} - 1; 1]\,. \tag{4.21}$$

that is readily confirmed by familiar methods (see eq. (A.28) of [32]).

From (4.11), (4.12), (4.17), and (4.18) we find that the left and right parts of the classical propagator act on a slanted wedge $[a;b]$ as

$$\begin{aligned} e^{-sL_R} e^{-s^\star L^\star_R}\,[a;b] &= [a;b] * [\tfrac{1}{2}(1+e^{s-s^\star}) - e^{-s^\star}\,;\, e^{s-s^\star}]\,, \\ e^{-sL_L} e^{-s^\star L^\star_L}\,[a;b] &= [\tfrac{1}{2}(1+e^{s^\star-s}) - e^{-s}\,;\, e^{s^\star-s}] * [a;b]. \end{aligned} \tag{4.22}$$

It now follows that the action of the classical propagator (4.10) on a slanted wedge $[a;b]$ is given by:

$$e^{-sL}e^{-s^\star L^\star}[a;b] = [\,\tfrac{1}{2}(1+b)(1+e^{s^\star-s}-2e^{-s})+a\,e^{s^\star-s}\,;\,b\,]\,. \tag{4.23}$$

On wedge states $[a;1]$, this simplifies to

$$e^{-sL}e^{-s^\star L^\star}[a;1] = \left[1-2e^{-s}+(1+a)e^{s^\star-s}\,;\,1\right]. \tag{4.24}$$

As we have emphasized, there are no states associated with slanted wedges $[a;b]$ for $b\neq 1$. Such surfaces are incomplete, they have a *hidden* vertical boundary segment at $i\infty$. Since eventually no hidden boundary can remain, a surface $[a;b]$ with $b\neq 1$, will have its hidden boundary glued to that of a compensating surface $[\hat{a};1/b]$ with inverse slant factor. This will be especially relevant when we build general one-loop diagrams in section 6. There we construct compensating slanted wedges $[a;e^{s_{\rm eff}}]$ and $[\hat{a};e^{-s_{\rm eff}}]$ which can then be mapped to the annulus. For tree diagrams the situation is simpler: the total surface representing the diagram is always of the form $[a;1]$, with horizontal identifications applied to the vertical edges.

4.3 Keeping track of insertions on slanted wedges

The open string moduli are encoded in the positions of punctures on the corresponding Riemann surfaces. As we will use slanted wedges to describe these surfaces, we need to keep track of operator insertions on slanted wedges. We denote by

$$[\,a;b\,|x_1,x_2,\ldots,x_k\,]\,,\quad \text{with}\quad \frac{1}{2}\le x_1\le x_2\le\ldots\le x_k\le\frac{1}{2}+a\,, \tag{4.25}$$

a slanted wedge with marked points at real coordinates x_i. The wedge is presented, as usual, with its left boundary above $z=\frac{1}{2}$. When star multiplying two slanted wedges, the position x of a marked point on the first slanted wedge is unaffected:

$$[\,a;b\,|x\,]*[\,a';b'\,] = [a+ba';bb'\,|\,x\,]\,. \tag{4.26}$$

A puncture at x' on the second wedge, on the other hand, is displaced and experiences scaling:

$$[\,a;b\,]*[\,a';b'\,|x'\,] = [a+ba';bb'\,|\,\tfrac{1}{2}+a+b\Big(x'-\tfrac{1}{2}\Big)\,]\,. \tag{4.27}$$

From this one can readily verify that

$$\begin{aligned}
e^{-sL_L}[\,a;b\,|x\,] &= [\;\ldots\,;\ldots\;|\;1-e^{-s}+e^{-s}x\,]\,,\\
e^{-sL_R}[\,a;b\,|x\,] &= [\;\ldots\,;\ldots\;|\;x\,]\,,\\
e^{-s^\star L^\star_L}[\,a;b\,|x\,] &= [\;\ldots\,;\ldots\;|\;e^{s^\star}x\,]\,,\\
e^{-s^\star L^\star_R}[\,a;b\,|x\,] &= [\;\ldots\,;\ldots\;|\;x\,]\,.
\end{aligned} \tag{4.28}$$

We put dots $\ldots$ on the width and slant parameters of the resulting wedges because these values are unaffected by the punctures and were given earlier. Note that the exponentials of right operators do not affect the position since they add a slanted wedge from the right. It follows from the above relations that

$$e^{-sL}\,e^{-s^\star L^\star}\,[\,a;b\,|x\,] = [\;\ldots\,;\ldots\;|\;1-e^{-s}+e^{s^\star-s}x\,]\,. \tag{4.29}$$

This formula generalizes easily to the case of additional punctures: all $x_i\to 1-e^{-s}+e^{s^\star-s}x_i$.

4.4 Representation of the L, $L^\star$ algebra on slanted wedges

It is known that one can view $L, L^\star, L^+ = L + L^\star$ as well as L^+_L and L^+_R as differential operators acting on the familiar wedge states. As we have learned, the left and right parts of L and $L^\star$ only act naturally on slanted wedges (acting on an ordinary wedge they will give a slanted wedge). In this section we represent $L_L, L_R, L^\star_L$ and $L^\star_R$, as differential operators on slanted wedges. This provides some further insight into slanted wedges, a check of this formalism and, as a by product, a tool to derive (or rederive) some identities.

Let us focus on the right part of the L and $L^\star$ operators. From (4.11) and (4.17) we have

$$\begin{aligned} L_R[a;b] &= -\frac{d}{ds}\Big|_{s=0} e^{-sL_R}\ [a;b] = \Big(-\frac{1}{2}b\partial_a - b\partial_b\Big)[a;b]\,, \\ L^\star_R[a;b] &= -\frac{d}{ds^\star}\Big|_{s^\star=0} e^{-s^\star L^\star_R}[a;b] = \Big(-\frac{1}{2}b\partial_a + b\partial_b\Big)[a;b]\,, \end{aligned} \tag{4.30}$$

and we identify the representation

$$L_R = -\frac{1}{2}b\partial_a - b\partial_b\,, \qquad L^\star_R = -\frac{1}{2}b\partial_a + b\partial_b\,. \tag{4.31}$$

For the left counterparts a similar calculation gives

$$L_L = (a - \frac{1}{2})\partial_a + b\partial_b\,, \qquad L^\star_L = -\Big(a + \frac{1}{2}\Big)\partial_a - b\partial_b\,. \tag{4.32}$$

One can readily confirm that acting on slanted wedges the operators L_R and L_L commute, and so do $L^\star_R$ and $L^\star_L$. One can now recover the more familiar differential operators

$$L = -\Big(\frac{1}{2}(1+b) - a\Big)\partial_a\,, \quad L^\star = -\Big(\frac{1}{2}(1+b) + a\Big)\partial_a\,, \quad L^+ = L + L^\star = -(1+b)\partial_a\,. \tag{4.33}$$

It is now possible to calculate the commutator $[L, L^\star]$ by imagining it acting on a wedge state,

$$[L, L^\star] = [-\Big(\tfrac{1}{2}(1+b) + a\Big)\partial_a\,, -\Big(\tfrac{1}{2}(1+b) - a\Big)\partial_a] = -(1+b)\partial_a = L^+\,, \tag{4.34}$$

which is the expected result. In fact, even the right parts of $L, L^\star$, and L^+ obey the same equation, as one would expect,

$$[L_R, L^\star_R] = \big[-\tfrac{1}{2}b\partial_a + b\partial_b\,, -\tfrac{1}{2}b\partial_a - b\partial_b\big] = -b\partial_a = L^+_R\,. \tag{4.35}$$

Let us illustrate how one derives identities using the above representation of operators. Note first that

$$L^+_R \equiv L_R + L^\star_R = -b\partial_a\,. \tag{4.36}$$

It then follows that

$$e^{-s^+ L^+_R}[a;b] = [a + bs^+; b] = [a;b] * [s^+; 1]\,, \tag{4.37}$$

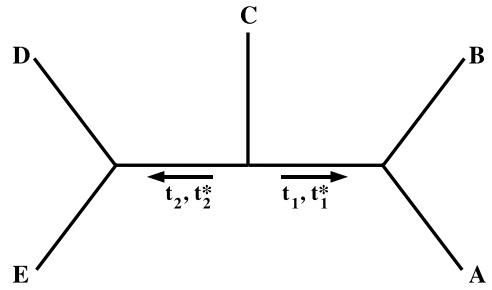

(a)

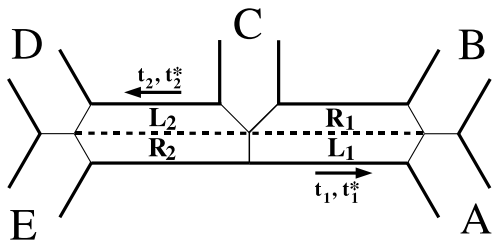

(b)

Figure 12: (a) A Feynman diagram for a five-point amplitude. (b) The topology of the corresponding Riemann surface.

showing that $e^{-s^+ L_R^+}$ acts by right multiplying a wedge of length s^+. Additionally, for wedge states $[a;1]$ of width a we have

$$-L_R^+[a;1] = \partial_a[a;1]\,, \qquad [a;1] = e^{-aL_R^+}\,[0;1]\,, \tag{4.38}$$

where the zero-length wedge $[0;1]$ is the identity state $|\mathcal{I}\rangle$. Another example uses (4.22) and (4.37):

$$e^{-tL_R}e^{-tL_R^\star}\,[a;b] = [a;b] * [1-e^{-t}\,;\,1] = e^{-(1-e^{-t})L_R^+}\,[a;b]\,, \tag{4.39}$$

leading us to conclude that $e^{-tL_R}e^{-tL_R^\star} = e^{-(1-e^{-t})L_R^+}$.

5. Riemann surfaces for tree-level diagrams

In this section we will use the technology of slanted wedges developed in the previous section to construct the punctured disks associated with tree diagrams. We start with the particularly simple case of a diagram with five external lines. We then sketch the construction for arbitrary tree-level diagrams.

5.1 The five-point diagram

Let us use the formalism of section 4 to construct the surface corresponding to the tree-level five-point diagram shown in figure 12. Our goal is to determine the relative angles of

the operator insertions on the unit disk. These are the open string moduli. There are, of course, no closed string moduli. All other diagrams contributing to the five point function are permutations of the external states in the diagram of figure 12.

The diagram contains two internal propagators, parameterized by the Schwinger parameters $t_i, t_i^\star$ with $i = 1, 2$. Here and in the following we use the letter t for Schwinger parameters of propagators in tree diagrams (or subtrees of loop diagrams). As this is a tree-level diagram, the classical propagator (4.10) must be used on both lines. We use arrows to assign a direction to each propagator line in the diagram. At fixed Schwinger parameters the classical propagator on the i-th line acts as the operator $e^{-t_i L} BQB^\star e^{-t_i^\star L^\star}$ in the indicated direction, i.e. on the state representing the surface in the direction of the arrow. Equivalently, it acts as the BPZ conjugate operator $e^{-t_i^\star L} BQB^\star e^{-t_i L^\star}$ in the direction opposite to the arrow. Since the full propagator is BPZ invariant, amplitudes do not depend on this assignment after integration over Schwinger parameters. The selection of specific arrows is simply a convention that fixes which Schwinger parameter we call t_i and which one we call $t_i^\star$.

Let us consider the part of the diagram consisting of the first propagator (t_1,$t_1^\star$) and the Fock space states $|F_A\rangle$, $|F_B\rangle$. Each Fock space state is of the form $[1;1|1]$. Together, and acted by the propagator, they form the twice-punctured surface state

$$\begin{aligned}
[a_1;1\,|\,x_A,x_B] &\equiv e^{-t_1 L} e^{-t_1^\star L^\star} \big([1;1|1]_A * [1;1\,|1]_B\big) \\
&= e^{-t_1 L} e^{-t_1^\star L^\star}\, [2;1|1,2] \\
&= [1-2e^{-t_1}+3e^{t_1^\star - t_1};1\,|\,x_A,x_B]\ , \\
\text{with}\qquad x_A &= 1-e^{-t_1}+e^{t_1^\star-t_1} \\
x_B &= 1-e^{-t_1}+2e^{t_1^\star-t_1}\,,
\end{aligned} \tag{5.1}$$

where we used (4.24) to calculate the wedge parameters and (4.29) to calculate the positions x_A and x_B of the punctures on the resulting wedge. Similarly, we can analyze the part of the diagram with the second propagator (t_2,$t_2^\star$) and the Fock space states $|F_D\rangle$, $|F_E\rangle$. They form the surface state

$$[a_2;1\,|\,x_D,x_E] \equiv e^{-t_2 L} e^{-t_2^\star L^\star} \big([1;1|1]_D * [1;1|1]_E\big) = [1-2e^{-t_2}+3e^{t_2^\star-t_2};1|x_D,x_E\,]\,, \tag{5.2}$$

with the operator insertions corresponding to $|F_D\rangle$ and $|F_E\rangle$ located at

$$\begin{aligned}
x_D &= 1-e^{-t_2}+e^{t_2^\star-t_2}\,, \\
x_E &= 1-e^{-t_2}+2e^{t_2^\star-t_2}\,.
\end{aligned} \tag{5.3}$$

To assemble the Riemann surface corresponding to the five-point diagram we glue the surfaces $[a_1;1|x_A,x_B]$, $[1;1|1]_C$ (corresponding to $|F_C\rangle$) and $[a_2;1|x_D,x_E]$. We obtain the surface Σ given by

$$\begin{aligned}
\Sigma &\equiv [a_1;1|x_A,x_B] * [1;1|1]_C * [a_2;1|\,x_D,x_E] \\
&= [a_1+a_2+1;1|\,x_A,\ x_B,\ a_1+1,\ a_1+1+x_D,\ a_1+1+x_E]\,.
\end{aligned} \tag{5.4}$$

In particular, we notice that the wedge Σ is not slanted. The two vertical boundaries of Σ are thus identified horizontally and the resulting surface is mapped to the unit disk η via

$$\eta = \exp\left(\frac{2\pi i z}{a}\right), \quad a = a_1 + a_2 + 1\,. \tag{5.5}$$

A horizontal distance Δx along the boundary of Σ translates into an angular separation $\Delta\phi$ on the unit disk given by

$$\frac{\Delta\phi}{2\pi} = \frac{\Delta x}{a}\,. \tag{5.6}$$

For the relative angles of the operator insertions on the boundary of the unit disk we thus obtain

$$\begin{aligned}
\frac{\phi_B - \phi_A}{2\pi} &= \frac{x_B - x_A}{a} &&= \frac{e^{t_1^\star - t_1}}{3 - 2e^{-t_1} - 2e^{-t_2} + 3e^{t_1^\star - t_1} + 3e^{t_2^\star - t_2}}\,,\\
\frac{\phi_C - \phi_A}{2\pi} &= \frac{a_1 + 1 - x_A}{a} &&= \frac{1 - e^{-t_1} + 2e^{t_1^\star - t_1}}{3 - 2e^{-t_1} - 2e^{-t_2} + 3e^{t_1^\star - t_1} + 3e^{t_2^\star - t_2}}\,,\\
\frac{\phi_D - \phi_A}{2\pi} &= \frac{a_1 + 1 + x_D - x_A}{a} &&= \frac{2 - e^{-t_1} + 2e^{t_1^\star - t_1} - e^{-t_2} + e^{t_2^\star - t_2}}{3 - 2e^{-t_1} - 2e^{-t_2} + 3e^{t_1^\star - t_1} + 3e^{t_2^\star - t_2}}\,,\\
\frac{\phi_E - \phi_A}{2\pi} &= \frac{a_1 + 1 + x_E - x_A}{a} &&= \frac{2 - e^{-t_1} + 2e^{t_1^\star - t_1} - e^{-t_2} + 2e^{t_2^\star - t_2}}{3 - 2e^{-t_1} - 2e^{-t_2} + 3e^{t_1^\star - t_1} + 3e^{t_2^\star - t_2}}\,.
\end{aligned} \tag{5.7}$$

This concludes the computation of angles for the string diagram in figure 12. Of course, the positions of three of the punctures can be fixed arbitrarily, so there are just two open string moduli. As usual for amplitudes in non BPZ-invariant gauges, we have twice as many Schwinger parameters as moduli of the corresponding Riemann surface. Indeed, we have four Schwinger parameters (t_1, $t_1^\star$, t_2, $t_2^\star$). This is not a problem because each of the two propagators is accompanied by a BRST operator Q. In [32, 31], the classical propagator (4.10) was rewritten as

$$\mathcal{P} = \frac{B}{L} + \text{ other terms }\,, \tag{5.8}$$

and it turned out that the B/L term by itself covered the moduli space of on-shell amplitudes for the four-point function. All other terms only contributed off-shell.

It is therefore interesting to ask if there is an assignment of B/L and $B^\star/L^\star$ to the propagator lines in the five-point diagram which produces all the requisite open string degenerations: as a Schwinger parameter becomes large the associated line produces the degeneration represented by a long strip. That degeneration, moreover, must occur independent of the values of the other Schwinger parameters, even if they also go to infinity. Not every assignment works. If we assign $B^\star/L^\star$ to *both* propagators (namely, $t_1 = t_2 = 0$) making one Schwinger parameter large is not sufficient to guarantee an open string degeneration. In fact, for $t_1^\star = t_2^\star \to \infty$ the angles of the five insertions on the unit circle spread out over the circle, a configuration that is clearly not degenerate. This is not too surprising. If we had regarded the left propagator as acting to the right, we would have encountered the operator combination $e^{-t_2^\star L_L} e^{-t_1^\star L_L^\star}$ acting on the Fock space state $|F_A\rangle$.

JHEP07(2008)063

This product of operators has been noticed to produce interesting subtleties in [32]. Although both Schwinger parameters in the operator diverge, the resulting Riemann surface is perfectly regular. Indeed, acting on any slanted wedge we have from (4.22):

$$\begin{aligned}\lim_{t_1^\star=t_2^\star\to\infty} e^{-t_2^\star L_L} e^{-t_1^\star L_L^\star}[a;b] &= \lim_{t_1^\star=t_2^\star\to\infty} [\tfrac{1}{2}+\tfrac{1}{2}e^{t_1^\star-t_2^\star}-e^{-t_2^\star}\,;e^{t_1^\star-t_2^\star}]*[a;b] = [1;1]*[a;b] \\ &= [a+1;b]\,.\end{aligned} \tag{5.9}$$

In this limit the operator simply inserts the unit wedge $[1;1]$. This is a surface of finite width and finite rescaling and cannot induce an open string degeneration in any diagram. For all other choices of assignments of B/L and $B^\star/L^\star$ to the two propagator lines, open string degenerations are always produced when we make any Schwinger parameter large. Details of this analysis are given in appendix A.

5.2 General tree diagrams

The construction of the surface for the five-string diagram was particularly simple. For general tree-level diagrams we need to be more systematic. As we did for the five-string diagram we assign an arrow to each propagator, indicating the direction in which it acts. This assignment is arbitrary and will not affect the total set of surfaces created as the Schwinger parameters vary over their full range because the propagator is BPZ-invariant.

We now rewrite the five-string diagram in a way that makes the case for the general rules to be stated below. Let us revisit the surface considered in (5.1):

$$e^{-t_1 L} e^{-t_1^\star L^\star}\big([1;1|1]_A * [1;1\,|1]_B\big) = e^{-t_1 L_L} e^{-t_1^\star L_L^\star} e^{-t_1 L_R} e^{-t_1^\star L_R^\star}\big([1;1|1]_A * [1;1\,|1]_B\big)\,. \tag{5.10}$$

Recalling (4.22), we then find

$$\begin{aligned}&e^{-t_1 L} e^{-t_1^\star L^\star}\big([1;1|1]_A * [1;1\,|1]_B\big) \\ &\quad = [\tfrac{1}{2}(1+e^{t_1^\star-t_1})-e^{-t_1}\,;e^{t_1^\star-t_1}]*[1;1|1]_A*[1;1\,|1]_B*[\tfrac{1}{2}(1+e^{t_1-t_1^\star})-e^{-t_1^\star}\,;e^{t_1-t_1^\star}] \\ &\quad = L_1 * [1;1|1]_A * [1;1\,|1]_B * R_1\,,\end{aligned} \tag{5.11}$$

where we have defined the slanted wedges L_i and R_i associated with the left and right part of the i-th propagator:

$$L_i \equiv [\tfrac{1}{2}(1+e^{t_i^\star-t_i})-e^{-t_i}\,;e^{t_i^\star-t_i}]\,, \qquad R_i \equiv [\tfrac{1}{2}(1+e^{t_i-t_i^\star})-e^{-t_i^\star}\,;e^{t_i-t_i^\star}]\,. \tag{5.12}$$

It is now clear that (5.2) becomes:

$$e^{-t_2 L} e^{-t_2^\star L^\star}\big([1;1|1]_D * [1;1|1]_E\big) = L_2 * [1;1|1]_D * [1;1\,|1]_E * R_2\,. \tag{5.13}$$

Assembling now the full surface Σ as in (5.4) we have

$$\Sigma = L_1 * [1;1|1]_A * [1;1\,|1]_B * R_1 * [1;1|1]_C * L_2 * [1;1|1]_D * [1;1\,|1]_E * R_2\,. \tag{5.14}$$

JHEP07(2008)063

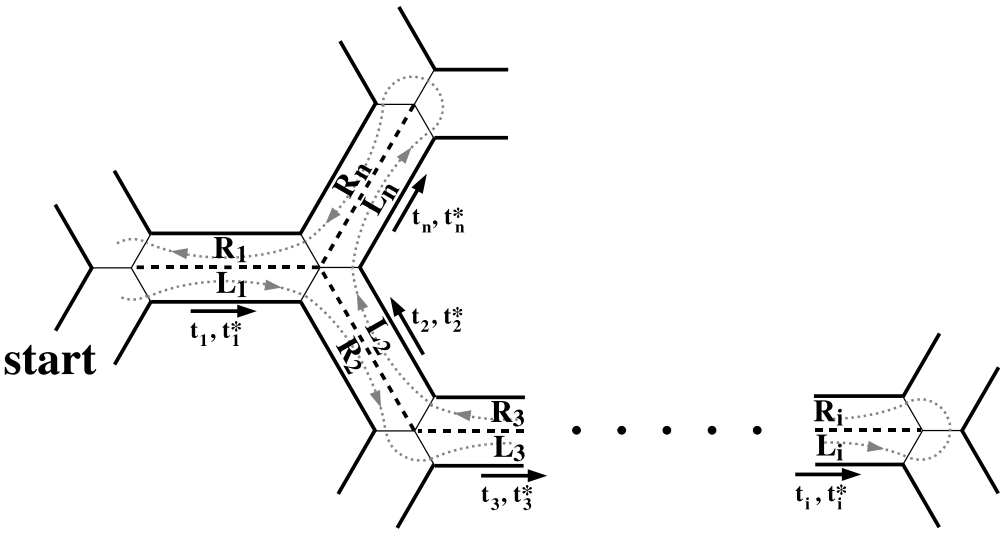

Figure 13: The surface Σ for general tree diagrams is built by tracing the grey dotted line counterclockwise around the diagram, starting at an arbitrary external state. When tracing along the i-th propagator one picks up either the slanted wedge corresponding to the left part (L_i) or right part (R_i) of the propagator. This depends on the direction of the propagator (black arrows).

Note that Σ is a wedge of unit slant factor (an ordinary wedge) because the slant factors of L_i and R_i are multiplicative inverses of each other. Since the right and left edges of Σ are to be identified, we can slide part of the wedge state from left to right, cyclically. We write, for convenience,

$$\Sigma = [1;1|1]_A * [1;1\,|1]_B * R_1 * [1;1|1]_C * L_2 * [1;1|1]_D * [1;1\,|1]_E * R_2 * L_1\,. \tag{5.15}$$

The rule for building the surface Σ for general tree diagrams is now clear: *Begin at some external state and trace around the diagram in the counterclockwise direction. For each external state add the factor* $[1;1|1]$. *For each line i traversed against the propagator arrow add a factor R_i. For each line i traversed along the propagator arrow add a factor L_i. All factors are added from the right.* The formula in (5.15) results from the application of this rule to the diagram in figure 12, starting at the external state $|F_A\rangle$. Note that the rules build the surface using half strings. If we are tracing in the direction of the arrow on the i line, we multiply by the surface L_i because the propagator acts from the left on the surface to be built. If we are tracing against the arrow of the propagator, we multiply by the surface R_i because, in this case, the propagator acts from the right on the surface we have already built.

For the more complicated diagram in figure 13 the rules are still simple to follow. Although it is redundant information, the labels L_i and R_i in figure 13 represent the factors that must be included, as a result of the chosen assignment of arrows, when we follow the grey dotted curve along the diagram. We have,

JHEP07(2008)063

$$\begin{aligned}\Sigma = [1;1|1] * L_1 * R_2 * [1;1|1] * L_3 * \ldots * L_i * [2;1|1,2] * R_i * \ldots \\ \ldots * R_3 * L_2 * L_n * [2;1|1,2] * R_n * R_1 * [1;1|1]\,.\end{aligned} \tag{5.16}$$

The resulting surface is of unit slant (for each L_i there is an R_i) and takes the form

$$\Sigma = [a;1\,|\,x_1, x_2, \ldots x_k\,]\,, \tag{5.17}$$

for some calculable width a and some calculable positions x_i. The left and right boundaries of Σ are identified through translation by a. We can therefore map the glued Σ surface to a unit disk using $\eta = \exp(2\pi i z/a)$. To determine the moduli of the surface, we only need to know the angular separation between operator insertions on the unit circle. If insertions are separated by Δx on Σ, their relative angle $\Delta\phi$ on the unit circle is simply given by

$$\frac{\Delta\phi}{2\pi} = \frac{\Delta x}{a}\,. \tag{5.18}$$

This concludes our discussion of Riemann surfaces for general tree-level diagrams.

6. Riemann surfaces for general one-loop diagrams

In section 3 we built the surface corresponding to the tadpole diagram in Schnabl gauge using the simplified propagator B/L (i.e. $s^\star = 0$). Using the z frame we built separately the parts of the surface that contain the inner and outer boundary components of the annulus, as displayed in figure 7(b). Let us now review this construction using the algebra of slanted wedges.

On the outer boundary (the right strip in the z frame) there is a Fock space state $[1;1|1]$. It is acted by the right part e^{-sL_R} of the propagator so we get a slanted wedge Σ given by

$$\Sigma = e^{-sL_R}[1;1|1] = [\tfrac{1}{2}(1+e^s); e^s|1\,]\,, \tag{6.1}$$

where we made use of (4.11) and (4.28). On the inner boundary there is only the remaining left part e^{-sL_L} of the propagator so the resulting slanted wedge $\widehat{\Sigma}$ is just

$$\widehat{\Sigma} \equiv [\tfrac{1}{2}(1-e^{-s}); e^{-s}]\,, \tag{6.2}$$

making use of (4.12). The slanted wedges Σ and $\widehat{\Sigma}$ are glued to each other at their hidden boundaries at $i\infty$, as discussed in section 3 using λ-regularization.

We need to place the surfaces Σ and $\widehat{\Sigma}$ in the z-plane in such a way that: (i) their hidden boundaries at $i\infty$ glue correctly, and (ii) the slanted identifications become translations in the w frame ($z = -\frac{1}{2}e^{-w}$). We refer to the result as the natural w-picture. For the identifications on Σ to be simple translations in the w frame, we shift Σ horizontally, so that the position of its right boundary is a rescaling by e^s of its left boundary. The translation is uniquely determined and Σ lands between the vertical lines given in (3.12). Similarly, we need to shift the position of $\widehat{\Sigma}$ in such a way that the position of its right boundary is a rescaling by e^{-s} of its left boundary. As $e^{-s} < 1$, this implies that we need to position $\widehat{\Sigma}$ in the region $\Re(z) < 0$. In fact, we readily see that $\widehat{\Sigma}$ must be placed as the region between $\Re(z) = -\frac{1}{2}$ and $\Re(z) = -\frac{1}{2}e^{-s}$.

But we are not done yet. The boundaries at $i\infty$ now do *not* glue correctly. By the definition of slanted wedges, the parameterizations of the left boundaries of Σ and $\widehat{\Sigma}$ match — indeed, they both have unit scaling factor. But for the hidden boundaries at $i\infty$ to glue nicely in the w frame, the parameterizations of the left boundary of Σ needs to match the parametrization of the *right* boundary of $\widehat{\Sigma}$.[4] We can achieve this simply by rescaling the shifted $\widehat{\Sigma}$ by e^s. Then $\widehat{\Sigma}$ is positioned between $\Re(z) = -\frac{1}{2}e^s$ and $\Re(z) = -\frac{1}{2}$. This is precisely the configuration of surfaces that we ended up with and fully justified in section 3.

The above steps can easily be generalized to one-loop diagrams of arbitrary complexity. We will now show how this is done. A detailed justification of the procedure is given in section 8, where we discuss the λ-regulation explicitly.

6.1 The natural w-picture

For a one-loop diagram, we construct two complementary surfaces

$$\Sigma \equiv [a; e^{s_{\rm eff}} \,|\, \vec{x}\,] \quad \text{and} \quad \widehat{\Sigma} \equiv [\hat{a}; e^{-s_{\rm eff}} \,|\, \vec{\hat{x}}\,], \tag{6.3}$$

where $\vec{x}$ and $\vec{\hat{x}}$ collectively represent the positions of all punctures on Σ and $\widehat{\Sigma}$, respectively. These surfaces are said to be complementary because their scaling factors multiply to one. On each surface, the left and the right boundaries are identified, and the two surfaces are glued to each other at their hidden boundaries at $i\infty$.

The *natural w picture* is one in which the hidden boundaries of Σ and $\widehat{\Sigma}$ glue nicely and the identifications on Σ and $\widehat{\Sigma}$ are horizontal translations by $s_{\rm eff}$. To obtain this picture we need to place the surfaces Σ and $\widehat{\Sigma}$ correctly in the z frame. First, we shift the surfaces Σ and $\widehat{\Sigma}$ by real constants a_0 and $\hat{a}_0$, respectively, so that the position of their right boundaries is a rescaling of the left boundaries by $e^{s_{\rm eff}}$ and $e^{-s_{\rm eff}}$, respectively. Recall that by definition all slanted wedges start out with their left boundary at $\Re(z) = \frac{1}{2}$. The required shifts are thus determined by the relations

$$e^{s_{\rm eff}} = \frac{a_0 + a + \frac{1}{2}}{a_0 + \frac{1}{2}}\,, \qquad e^{-s_{\rm eff}} = \frac{\hat{a}_0 + \hat{a} + \frac{1}{2}}{\hat{a}_0 + \frac{1}{2}}\,. \tag{6.4}$$

Thus

$$a_0 = \frac{a}{e^{s_{\rm eff}} - 1} - \frac{1}{2}\,, \qquad \hat{a}_0 = -\frac{\hat{a}}{1 - e^{-s_{\rm eff}}} - \frac{1}{2}\,. \tag{6.5}$$

This shift places the surface Σ at

$$\text{Final } \Sigma \text{ region:} \quad a_0 + \frac{1}{2} \le \Re(z) \le e^{s_{\rm eff}} \left(a_0 + \frac{1}{2}\right). \tag{6.6}$$

As we discussed for the tadpole example above, we then rescale $\widehat{\Sigma}$ by a factor of $e^{s_{\rm eff}}$ so that it has the canonical parametrization on its *right* boundary. With this scaling $\widehat{\Sigma}$ ends up in the location

$$\text{Final } \widehat{\Sigma} \text{ region:} \quad e^{s_{\rm eff}} \left(\hat{a}_0 + \frac{1}{2}\right) \le \Re(z) \le \hat{a}_0 + \frac{1}{2}\,. \tag{6.7}$$

[4]This requirement will lead to the established result for this diagram, but will be justified in more generality using λ-regularization in section 8.3.

After positioning Σ and $\widehat{\Sigma}$ in this way we map to the w frame via (2.9) and to the annulus frame ζ via

$$\zeta = e^{-\frac{2\pi i}{s_{\rm eff}}(w-i\pi)}\,. \tag{6.8}$$

The modulus M of the annulus was defined in (2.32). We can read it off from (6.8) as

$$M = \frac{\pi}{|s_{\rm eff}|}\,. \tag{6.9}$$

A point x on Σ with $\frac{1}{2} \le x \le \frac{1}{2} + a$ is located at $z = x + a_0$ in the shifted Σ region (6.6). Using (2.31), we see that it ends on a boundary of the annulus at an angle

$$\phi = \frac{2\pi}{s_{\rm eff}} \ln(2|a_0 + x|) = \frac{2\pi}{s_{\rm eff}} \ln\Big(2\Big|x - \frac{1}{2} + \frac{a}{e^{s_{\rm eff}} - 1}\Big|\Big)\,. \tag{6.10}$$

Similarly, any point $\hat{x}$ on $\widehat{\Sigma}$ is located at $z = e^{s_{\rm eff}}(\hat{x} + \hat{a}_0)$ in the final $\widehat{\Sigma}$ region (6.7) and lands at an angle

$$\hat{\phi} = \frac{2\pi}{s_{\rm eff}} \ln(2e^{s_{\rm eff}}|\hat{x} + \hat{a}_0|) = \frac{2\pi}{s_{\rm eff}} \ln\Big(2\Big|\frac{1}{2} - \hat{x} + \frac{\hat{a}}{1 - e^{-s_{\rm eff}}}\Big|\Big)\,. \tag{6.11}$$

All points in $\vec{x}$ land on the same boundary component and all points in $\vec{\hat{x}}$ land on the other boundary component. With the maps written here, if $s_{\rm eff} > 0$ the points in $\vec{x}$ lie on the outer component and if $s_{\rm eff} < 0$ they lie on the inner component. Of course, there is no invariant distinction between these components as they can be exchanged by a conformal map.

6.2 General one-loop diagrams

Let us now build the complementary surfaces Σ and $\widehat{\Sigma}$ in (6.3) for a general one-loop diagram. Let n be the number of propagators running in the loop. It follows that there are also n vertices within the loop. These vertices will be labeled 1 to n as we move counterclockwise in the loop (see figure 14(a)). Two lines of each cubic vertex in the loop connect to loop propagators. The remaining line can lead to a single external state or to a subtree diagram with a set of external states. In either case, the additional external state(s) at this vertex are all on one specific boundary of the annulus. We let Σ represent the part of the diagram which is drawn on the outer side of the loop and $\widehat{\Sigma}$ represent the part of the diagram on the inside of the loop. Eventually, we will glue the surfaces Σ and $\widehat{\Sigma}$ along their hidden boundaries, shown as dashed lines in figure 14(b). In section 6.1 we have learned how to perform this gluing.

If the external states at the i-th vertex are on the Σ-side of the annulus, they add to Σ a surface

$$[a_i; 1\,|\,\vec{y_i}\,] = [a_i; 1\,|\,y_i^1, \ldots, y_i^{m_i}\,] \quad \text{with } a_i > 0\,, \tag{6.12}$$

where the y_i^α are the positions of the punctures and $\alpha = 1, \ldots m_i$ is an index that enumerates them. If only a Fock space state is connected to vertex i, the surface in (6.12) is $[1; 1|1]$. As shown in figure 14(a), the surface in (6.12) can in general represent a complicated subtree diagram. The slant factor is one because the subdiagram is a tree. As the

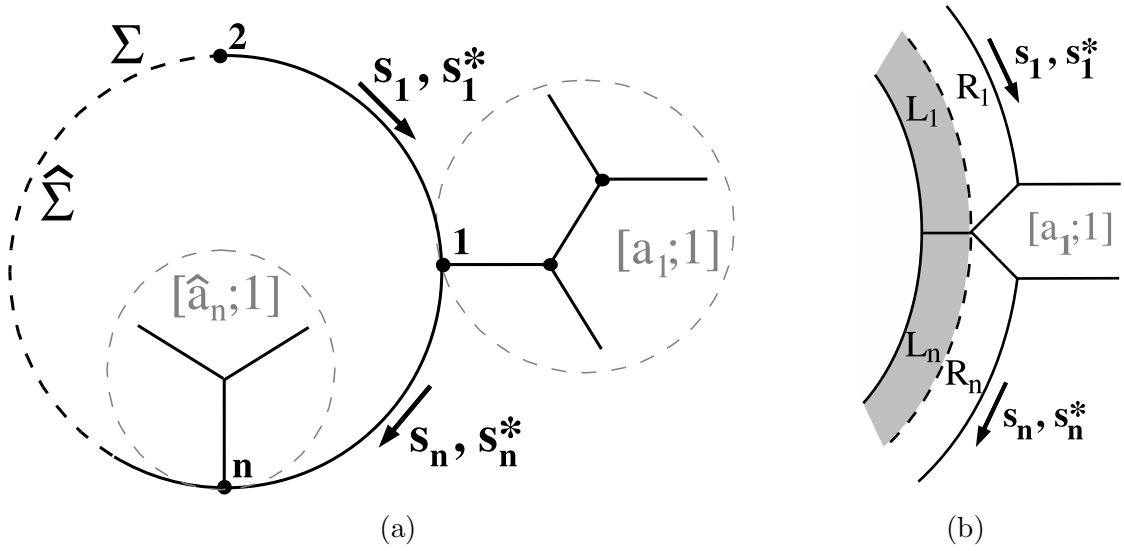

Figure 14: (a) A general one-loop diagram with n vertices and n propagators in the loop. At each vertex the external states can either contribute to Σ or $\widehat{\Sigma}$ and thus end up on either boundary of the annulus. (b) The topology of the surfaces at vertex one. The right part R_i of the i-th propagator contributes to Σ. The left part L_i of the i-th propagator (shaded) contributes to $\widehat{\Sigma}$. Σ and $\widehat{\Sigma}$ are glued along the hidden boundaries represented by the dashed lines.

external states of the i-th vertex are on the Σ-side of the diagram, they do not affect the $\widehat{\Sigma}$-side. In order to treat both Σ and $\widehat{\Sigma}$ symmetrically, we also insert a surface on $\widehat{\Sigma}$, the trivial "identity surface"

$$[\hat{a}_i; 1] = [0; 1]\,. \tag{6.13}$$

If, on the other hand, the external states are on the boundary corresponding to $\widehat{\Sigma}$, we have a surface insertion

$$[\hat{a}_i; 1\,|\,\vec{\hat{y}}_i\,] = [\hat{a}_i; 1\,|\,\hat{y}_i^1, \ldots, \hat{y}_i^{\hat{m}_i}\,] \quad \text{with } \hat{a}_i > 0 \tag{6.14}$$

on $\widehat{\Sigma}$ accompanied by a trivial insertion $[a_i; 1] = [0; 1]$ on the Σ side. Thus the n vertices in the loop are described by $2n$ wedges, only n of which are non-trivial.

The propagators in the loop are in general complicated, because their geometric action depends on the ghost number of the state that they act on [34]. Since states of all ghost numbers circulate in the loop we cannot use the classical propagator (4.10). We choose the alternating gauge introduced in [34] for the FP gauge fixing procedure of Schnabl gauge. This yields the propagator

$$\mathcal{P} = \mathcal{P}_+\,\Pi_+ + \mathcal{P}_-\,\Pi_-\,, \tag{6.15}$$

where Π_+ (Π_-) is the projector on even (odd) ghost number, and $\mathcal{P}_\pm$, for the i-th propagator, are defined by

$$\mathcal{P}_+ = \int ds_i ds_i^\star\, e^{-s_i L}\, B\, Q\, B^\star e^{-s_i^\star L^\star}\,, \qquad \mathcal{P}_- = \int ds_i ds_i^\star\, e^{-s_i^\star L^\star}\, B^\star\, Q\, B e^{-s_i L}\,. \tag{6.16}$$

JHEP07(2008)063

The classical propagator is $\mathcal{P}_+$ since it acts on ghost number two sources to give ghost number one classical states. With external physical states of ghost number one, all non-trivial surface insertions at the loop insert states of ghost number one. Since the three string vertex couples states whose ghost numbers add up to three, the states on the two loop-propagators that attach to the vertex must both have either even or odd ghost number. Consequently the states running over *all* the propagators in the loop are either of even ghost number or odd ghost number. It follows that in alternating gauge we only need to consider two types of Riemann surfaces for every diagram at one loop level. The first surface is constructed by including a projector onto states of even ghost number anywhere in the loop and using $\mathcal{P}_+$ for all lines in the loop. The second surface is constructed with a projector onto odd ghost numbers in the loop and using $\mathcal{P}_-$ for all lines in the loop.

As mentioned before, the final set of surfaces is independent of the chosen direction on the propagator on each line. For simplicity, however, we orient all propagators in the loop clockwise. Tracing the outer loop counterclockwise, the right part of the propagator contributes to the surface Σ on each line. The inner loop must be traced clockwise so the left part of the propagator contributes to the surface $\widehat{\Sigma}$ on each line. This has been illustrated in figure 14(b).

At fixed Schwinger parameters, the right part of $\mathcal{P}_+$ adds to Σ the slanted wedge corresponding to the operator $e^{-s_i L_R} e^{-s_i^\star L_R^\star}$, which is calculated in (4.22). The right part of $\mathcal{P}_-$, on the other hand, adds the slanted wedge corresponding to $e^{-s_i^\star L_R^\star} e^{-s_i L_R}$ to Σ, which is calculated using (4.11) and (4.17). We conclude that the i-th propagator contributes to Σ the slanted wedge R_i given by

$$R_i \equiv [r_i; e^{s_i - s_i^\star}] \quad \text{with} \quad \begin{cases} r_i = \frac{1}{2}(1 + e^{s_i - s_i^\star}) - e^{-s_i^\star} & \text{for even ghost number } (\mathcal{P}_+) \\ \\ r_i = e^{s_i} - \frac{1}{2}(1 + e^{s_i - s_i^\star}) & \text{for odd ghost number } (\mathcal{P}_-)\,. \end{cases} \tag{6.17}$$

Similarly, the left part of the propagator contributes to $\widehat{\Sigma}$ the slanted wedge L_i given by $e^{-s_i L_L} e^{-s_i^\star L_L^\star}$ for $\mathcal{P}_+$ and $e^{-s_i^\star L_L^\star} e^{-s_i L_L}$ for $\mathcal{P}_-$. We readily find

$$L_i \equiv [l_i; e^{s_i^\star - s_i}] \quad \text{with} \quad \begin{cases} l_i = \frac{1}{2}(1 + e^{s_i^\star - s_i}) - e^{-s_i} & \text{for even ghost number } (\mathcal{P}_+) \\ \\ l_i = e^{s_i^\star} - \frac{1}{2}(1 + e^{s_i^\star - s_i}) & \text{for odd ghost number } (\mathcal{P}_-)\,. \end{cases} \tag{6.18}$$

The definitions (6.17) and (6.18) generalize (5.12) from the classical propagators of tree diagrams to loop propagators in alternating gauge.

We now assemble the complete surfaces Σ and $\widehat{\Sigma}$. We construct Σ by gluing the surfaces of propagators and external states counterclockwise, starting at vertex 1. We obtain

$$\Sigma \equiv [a; e^{s_{\rm eff}} |\vec{x}\,] = [a_1; 1|\vec{y}_1] * R_1 * \cdots * [a_n; 1|\vec{y}_n] * R_n\,, \tag{6.19}$$

Similarly, we construct $\widehat{\Sigma}$ by gluing the surfaces of propagators and external states. We trace clockwise starting right below vertex 1 and get

$$\widehat{\Sigma} \equiv [\hat{a}; e^{-s_{\rm eff}} |\,\vec{\hat{x}}\,] = L_n * [\hat{a}_n; 1|\,\vec{\hat{y}}_n\,] * \cdots * L_1 * [\hat{a}_1; 1|\,\vec{\hat{y}}_1\,]\,. \tag{6.20}$$

It is clear from (6.19) and (6.20) that

$$s_{\rm eff} = \sum_{i=1}^{n} (s_i - s_i^\star)\,. \tag{6.21}$$

It follows that the modulus M of the annulus is given by

$$M = \frac{\pi}{|s_{\rm eff}|}\,. \tag{6.22}$$

To calculate the positions of the punctures we first determine the total lengths a and $\hat{a}$ of Σ and $\widehat{\Sigma}$. Looking at (6.19) we see that

$$a = a_1 + r_1 + e^{s_1 - s_1^\star}\big(a_2 + r_2 + e^{s_2 - s_2^\star}(a_3 + r_3 + \dots \quad . \tag{6.23}$$

This is readily seen to give

$$a = \sum_{i=1}^{n} e^{\sum_{j=1}^{i-1} s_j - s_j^\star}(a_i + r_i) = \sum_{i=1}^{n} b_i\,(a_i + r_i)\,. \tag{6.24}$$

where we defined

$$b_i \equiv e^{\sum_{j=1}^{i-1} s_j - s_j^\star}\,. \tag{6.25}$$

We can view b_i as a *local scaling factor*. It is the product of the slant factors of the surfaces R_1, $R_2, \dots$, up to R_{i-1}. It is the scaling factor that must apply to R_i when it is glued in to form Σ in (6.19).

The value of $\hat{a}$ is computed similarly. Looking at (6.20) we write

$$\hat{a} = e^{s_n^\star - s_n}\hat{a}_n + l_n + e^{s_n^\star - s_n}\big(e^{s_{n-1}^\star - s_{n-1}}\,\hat{a}_{n-1} + l_{n-1} + \dots \quad , \tag{6.26}$$

which gives

$$\hat{a} = \sum_{i=1}^{n} e^{\sum_{j=i+1}^{n} s_j^\star - s_j}(e^{s_i^\star - s_i}\hat{a}_i + l_i)\,. \tag{6.27}$$

Noticing that $e^{s_i - s_i^\star} l_i = r_i$ (see (6.17) and (6.18)) we can also rewrite $\hat{a}$ as

$$\hat{a} = e^{-s_{\rm eff}} \sum_{i=1}^{n} e^{\sum_{j=1}^{i-1} s_j - s_j^\star}(\hat{a}_i + r_i) = e^{-s_{\rm eff}} \sum_{i=1}^{n} b_i\,(\hat{a}_i + r_i)\,. \tag{6.28}$$

For insertions at positions y_k^α and $\hat{y}_k^\alpha$ we denote by x_k^α and $\hat{x}_k^\alpha$ their final coordinates on Σ and $\widehat{\Sigma}$. The collection of these insertions were represented by $\vec{x}$ and $\vec{\hat{x}}$ in (6.19) and (6.20). Short calculations using (4.27) show that these positions are given by

$$\begin{aligned} x_k^\alpha - \frac{1}{2} &= b_k\left(y_k^\alpha - \frac{1}{2}\right) + \sum_{i=1}^{k-1} b_i\,(a_i + r_i)\,, \\ \hat{x}_k^\alpha - \frac{1}{2} &= e^{-s_{\rm eff}}\left(b_k\left(\hat{y}_k^\alpha - \frac{1}{2} + r_k\right) + \sum_{i=k+1}^{n} b_i\,(\hat{a}_i + r_i)\right). \end{aligned} \tag{6.29}$$

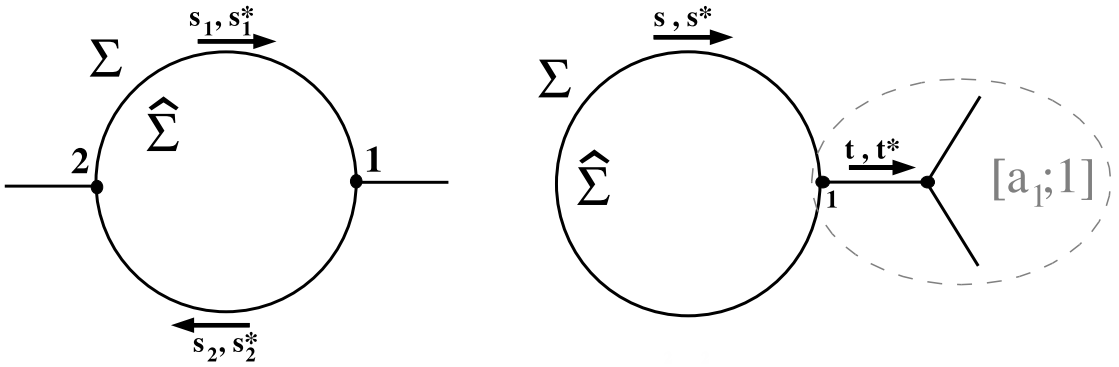

(a) (b)

Figure 15: The two diagrams contributing to the two-point function with both insertions on the same boundary.

It follows immediately from (6.10) and (6.11) that in the annulus frame ζ these positions translate into the angles

$$\phi_k^\alpha = \frac{2\pi}{s_{\text{eff}}} \ln\Big(2\Big|x_k^\alpha - \frac{1}{2} + \frac{a}{e^{s_{\text{eff}}}-1}\Big|\Big)\,, \qquad \hat\phi_k^\alpha = \frac{2\pi}{s_{\text{eff}}} \ln\Big(2\Big|\frac{1}{2} - \hat x_k^\alpha + \frac{\hat a}{1-e^{-s_{\text{eff}}}}\Big|\Big)\,. \tag{6.30}$$

Up to a trivial overall rotation of the annulus, the angles (6.30) represent the open string moduli of the one-loop diagram. This concludes our construction of moduli for general one-loop diagrams in Schnabl gauge.

7. The one-loop two-point diagram

We now apply the general construction of section 6 to the one-loop two-point diagram. In the following analysis we will restrict ourselves to the Riemann surfaces generated by even ghost-number propagators running in the loop, i.e. we use the propagator $\mathcal{P}_+$ in the loop. The other Riemann surface, which is generated by putting $\mathcal{P}_-$ on all loop propagator lines, can be calculated analogously.

7.1 Riemann surfaces with both insertions on the same boundary

Let us consider the one-loop two-point function with both insertions on the same boundary component of the annulus — the so-called planar contributions. There are two diagrams that contribute, as shown in figure 15.

7.1.1 First diagram

In the first diagram (figure 15(a)) we have two propagators in the loop ($n = 2$) and two Fock space surfaces $[1;1|1]$ connected directly to vertices in the loop, on the side that we choose to call the surface Σ. The Fock space surfaces do not contribute to $\widehat\Sigma$. In the notation of (6.12)

$$a_1 = a_2 = 1\,, \qquad y_1^1 = y_2^1 = 1\,, \qquad \hat a_1 = \hat a_2 = 0\,. \tag{7.1}$$

We label the Schwinger parameters of the two propagators by s_1, $s_1^\star$, s_2, $s_2^\star$ and (6.21) gives

$$s_{\rm eff} = s_1 - s_1^\star + s_2 - s_2^\star \,. \tag{7.2}$$

The length a of the Σ surface follows from (6.24) and (6.17). We find

$$a = \tfrac{3}{2} + 2e^{s_1 - s_1^\star} - e^{-s_1^\star} + \frac{1}{2}\, e^{s_{\rm eff}} - e^{s_1 - s_1^\star - s_2^\star} \,. \tag{7.3}$$

The position of the punctures on Σ are found using (6.29) and (6.17). We obtain:

$$x_1^1 = 1 \,, \qquad x_2^1 = 2 + e^{s_1 - s_i^\star} - e^{-s_1^\star} \,. \tag{7.4}$$

The relevant open string modulus is the relative angle between the insertions. Making use of (6.30) a short calculation gives

$$\Delta\phi = \phi_2^1 - \phi_1^1 = \frac{2\pi}{s_{\rm eff}} \ln \frac{2 - e^{-s_1^\star} + e^{s_1 - s_1^\star} + e^{s_2^\star - s_2} - e^{-s_2}}{1 - e^{-s_1^\star} + 2e^{s_1 - s_1^\star} - e^{s_1 - s_1^\star - s_2^\star} + e^{s_{\rm eff}}} \,. \tag{7.5}$$

Just like for the five-point diagram, let us consider the Riemann surfaces generated by the simplified propagator B/L. We thus set $s_1^\star = s_2^\star = 0$ and (7.5) becomes

$$\Delta\phi = \frac{2\pi}{s_1 + s_2} \ln\Big(\frac{1 + e^{s_1}}{e^{s_1} + e^{s_1 + s_2}}\Big) \;=\; \pi + \frac{2\pi}{s_1 + s_2} \ln\Big(\frac{\cosh\frac{s_1}{2}}{\cosh\frac{s_2}{2}}\Big) \,. \tag{7.6}$$

It is convenient to study this angle for fixed modulus of the annulus: $s_{\rm eff} = s_1 + s_2 = \text{const}$. We then have

$$\Delta\phi = \pi + \frac{2\pi}{s_{\rm eff}} \ln\Big(\frac{\cosh\frac{s_1}{2}}{\cosh\frac{s_{\rm eff} - s_1}{2}}\Big) \,. \tag{7.7}$$

For $s_1 = \frac{1}{2} s_{\rm eff}$ the two punctures are maximally separated: $\Delta\phi = \pi$. As we vary s_1 the separation angle varies within an interval centered at π. The maximal (minimal) angle $\Delta\phi_+$ ($\Delta\phi_-$) is obtained for $s_1 = s_{\rm eff}$ ($s_1 = 0$), and it is given by

$$\Delta\phi_\pm = \pi \pm \frac{2\pi}{s_{\rm eff}} \ln\cosh\tfrac{s_{\rm eff}}{2} \,. \tag{7.8}$$

Close to closed string degeneration, i.e. for $s_{\rm eff} \ll 1$, we obtain the simplified expression

$$\Delta\phi_\pm = \pi \pm \frac{\pi}{4} s_{\rm eff} \qquad \text{for} \quad s_{\rm eff} \ll 1 \,. \tag{7.9}$$

Thus near closed string degeneration the diagram just generates a region of moduli in which the punctures are nearly opposite. Close to open string degeneration ($s_{\rm eff} \to \infty$) equation (7.8) shows that almost the entire range of the position modulus is covered. In general, not all of the range of the position modulus is obtained. In figure 16 we show the region of the complete two-dimensional moduli space $(s_{\rm eff}, \Delta\phi)$ that the present, first diagram covers. The remaining region, as we will see now, is generated by second diagram contributing to the amplitude.

JHEP07(2008)063

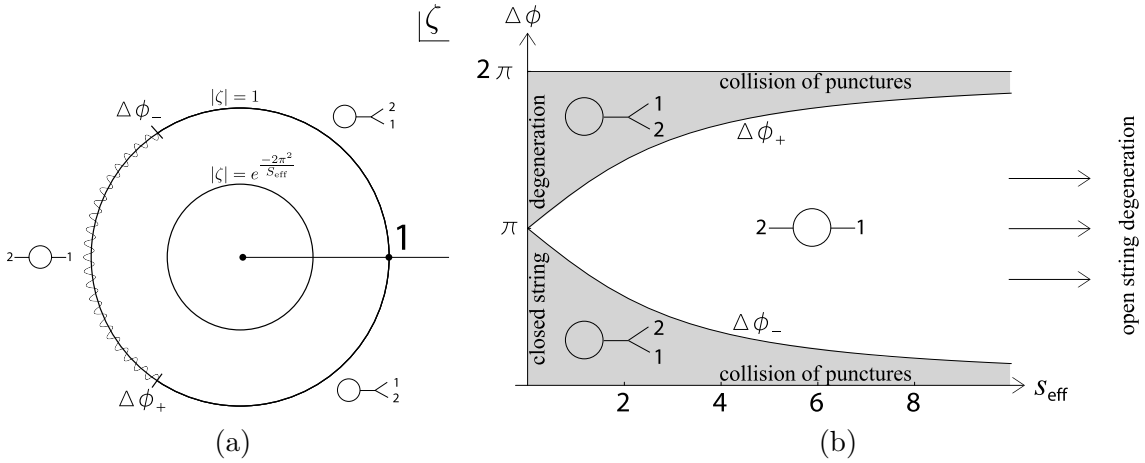

Figure 16: (a) The ζ-frame annulus for the planar one-loop two-point function. Insertion 1 is fixed at angle $\phi = 0$ and the position modulus is the angle $\Delta\phi$ for insertion 2. Both string diagrams in figure 15 are needed to generate the full position range $0 \leq \Delta\phi \leq 2\pi$. (b) The space $(s_{\rm eff}, \Delta\phi)$ of closed and open moduli is covered fully by the indicated string diagrams.

7.1.2 Second diagram

In the second diagram (figure 15(b)) there is only one propagator in the loop ($s^\star$, s) and both external states are connected to the loop through another internal propagator (t, $t^\star$). We then have

$$[a_1; 1|\, y_1^1, y_1^2] = e^{-tL} e^{-t^\star L^\star} [2; 1|1, 2] = [1 - 2e^{-t} + 3e^{t^\star - t}; 1|y_1^1, y_1^2]\,, \tag{7.10}$$

where we use (4.23) and (4.29) to obtain

$$a_1 = 1 - 2e^{-t} + 3e^{t^\star - t}\,, \quad y_1^1 = 1 - e^{-t} + e^{t^\star - t}\,, \quad y_1^2 = 1 - e^{-t} + 2e^{t^\star - t}\,, \quad \hat{a}_1 = 0\,. \tag{7.11}$$

To build Σ we use (6.19) with $n = 1$ and find

$$\Sigma \equiv [a; e^{s-s^\star}|x_1^1, x_1^2] = [a_1; 1|\, y_1^1, y_1^2] * [r_1; e^{s-s^\star}]\,, \qquad r_1 = \frac{1}{2}(1 + e^{s-s^\star}) - e^{-s^\star}\,, \tag{7.12}$$

and thus

$$a = a_1 + r_1 = \tfrac{3}{2} - 2e^{-t} + 3e^{t^\star - t} - e^{-s^\star} + \frac{1}{2} e^{s-s^\star}\,. \tag{7.13}$$

As $[a_1; 1|\, y_1^1, y_1^2]$ is the left-most surface in Σ, the positions of insertions on Σ coincide with the positions of insertions on $[a_1; 1]$: we have $x_1^1 = y_1^1$ and $x_1^2 = y_1^2$. For the relative angle $\Delta\phi$ between the two insertions we use (6.30) to obtain

$$\Delta\phi = \frac{2\pi}{s_{\rm eff}} \ln\!\left(\frac{1 - e^{-s^\star} + e^{s-s^\star} - e^{-t} + e^{t^\star - t} - e^{s-s^\star-t} + 2e^{s-s^\star+t^\star-t}}{1 - e^{-s^\star} + e^{s-s^\star} - e^{-t} + 2e^{t^\star-t} - e^{s-s^\star-t} + e^{s-s^\star+t^\star-t}} \right), \tag{7.14}$$

with $s_{\rm eff} = s - s^\star$.

Let us again focus on the surfaces generated by the simplified propagators $B^\star/L^\star$ or B/L. We have two options.

- $s^\star = t = 0$ (The case $s = t = 0$ gives similar results)
  In this case $s_{\rm eff} = s$ and $\Delta\phi$ reduces to

$$\Delta\phi = \frac{2\pi}{s_{\rm eff}} \ln\left(\frac{e^{t^\star} + 2e^{s_{\rm eff}+t^\star} - 1}{2e^{t^\star} + e^{s_{\rm eff}+t^\star} - 1}\right). \tag{7.15}$$

  For $t^\star \to 0$, this gives

$$\Delta\phi = \frac{2\pi}{s_{\rm eff}} \ln\left(\frac{2e^{s_{\rm eff}}}{1+e^{s_{\rm eff}}}\right) = \pi - \frac{2\pi}{s_{\rm eff}} \ln\cosh\tfrac{s_{\rm eff}}{2} \quad \text{for } t^\star \to 0\,, \tag{7.16}$$

  and matches smoothly to the first diagram's $\Delta\phi_-$ as given in (7.8).

  For $t^\star \to \infty$, however, there is no collision between the insertions. Instead, we obtain

$$\Delta\phi = \frac{2\pi}{s_{\rm eff}} \ln\left(\frac{1+2e^{s_{\rm eff}}}{2+e^{s_{\rm eff}}}\right) \quad \text{for } \; t^\star \to \infty\,. \tag{7.17}$$

  Thus diagram two with propagator $B^\star/L^\star$ in the subtree does *not* cover moduli space together with diagram one. This is not surprising because tracing along the Σ boundary of the Feynman diagram we encounter the operator combination $e^{-t^\star L_L} e^{-s_{\rm eff} L_L^\star} e^{-t^\star L_L^\star}$. At fixed annulus modulus, i.e. for $s_{\rm eff} = const$, this operator does not produce open string degeneration for $t^\star \to \infty$. In fact,

$$\lim_{t^\star\to\infty} e^{-t^\star L_L} e^{-s_{\rm eff} L_L^\star} e^{-t^\star L_L^\star}[a;b] = [a + \tfrac{1}{2}(e^{s_{\rm eff}}+1); e^{s_{\rm eff}} b]\,, \tag{7.18}$$

  which is a perfectly regular surface.

- $s^\star = t^\star = 0$ (The case $s = t^\star = 0$ gives similar results)
  Again, $s_{\rm eff} = s$ and this choice corresponds to B/L as the propagator in the tree. This time we obtain

$$\Delta\phi = \frac{2\pi}{s_{\rm eff}} \ln\left(\frac{e^{s_{\rm eff}} + e^{s_{\rm eff}-t}}{e^{s_{\rm eff}} + e^{-t}}\right) = \pi - \frac{2\pi}{s_{\rm eff}} \ln\left(\frac{\cosh\frac{t+s_{\rm eff}}{2}}{\cosh\frac{t}{2}}\right). \tag{7.19}$$

  For $t = 0$ we again match to $\Delta\phi_-$ in the first diagram. This time, all angles $0 < \Delta\phi < \Delta\phi_-$ are covered. Indeed,

$$\Delta\phi \to 0 \quad \text{for} \quad t \to \infty\,. \tag{7.20}$$

  This is sufficient to cover moduli space together with diagram one, as shown in figure 16. The diagram gives the shaded region $0 < \Delta\phi < \Delta\phi_-$. Of course, since external states are distinguishable, the region $\Delta\phi_+ < \Delta\phi < 2\pi$ is generated by the string diagram in which the order of the Fock space state insertions is reversed.

7.2 Riemann surfaces with insertions on both boundaries

Let us consider a one-loop amplitude with one Fock space state insertion on the outer boundary and one Fock space state insertion on the inner boundary. This nonplanar string diagram in shown in figure 17. As $[a_1;1|1]$ and $[\hat{a}_2;1|1]$ are the Fock space surfaces, we

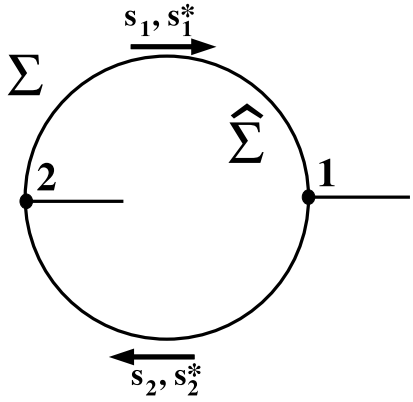

Figure 17: The diagram of the two-point function with insertions on both boundaries.

have

$$a_1 = \hat{a}_2 = 1\,, \qquad a_2 = \hat{a}_1 = 0\,, \qquad y_1^1 = 1\,, \qquad \hat{y}_2^1 = 1\,. \tag{7.21}$$

We have two propagators running in the loop. The relevant surfaces, using (6.19) and (6.20) are

$$\begin{aligned} \Sigma &\equiv [a; 1|x_1^1] = [1; 1|1] * R_1 * R_2 \\ \widehat{\Sigma} &\equiv [\hat{a}; 1|\hat{x}_2^1] = L_2 * [1; 1|1] * L_1\,. \end{aligned} \tag{7.22}$$

The relevant parameters above are readily calculated:

$$\begin{aligned} a &= \frac{3}{2} - e^{-s_1^\star} + e^{s_1 - s_1^\star}\left(1 - e^{-s_2^\star} + \frac{1}{2}e^{s_2 - s_2^\star}\right) \\ \hat{a} &= e^{-s_{\text{eff}}}\left(\frac{1}{2} - e^{-s_1^\star} + e^{s_1 - s_1^\star}\left(2 - e^{-s_2^\star} + \frac{1}{2}e^{s_2 - s_2^\star}\right)\right), \\ s_{\text{eff}} &= s_1 - s_1^\star + s_2 - s_2^\star\,, \\ x_1^1 &= 1\,, \\ \hat{x}_2^1 &= e^{s_2^\star - s_2} - e^{s_2} + 1\,. \end{aligned} \tag{7.23}$$

A calculation using the above results and (6.30) gives us the difference in insertion angles

$$\Delta\phi = \hat{\phi}_2^1 - \phi_1^1 = \frac{2\pi}{s_{\text{eff}}} \ln \frac{1 - e^{-s_1^\star} + e^{s_1 - s_1^\star} - e^{-s_2} + e^{s_2^\star - s_2}}{1 - e^{-s_1^\star} + e^{s_1 - s_1^\star} - e^{s_1 - s_1^\star - s_2^\star} + e^{s_{\text{eff}}}}\,. \tag{7.24}$$

Let us consider two cases of simplified propagators. If both propagators are B/L, then we can set $s_1^\star = s_2^\star = 0$ (similarly for $B^\star/L^\star$ and $s_1 = s_2 = 0$) and obtain

$$\Delta\phi = \frac{2\pi}{s_1 + s_2} \ln \frac{e^{s_1}}{e^{s_{\text{eff}}}} = 2\pi\, \frac{s_1}{s_1 + s_2}\,. \tag{7.25}$$

Moduli space is covered: for fixed $s_{\text{eff}} = s_1 + s_2$, $\Delta\phi$ takes on all values between 0 and 2π.

To examine the case of mixed propagators B/L and $B^\star/L^\star$ we set $s_1^\star = s_2 = 0$. Then,

$$\Delta\phi = \frac{2\pi}{s_1 - s_2^\star} \ln(e^{s_1 - s_2^\star} - e^{-s_2^\star} + 1)\,. \tag{7.26}$$

Since $s_1 = s_{\rm eff} + s_2^\star$ and $s_1, s_2^* \geq 0$, for fixed $s_{\rm eff} > 0$ we have a constraint in the range of s_1. Moduli space is not fully covered. In fact, for $s_{\rm eff} \to \infty$ we have $\Delta\phi \to 2\pi$ for the entire range of permissible s_1, $s_2^\star$. In this limit the open string modulus is stuck at the collision of punctures.

8. A regularized view on one-loop diagrams

In section 6 we presented a prescription to map the Riemann surface of a general one-loop diagram to the annulus while keeping track of the operator insertions of external states. This allowed us to calculate the closed and open string moduli of the surface as simple functions of the Schwinger parameters. The treatment was entirely in Schnabl gauge and used the formalism of slanted wedges. To justify our prescription, however, we need to revisit the construction by regularizing Schnabl gauge. This analysis extends the proof for the one-loop tadpole given in section 3.3 to general one-loop diagrams. Again, we use the λ-regularization introduced in [34]. To confirm our prescription we need to examine the three types of operations that are used. These operations are the multiplication of slanted wedges, the gluing between left and right boundaries on both Σ and $\widehat{\Sigma}$, and the gluing of Σ and $\widehat{\Sigma}$ to each other at their hidden boundaries. Before we check these operations, let us analyze the relevant gluing boundaries in more detail.

8.1 The boundaries of regularized slanted wedges

To examine the gluing curves, it is convenient to represent the coordinate curve $f^\lambda(e^{i\theta})$ in the z frame in terms of the parameterized curves γ_R^λ and γ_L^λ defined in (2.25) and shown in figure 1(c). Regarded as the regulated surface $[1;1|1]$, a Fock space state is then bounded by $\frac{1}{2} + \gamma_L^\lambda$ and $\frac{3}{2} + \gamma_R^\lambda$. The boundaries touch at the midpoint $\theta = \pi/2$.

Similarly, the regularized slanted wedge corresponding to $e^{-sL_R^\lambda}$ is bounded by the curves $\frac{1}{2} + \gamma_R^\lambda$ and $e^s(\frac{1}{2} + \gamma_R^\lambda)$. Its left boundary glues nicely to a Fock space state. The right boundary is a simple rescaling of the left boundary by e^s. This was illustrated in the context of the tadpole graph in figure 6(b). The two boundaries of $e^{-sL_R^\lambda}$ do not touch for $\theta = \frac{\pi}{2}$. In fact, $e^{-sL_R^\lambda}$ has a vertical boundary on the imaginary axis from $i\Lambda$ to $ie^s\Lambda$, as discussed in section 3. This vertical line segment connects the endpoints of the left and right boundary of $e^{-sL_R^\lambda}$.

The regularized slanted wedge corresponding to $e^{-s^\star(L_R^\lambda)^\star}$ is more delicate. Recall that in figure 11 we *flipped* the surface around its right vertical boundary to be able to interpret $e^{-s^\star L_R^\star}$ as the slanted wedge $[\frac{1}{2}(1-e^{-s^\star}); e^{-s^\star}]$. We conclude that the regularized boundaries of $e^{-s^\star(L_R^\lambda)^\star}$ are given by $\frac{1}{2} + \gamma_L^\lambda$ and $\frac{1}{2} + \frac{1}{2}(1 - e^{-s^\star}) + e^{-s^\star}\gamma_L^\lambda$. The surface of $e^{-s^\star(L_R^\lambda)^\star}$ also has a hidden vertical boundary. It is located between $1 + ie^{-s^\star}\Lambda$ and $1 + i\Lambda$. These facts are illustrated in figure 18, where we also show the surface for $e^{-s^\star(L_L^\lambda)^\star}$, which needs

JHEP07(2008)063

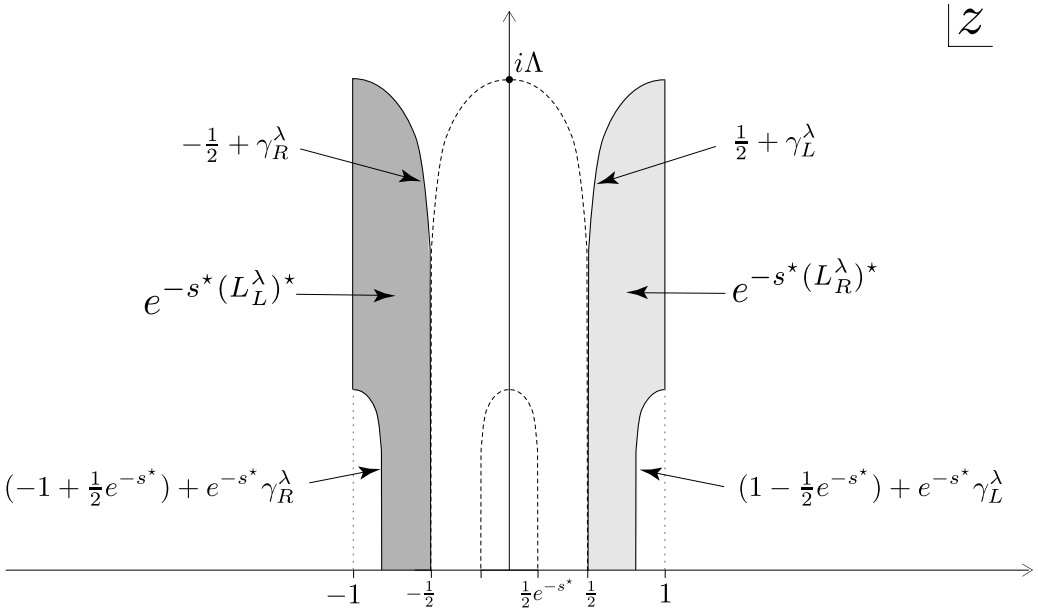

Figure 18: The regularized version of the slanted wedges corresponding to $e^{-s^\star(L_L^\lambda)^\star}$ and $e^{-s^\star(L_R^\lambda)^\star}$.

further displacement and rescaling to be presented as a regularization of a conventional slanted wedge.

In our construction, we build surfaces from slanted wedges associated with propagators and Fock space states. From this it is clear, that the slanted wedges $[a;b]$ relevant to our construction will, after regularization, be bounded on the left by either $\frac{1}{2}+\gamma_L^\lambda$ or $\frac{1}{2}+\gamma_R^\lambda$ and will be bounded on the right by either $\frac{1}{2}+a+b\gamma_L^\lambda$ or by $\frac{1}{2}+a+b\gamma_R^\lambda$. Furthermore, the slanted wedges associated with the left and right parts of e^{-sL} and $e^{-s^\star L^\star}$ carry a hidden boundary that needs to be glued to the hidden boundary of a complementary surface.

For $\lambda \to 0$, the curves $\gamma_{L/R}^\lambda(\theta)$ both approach the canonical vertical sliver parametrization $\gamma(\theta)$ defined in (2.26). One may therefore wonder why it is not trivial that regularized slanted wedges glue nicely for $\lambda \to 0$. The problem is that the convergence of $\gamma_{L/R}^\lambda(\theta)$ to the curve $\gamma(\theta)$ in the limit $\lambda \to 0$ is not *uniform* on the full interval $0 \le \theta \le \frac{\pi}{2}$. In fact, for any $\lambda > 0$, the curves $\gamma_{L/R}^\lambda$ start deviating significantly from γ in the region where $\Im(z)$ is of order Λ, as discussed in section 2.1. This effect can be neglected for tree-level amplitudes. In fact, the relevant frame for the calculation of moduli and correlators in tree amplitudes is the disk frame η, which is related to the z frame through

$$\eta = \exp\left(\frac{2\pi i z}{a}\right) . \tag{8.1}$$

Here, $a > 0$ is a function of the Schwinger parameters and independent of λ. All points with large imaginary values in the z frame converge to the point $\eta = 0$. In the η-frame, the deviations of $\gamma_{L/R}^\lambda$ from γ are thus suppressed by a factor of $e^{-\frac{2\pi\Lambda}{a}}$, which vanishes for $\lambda \to 0$.

JHEP07(2008)063

For one-loop diagrams the natural frame to consider for the gluing is either the ζ-frame of the annulus or the w frame, in which the annulus is "unwrapped". The w coordinate is given by

$$w = -\ln(2z) + i\pi\,. \tag{8.2}$$

Clearly, not all points z with large imaginary values converge to a single point in the w frame. Therefore the analysis for one-loop diagrams is more subtle than for trees. The mapping of the boundary curves $\gamma^\lambda_{L/R}$ to the w frame have been analyzed in the context of the simplified tadpole diagram. Indeed, in section 3 we have proven that when mapped to the w frame, the left boundary of the Fock space state is a translation by s of the right boundary of e^{-sL_R}. Concretely, we showed in claim (2) of section 3.3 that

$$\lim_{\lambda\to 0} w\Big(a_0 + \frac{1}{2} + \gamma^\lambda_L\Big) - w\Big(e^s\Big(a_0 + \frac{1}{2} + \gamma^\lambda_R\Big)\Big) = s\,. \tag{8.3}$$

The limit holds uniformly on $0 \le \theta \le \frac{\pi}{2}$. This result can be easily generalized to the uniform convergence

$$\begin{aligned} &\lim_{\lambda\to 0}\ w\big(e^{s'}(d+\gamma^\lambda_{L/R})\big) - w\big(e^{s''}(d+\gamma^\lambda_{R/L})\big) = s''-s' \\ &\quad \forall\ d, s', s'' \in \mathbb{R} \text{ independent of } \lambda\,;\ d \neq 0\,. \end{aligned} \tag{8.4}$$

Note that only this case of mixed curves γ_L and γ_R is non-trivial. If both curves are either of the type γ_L or of the type γ_R, the identity analogous to (8.4) is exact for all λ:

$$w\big(e^{s'}(d+\gamma^\lambda_{L/R})\big) - w\big(e^{s''}(d+\gamma^\lambda_{L/R})\big) = s''-s' \quad \text{for all} \quad \lambda \ge 0\,. \tag{8.5}$$

This follows from the definition of the map (2.9) to the w frame.

8.2 Gluings and identifications on Σ

For one-loop diagrams, we know from (6.19) that the surface Σ is constructed by the multiplication of $2n$ slanted wedges. Let as analyze the validity of the gluing between any pair of neighboring slanted wedges in this product. To this end, we split the surface Σ into two slanted wedges. One of them comprises all the surfaces to the left of the gluing we are interested in, the other one comprises all the surfaces to the right of this gluing. We thus have

$$\Sigma = [a; e^{s_{\text{eff}}}] = [a_1; b_1] * [a_2; b_2]\,. \tag{8.6}$$

When multiplying the slanted wedges $[a_1; b_1]$ and $[a_2; b_2]$, we need to glue the right boundary of $[a_1; b_1]$ to the left boundary $[a_2; b_2]$. To see that our usual multiplication prescription is valid, we analyze this gluing of the two boundaries using λ-regulated slanted wedges. If these boundaries are either both of the type γ^λ_L or both of the type γ^λ_R, the gluing is natural for all λ and no limit needs to be taken. If the boundaries are of mixed type, the gluing curves do not match for $\Im(z)$ of order Λ. The surfaces thus either start overlapping or separating in this region. But using (8.4) in the form

$$\lim_{\lambda\to 0}\ w\Big(\frac{1}{2} + a_0 + a_1 + b_1\gamma^\lambda_L\Big) - w\Big(\frac{1}{2} + a_0 + a_1 + b_1\gamma^\lambda_R\Big) = 0\,, \tag{8.7}$$

we see that the boundaries match in the w frame for $\lambda \to 0$. The shift a_0, defined in (6.5), is independent of λ so that uniform convergence is guaranteed. We have thus shown that all the slanted wedges which are multiplied in the construction of Σ glue nicely to each other in the w frame when $\lambda \to 0$.

Eventually, we also have to glue the left and right boundaries of Σ to each other. This is done by the map from the w frame to the annulus ζ through (6.8). This map has the periodicity $w \sim w - s_{\text{eff}}$. It is thus sufficient to show that in the limit $\lambda \to 0$, the left and right boundaries of Σ are related through a translation by s_{eff} in the w frame. As shown in (8.5), if both boundaries of Σ are of type γ_L^λ or both are of type γ_R^λ, this relation in the w frame is exact by construction, even for finite λ. If one boundary is of the type γ_L^λ and the other boundary is of the type γ_R^λ, we can use (8.4) in the form

$$\lim_{\lambda\to 0}\ w\left(\frac{1}{2} + a_0 + \gamma_{L/R}^\lambda\right) - w\left(e^{s_{\text{eff}}}\left(\frac{1}{2} + a_0 + \gamma_{R/L}^\lambda\right)\right) = s_{\text{eff}} \tag{8.8}$$

to see that the two boundaries of Σ are related through a translation by s_{eff} in the w frame.

In summary, we have shown that the w-frame image of Σ, as $\lambda \to 0$, represents a smooth surface which is foliated by horizontal lines of length $|s_{\text{eff}}|$. Clearly, the same arguments as above also apply to the surface $\widehat{\Sigma}$. To complete the proof of our prescription, we still need to show that the surfaces Σ and $\widehat{\Sigma}$ also glue smoothly to each other at their hidden boundaries.

8.3 Gluing the hidden boundaries

In constructing one-loop amplitudes for Schnabl gauge, we cut the surfaces associated with $e^{-s_i L}$ and $e^{-s_i^\star L^\star}$ into two pieces associated with their left and right parts. As we saw using λ-regularization, these surfaces really have a hidden boundary at $i\infty$ at which they were cut, and we need to ensure that these hidden boundaries glue nicely when we form the annulus.

In the λ-regularized construction the hidden boundaries are of the general form

$$z = d + ix\Lambda \qquad \text{with} \quad e^{s'} \le x \le e^{s''}, \qquad d, s', s'' \in \mathbb{R} \ \text{ independent of } \lambda\,. \tag{8.9}$$

The parameters d, s', and s'' are thus suitable to characterize general hidden boundaries of slanted wedges. They emerge as actual vertical boundary segments once the slanted wedge is regularized, but we will still call them hidden boundaries, to avoid confusion with other types of boundaries. The hidden boundary of $e^{-s^\star (L^\lambda)_R^\star}$, for example, stretches from $1 + ie^{-s^\star}\Lambda$ to $1 + i\Lambda$, as we can see in figure 18. We thus have $d = 1$, $s' = -s^\star$, and $s'' = 0$ as the parameters of the hidden boundary of $e^{-s^\star L_R^\star}$. Note also that the parameters s' and s'' are just the logarithms of the scaling factors that apply to the left or right boundaries of the surface associated with $e^{-s^\star L_R^\star}$. The parameter s'' that defines the top endpoint of the hidden boundary arises from the left boundary which has a scale factor of one, thus $s'' = 0$. The parameter s' that defines the bottom endpoint of the hidden boundary arises from the right boundary, which has a scale factor of $e^{-s^\star}$, thus $s' = -s^\star$.

JHEP07(2008)063

Let us summarize the parameters of hidden boundaries for slanted wedges associated with propagators:

$$d=0 \qquad s'=0 \qquad s''=s \qquad \text{for the hidden boundary of } e^{-sL_R}\,, \tag{8.10}$$

$$d=1 \qquad s'=-s \qquad s''=0 \qquad \text{for the hidden boundary of } e^{-sL_L}\,, \tag{8.11}$$

$$d=1 \qquad s'=-s^\star \qquad s''=0 \qquad \text{for the hidden boundary of } e^{-s^\star L^\star_R}\,, \tag{8.12}$$

$$d=0 \qquad s'=0 \qquad s''=s^\star \qquad \text{for the hidden boundary of } e^{-s^\star L^\star_L}\,. \tag{8.13}$$

When we multiply regulated slanted wedges to form the surfaces Σ and $\widehat{\Sigma}$, hidden boundaries get shifted and rescaled. Of course they are then still of the general form (8.9).

In proving claim (1) of section 3.3 –that the hidden boundaries of e^{-sL_L} and e^{-sL_R} glue nicely in the tadpole graph– we showed that

$$\lim_{\lambda\to 0}\; w(ix\Lambda) - w(a_0+1+ix\Lambda) = 0 \qquad \text{for all} \quad 1\le x\le e^s\,. \tag{8.14}$$

More generally, consider two hidden boundaries of the form (8.9) with identical ranges of x so that they are related by just a horizontal translation. If the horizontal distance $\Delta d\in\mathbb{R}$ that separates these hidden boundaries is independent of λ, they glue nicely in the w frame in the limit $\lambda\to 0$. A straightforward generalization of the proof in section 3.3 indeed shows that the following limit holds uniformly

$$\lim_{\lambda\to 0}\; w(d+ix\Lambda) - w(d+\Delta d+ix\Lambda) = 0 \quad \forall\; e^{s'}\le x\le e^{s''} \;\text{ with }\; d,\Delta d,s',s''\in\mathbb{R}\,. \tag{8.15}$$

We now show that for one-loop diagrams all gluings of hidden boundaries work nicely in the w frame. Each propagator in the loop has two hidden boundaries, one from cutting e^{-sL} and one from cutting $e^{-s^\star L^\star}$. For definiteness, we analyze the k-th propagator in the loop and assume it is of type $\mathcal{P}_+$. This propagator is responsible for the insertion of the slanted wedge associated with

$$e^{-s_kL_R}\,\underline{e^{-s_k^\star L_R^\star}} \qquad \text{into}\;\; \Sigma\,. \tag{8.16}$$

The same propagator will be responsible for the insertion of the slanted wedge associated with

$$e^{-s_kL_L}\,\underline{e^{-s_k^\star L_L^\star}} \qquad \text{into}\;\; \widehat{\Sigma}\,. \tag{8.17}$$

We will focus on the underlined operators in the two expressions above. The first produces a hidden boundary in Σ and the second a hidden boundary in $\widehat{\Sigma}$. We aim to show that these hidden boundaries appear at the same height and have the same vertical range so that (8.15) implies that they glue correctly as the regulator is removed. More concretely, we want to show that these two hidden boundaries are characterized by (8.9) with identical parameters s' and s'', both independent of λ. The value of d for each boundary must also be λ-independent.

Let us begin with the hidden boundary generated by $e^{-s_k^\star L_R^\star}$ in Σ. Just before Σ is mapped to the w frame, the associated slanted wedge has its left boundary at a position x_L^k that is independent of λ (as is familiar from our calculations of positions in section 6,

positions just depend on Schwinger parameters). According to (8.12), the hidden boundary of $e^{-s_k^\star L_R^\star}$, as a canonically presented slanted wedge is positioned a distance $d - \frac{1}{2} = \frac{1}{2}$ to the right of its left boundary. We conclude that on Σ, it is positioned a distance $\frac{1}{2}b_k$ from its left boundary, i.e. at $d = x_L^k + \frac{1}{2}b_k$. The factor of b_k is necessary because it represents the *local scale factor*: it is the product of the scale factors of all the slanted wedges that precede the insertion of $e^{-s_k^\star L_R^\star}$ in Σ (see (6.19)). Note that the first operator in (8.16) does not contribute to the local scale factor because its slanted wedge ends up to the right of the one we are looking at. As both x_L^k and b_k are manifestly λ independent, so is the location d of the hidden boundary. This is all that matters, its specific value is not needed.

The parameters s' and s'' for $e^{-s_k^\star L_R^\star}$ listed in (8.12) get a contribution from the logarithm of the local scale factor b_k at the insertion. We thus have:

$$s' = -s_k^\star + \ln b_k\,, \quad s'' = 0 + \ln b_k = \ln b_k\,, \qquad \text{for } e^{-s_k^\star L_R^\star} \text{ on } \Sigma\,. \tag{8.18}$$

Let us now consider the insertion of $e^{-s_k^\star L_L^\star}$ on $\widehat{\Sigma}$, just before $\widehat{\Sigma}$ is mapped to the w frame. The position $\hat{x}_L^k$ of the associated slanted wedge, defined as the real value of its left boundary, is independent of λ. What we need is the local scale factor $b_{\rm loc}$ at this position. For this we recall that $\widehat{\Sigma}$ is rescaled by $e^{s_{\rm eff}}$ in such a way that its left boundary has scaling factor $e^{s_{\rm eff}}$ and the right boundary has unit scaling factor. It then follows from (6.20) that, in addition to $e^{s_{\rm eff}}$, we get the multiplicative contribution from the slant parameters of $L_n, L_{n-1}, \ldots, L_{k+1}$ *and* the slant parameter of the first operator in (8.17). This gives

$$b_{\rm loc} = e^{s_{\rm eff}} \cdot e^{\sum_{j=k+1}^n (s_j^\star - s_j)} \cdot e^{-s_k} = e^{\sum_{j=1}^k (s_j - s_j^\star)} \cdot e^{-s_k} = b_k e^{-s_k^\star}\,. \tag{8.19}$$

This time the s' and s'' parameters in (8.13) are modified by the addition of the logarithm of $b_{\rm loc}$. We thus get

$$s' = 0 + \ln b_{\rm loc} = -s_k^\star + \ln b_k\,, \quad s'' = s_k^\star + \ln b_{\rm loc} = \ln b_k\,, \qquad \text{for } e^{-s_k^\star L_L^\star} \text{ on } \widehat{\Sigma}\,. \tag{8.20}$$

Comparing (8.18) with (8.20), we see that the parameters s' and s'' match precisely. Therefore we conclude from (8.15) that the hidden boundaries of $e^{-s_k^\star L_R^\star}$ and $e^{-s_k^\star L_L^\star}$ glue nicely in the w frame.
A few remarks are in order.

- The hidden boundaries of $e^{-s_k L_R}$ and $e^{-s_k L_L}$ also glue seamlessly in the w frame. The proof is completely analogous to the one presented above.

- The propagators in subtrees also have hidden boundaries. The hidden boundaries associated with a subtree propagator are either both on Σ or both on $\widehat{\Sigma}$. These boundaries cannot be simply ignored because unlike in tree-amplitudes, the subtree is mapped to the annulus and *not* to the disk. Still, it is easy to see by a similar analysis as for loop propagators that these hidden boundaries glue nicely in the w frame.

- One might wonder if the question of gluing hidden boundaries could have been ignored. After all, these hidden boundaries are pushed off to $i\infty$ in the z frame and to

JHEP07(2008)063

$\frac{\pi}{2} - i\infty$ in the w frame and these seem to be well defined points. This naive argument, however, leads to wrong conclusions. It would allow *independent* z-frame rescalings of Σ and $\widehat{\Sigma}$, which is equivalent to shifting their relative horizontal position in the w frame. On the annulus, this corresponds to rotating the inner and outer boundaries of the annulus with respect to each other. But if we have insertions on both the inner and the outer boundary, the configuration after such a relative rotation is *not* conformally equivalent to the original one. We conclude that the naive expectation that the gluing in Schnabl gauge works out correctly automatically, leaves an ambiguity in the open string moduli. This ambiguity is fixed when we regulate and demand the gluing to work out nicely in the limit $\lambda \to 0$.

- While we did our analysis of the gluing of hidden boundaries using the λ-regulated gauges, any other family of regular linear b-gauges associated with zero modes in the frames $z = \tilde{f}^\lambda(\xi)$ could have been used, as long as this family approaches Schnabl gauge in the limit $\lambda \to 0$. By construction, for such a family the frames satisfy

$$\lim_{\lambda\to 0} \tilde{\Lambda} = \infty \quad \text{with} \quad i\tilde{\Lambda} \equiv \tilde{f}^\lambda(i)\,. \tag{8.21}$$

  The proof of consistent gluing of hidden boundaries goes through with $\Lambda \to \tilde{\Lambda}$.

This concludes the proof of our prescription for the construction of general one-loop Riemann surfaces in Schnabl gauge.

9. Concluding remarks

The open string midpoint has played a very subtle and important role in covariant open string field theory. The midpoint makes it non-trivial to formulate open string field theory as a theory of half-strings (see [43]). Spacetime diffeomorphisms are not quite open-string gauge symmetries because of the special status of the midpoint in the star product [44]. Nevertheless, closed string poles appear in open string loop diagrams, again because of the special role of the midpoint. Naively, the star algebra was expected to have no projectors. But again, open string surface states with singular behavior at the midpoint give rise to projectors that seem to be completely consistent.

It is perhaps no surprise then that the tachyon vacuum solution uses a gauge, Schnabl gauge, that is described by the conformal frame of a projector. So does the rolling tachyon solution that describes the decay of a D-brane. Since observables associated with these solutions probe closed string physics [28, 45, 46] it is natural to ask if the use of Schnabl gauge allows the correct incorporation of closed string physics. As a first step, we ask if Schnabl gauge, just like Siegel gauge, leads to correct loop amplitudes. Indeed, naive arguments suggested that the singular midpoint behavior in Schnabl gauge could ruin the validity of the gauge at loop level, precisely where closed string physics is revealed. In a nutshell, the string diagrams for one loop appeared to give a surface that is disconnected into two pieces, each of which contains one of the boundary components of the annulus.

The analysis presented in this paper gives reason for optimism and teaches us a few facts:

JHEP07(2008)063

- The left and right parts of the operator L (the Virasoro zero-mode in sliver frame) fail to commute. This non-commutation is required by consistency: it introduces a finite hidden boundary to each of the two disconnected surfaces that form the annulus. The gluing across the hidden boundaries restores the closed string moduli.
- Schnabl gauge string diagrams at one loop cover the (one-dimensional) closed string moduli space. This is no proof of complete consistency, but dispels the fear of inconsistency due to subtle midpoint effects.
- All moduli, open and closed, of one-loop amplitudes with arbitrary numbers of open string states are calculable in closed form. Schnabl gauge off-shell amplitudes may ultimately be recognized as simpler than those in the familiar Siegel or light-cone gauges.
- Wedge surfaces have a natural generalization in the form of *slanted* wedges. Only on slanted wedges we have a natural action of the left and right parts of the operators L and $L^\star$. The use of these surfaces allows us to give (for the first time) an explicit algorithm to construct arbitrarily complicated tree and one-loop diagrams.

The focus in this paper has been narrow. We have studied the moduli of the diagrams generated in Schnabl gauge. We have not calculated any loop amplitude in detail. For this one must, of course, deal with the antighost and BRST insertions. Even regarding moduli we have not answered everything. Though the specific examples we have analyzed in this paper are encouraging, it is not yet clear whether open string moduli are covered in general. This problem is in fact still unsolved at tree-level. We are lacking proof that even tree amplitudes are correctly reproduced in Schnabl gauge. The open string propagator has moduli associated with the operators B/L and $B^\star/L^\star$, but also contains the BRST operator Q, which acts as a total derivative on moduli space. Our analysis of the tree-level five-point function and the one-loop two-point function suggests that there might be an assignment of simplified propagators B/L and $B^\star/L^\star$ to the propagator lines so that the string diagram has all the requisite degenerations. Finding such an assignment could be the next step in a proof of consistency of Schnabl gauge.

The λ-regularized gauges are fully consistent and Schnabl gauge amplitudes can in principle be defined by the limit $\lambda \to 0$ of λ-regulated amplitudes. Calculating regularized amplitudes is problematic, because even at small (but fixed) λ, the geometry differs significantly from the Schnabl geometry when any Schwinger parameter becomes large, i.e. of order $\mathcal{O}(\log\log\lambda^{-1})$. When one imposes cutoffs on the integration region of Schwinger parameters, the limit of removing these cutoffs and the limit $\lambda \to 0$ do not, in general, commute. It would be interesting to determine a cutoff prescription for which these limits commute and thus define consistent amplitudes for Schnabl gauge. A possible candidate for such a prescription is a generalization of the symmetric limit defined for the four-point amplitude in [32]. Note that, in this paper, we took the limit $\lambda \to 0$ at fixed Schwinger parameters and any amplitude calculated using these surfaces is thus a true Schnabl-gauge amplitude and needs to be supplemented with a suitable prescription on the integration over Schwinger parameters.

JHEP07(2008)063

The conformal field theory boundary state of the rolling tachyon has been studied to extract the time-dependent pressure profile of tachyon condensation (see [47] and references therein). The result suggests that the pressure goes to zero at late times, consistent with the expectation that the D-brane decays into heavy non-relativistic closed strings. The conformal field theory analysis of the closed string production in the background of the rolling tachyon encounters UV divergences [48]. As the corresponding analytic solution of string field theory has been found, this problem can now also be studied within open string field theory.[5] It would be interesting to extract a boundary state from the one-loop open-string vacuum amplitude in the background of the rolling tachyon solution. This string field theory boundary state may confirm the expected late time behavior of the pressure and could help us understand the role of observables in open string field theory.

All in all, our work shows that Schnabl gauge is not only a convenient gauge for analytic solutions in string field theory but also simplifies string perturbation theory considerably. While the ultimate consistency proof is still pending, we hope that the tools developed here will help construct this proof and lead to new insights into the role of closed strings in open string field theory.

Acknowledgments

We would like to thank Ashoke Sen for helpful discussions and for collaboration in the initial stages of this project. We also thank Yuji Okawa and Martin Schnabl for valuable comments on a draft version of this paper. The work of M.K. and B.Z. is supported in part by the U.S. DOE grant DE-FC02-94ER40818.

A. Covering of moduli space in the five-point diagram

In this appendix we will analyze which assignment of B/L and $B^\star/L^\star$ to the propagators in the five-point amplitude always produces open string degenerations when a Schwinger parameter becomes large. To do so, we will set one of the Schwinger parameters of each propagator to zero in our result for the angles of operator insertions on the unit circle (5.7). Notice that the only degenerations we expect from the diagram in figure 12 are the collision of the insertions of $|F_A\rangle$ and $|F_B\rangle$, and the collision of the insertions of $|F_D\rangle$ and $|F_E\rangle$. There are three distinct cases of B/L and $B^\star/L^\star$ assignments.

- **case 1:** $t_1 = t_2 = 0$ **(propagator 1:** $B^\star/L^\star$**; propagator 2:** $B^\star/L^\star$**)**
  The angles of operator insertions for this case can be calculated from (5.7). They are given in Table 1.

  The angles ϕ_C, ϕ_D, and ϕ_E approach each other for $t_1^\star \to \infty$, if $t_2^\star$ stays finite. This is conformally equivalent to ϕ_A and ϕ_B coming close together. But this cannot be a stable degeneration, because if $t_2^\star$ also becomes large, the angles ϕ_A and ϕ_B are no longer degenerate. In fact, for $t_1^\star = t_2^\star \to \infty$ all insertions are separated by finite angles from each other! Thus this is not a consistent assignment of B/L and $B^\star/L^\star$.

[5] For an interesting recent analysis of observables associated with on-shell closed string states, see [28].

	finite $t_1^\star$, $t_2^\star$	$t_1^\star \to \infty$	$t_2^\star \to \infty$	$t_1^\star = t_2^\star \to \infty$
$\frac{\phi_B - \phi_A}{2\pi}$	$\frac{e^{t_1^\star}}{3e^{t_1^\star}+3e^{t_2^\star}-1}$	$\frac{1}{3}$	0	$\frac{1}{6}$
$\frac{\phi_C - \phi_A}{2\pi}$	$\frac{2e^{t_1^\star}}{3e^{t_1^\star}+3e^{t_2^\star}-1}$	$\frac{2}{3}$	0	$\frac{1}{3}$
$\frac{\phi_D - \phi_A}{2\pi}$	$\frac{2e^{t_1^\star}+e^{t_2^\star}}{3e^{t_1^\star}+3e^{t_2^\star}-1}$	$\frac{2}{3}$	$\frac{1}{3}$	$\frac{1}{2}$
$\frac{\phi_E - \phi_A}{2\pi}$	$\frac{2e^{t_1^\star}+2e^{t_2^\star}}{3e^{t_1^\star}+3e^{t_2^\star}-1}$	$\frac{2}{3}$	$\frac{2}{3}$	$\frac{2}{3}$

Table 1: The angles of operator insertions in the five-point diagram for case 1: $t_1 = t_2 = 0$.

	finite t_1, t_2	$t_1 \to \infty$	$t_2 \to \infty$	$t_1 = t_2 \to \infty$
$\frac{\phi_B - \phi_A}{2\pi}$	$\frac{e^{-t_1}}{3+e^{-t_1}+e^{-t_2}}$	0	$\frac{e^{-t_1}}{3+e^{-t_1}}$	0
$\frac{\phi_C - \phi_A}{2\pi}$	$\frac{1+e^{-t_1}}{3+e^{-t_1}+e^{-t_2}}$	$\frac{1}{3+e^{-t_2}}$	$\frac{1+e^{-t_1}}{3+e^{-t_1}}$	$\frac{1}{3}$
$\frac{\phi_D - \phi_A}{2\pi}$	$\frac{2+e^{-t_1}}{3+e^{-t_1}+e^{-t_2}}$	$\frac{2}{3+e^{-t_2}}$	$\frac{2+e^{-t_1}}{3+e^{-t_1}}$	$\frac{2}{3}$
$\frac{\phi_E - \phi_A}{2\pi}$	$\frac{2+e^{-t_1}+e^{-t_2}}{3+e^{-t_1}+e^{-t_2}}$	$\frac{2+e^{-t_2}}{3+e^{-t_2}}$	$\frac{2+e^{-t_1}}{3+e^{-t_1}}$	$\frac{2}{3}$

Table 2: The angles of operator insertions in the five-point diagram for case 2: $t_1^\star = t_2^\star = 0$.

- **case 2:** $t_1^\star = t_2^\star = 0$ **(propagator 1:** B/L**; propagator 2:** B/L**)**
  The angles of operator insertions for this case are given in Table 2. The angles ϕ_A and ϕ_B come close together for $t_1 \to \infty$. Making t_2 also large cannot prevent the degeneration. Similarly, the degeneration of ϕ_D and ϕ_E in the limit $t_2 \to \infty$ cannot be undone by making t_1 comparably large. Thus, this is a good assignment of propagators.
- **case 3:** $t_1^\star = t_2 = 0$ **(propagator 1:** B/L **, propagator 2:** $B^\star/L^\star$**)**
  The angles of operator insertions for this case are given in Table 3. The angles ϕ_A and ϕ_B come close together for $t_1 \to \infty$. Making $t_2^\star$ also large, cannot prevent the degeneration. Similarly, for $t_2^\star$ very large, ϕ_A, ϕ_B and ϕ_C approach each other. This is conformally equivalent to ϕ_D and ϕ_E coming close together. Again, this cannot be undone by making t_1 comparably large. Thus, this is also a good assignment of propagators.

JHEP07(2008)063

	finite t_1, $t_2^\star$	$t_1 \to \infty$	$t_2^\star \to \infty$	$t_1 = t_2^\star \to \infty$
$\frac{\phi_B - \phi_A}{2\pi}$	$\frac{e^{-t_1}}{1+e^{-t_1}+3e^{t_2^\star}}$	0	0	0
$\frac{\phi_C - \phi_A}{2\pi}$	$\frac{1+e^{-t_1}}{1+e^{-t_1}+3e^{t_2^\star}}$	$\frac{1}{1+3e^{t_2^\star}}$	0	0
$\frac{\phi_D - \phi_A}{2\pi}$	$\frac{1+e^{-t_1}+e^{t_2^\star}}{1+e^{-t_1}+3e^{t_2^\star}}$	$\frac{1+e^{t_2^\star}}{1+3e^{t_2^\star}}$	$\frac{1}{3}$	$\frac{1}{3}$
$\frac{\phi_E - \phi_A}{2\pi}$	$\frac{1+e^{-t_1}+2e^{t_2^\star}}{1+e^{-t_1}+3e^{t_2^\star}}$	$\frac{1+2e^{t_2^\star}}{1+3e^{t_2^\star}}$	$\frac{2}{3}$	$\frac{2}{3}$

Table 3: The angles of operator insertions in the five-point diagram for case 3: $t_1^\star = t_2 = 0$.

References

[1] M. Schnabl, *Analytic solution for tachyon condensation in open string field theory*, *Adv. Theor. Math. Phys.* **10** (2006) 433 [hep-th/0511286].

[2] E. Witten, *Noncommutative geometry and string field theory*, *Nucl. Phys.* **B 268** (1986) 253.

[3] W. Siegel, *Covariantly second quantized string*, *Phys. Lett.* **B 142** (1984) 276; *Covariantly second quantized string.* 2, *Phys. Lett.* **B 149** (1984) 157 [*Phys. Lett.* **B 151** (1985) 391]; *Covariantly second quantized string.* 3, *Phys. Lett.* **B 149** (1984) 162 [*Phys. Lett.* **B 151** (1985) 396].

[4] Y. Okawa, *Comments on Schnabl's analytic solution for tachyon condensation in Witten's open string field theory*, *JHEP* **04** (2006) 055 [hep-th/0603159].

[5] E. Fuchs and M. Kroyter, *On the validity of the solution of string field theory*, *JHEP* **05** (2006) 006 [hep-th/0603195].

[6] E. Fuchs and M. Kroyter, *Schnabl's $L(0)$ operator in the continuous basis*, *JHEP* **10** (2006) 067 [hep-th/0605254].

[7] L. Rastelli and B. Zwiebach, *Solving open string field theory with special projectors*, *JHEP* **01** (2008) 020 [hep-th/0606131].

[8] I. Ellwood and M. Schnabl, *Proof of vanishing cohomology at the tachyon vacuum*, *JHEP* **02** (2007) 096 [hep-th/0606142].

[9] E. Fuchs and M. Kroyter, *Universal regularization for string field theory*, *JHEP* **02** (2007) 038 [hep-th/0610298].

[10] Y. Okawa, L. Rastelli and B. Zwiebach, *Analytic solutions for tachyon condensation with general projectors*, hep-th/0611110.

[11] T. Erler, *Split string formalism and the closed string vacuum*, *JHEP* **05** (2007) 083 [hep-th/0611200].

[12] T. Erler, *Split string formalism and the closed string vacuum. II*, *JHEP* **05** (2007) 084 [hep-th/0612050].

JHEP07(2008)063

[13] M. Schnabl, *Comments on marginal deformations in open string field theory*, *Phys. Lett.* **B 654** (2007) 194 [hep-th/0701248].

[14] M. Kiermaier, Y. Okawa, L. Rastelli and B. Zwiebach, *Analytic solutions for marginal deformations in open string field theory*, *JHEP* **01** (2008) 028 [hep-th/0701249].

[15] T. Erler, *Marginal solutions for the superstring*, *JHEP* **07** (2007) 050 [arXiv:0704.0930].

[16] Y. Okawa, *Analytic solutions for marginal deformations in open superstring field theory*, *JHEP* **09** (2007) 084 [arXiv:0704.0936].

[17] E. Fuchs, M. Kroyter and R. Potting, *Marginal deformations in string field theory*, *JHEP* **09** (2007) 101 [arXiv:0704.2222].

[18] Y. Okawa, *Real analytic solutions for marginal deformations in open superstring field theory*, *JHEP* **09** (2007) 082 [arXiv:0704.3612].

[19] I. Ellwood, *Rolling to the tachyon vacuum in string field theory*, *JHEP* **12** (2007) 028 [arXiv:0705.0013].

[20] E. Fuchs and M. Kroyter, *Marginal deformation for the photon in superstring field theory*, *JHEP* **11** (2007) 005 [arXiv:0706.0717].

[21] M. Kiermaier and Y. Okawa, *Exact marginality in open string field theory: a general framework*, arXiv:0707.4472.

[22] T. Erler, *Tachyon vacuum in cubic superstring field theory*, *JHEP* **01** (2008) 013 [arXiv:0707.4591].

[23] M. Kiermaier and Y. Okawa, *General marginal deformations in open superstring field theory*, arXiv:0708.3394.

[24] O.-K. Kwon, B.-H. Lee, C. Park and S.-J. Sin, *Fluctuations around the tachyon vacuum in open string field theory*, *JHEP* **12** (2007) 038 [arXiv:0709.2888].

[25] B.-H. Lee, C. Park and D.D. Tolla, *Marginal deformations as lower dimensional D-brane solutions in open string field theory*, arXiv:0710.1342.

[26] O.-K. Kwon, *Marginally deformed rolling tachyon around the tachyon vacuum in open string field theory*, arXiv:0801.0573.

[27] S. Hellerman and M. Schnabl, *Light-like tachyon condensation in open string field theory*, arXiv:0803.1184.

[28] I. Ellwood, *The closed string tadpole in open string field theory*, arXiv:0804.1131.

[29] T. Kawano, I. Kishimoto and T. Takahashi, *Gauge invariant overlaps for classical solutions in open string field theory*, arXiv:0804.1541.

[30] T. Kawano, I. Kishimoto and T. Takahashi, *Schnabl's solution and boundary states in open string field theory*, arXiv:0804.4414.

[31] H. Fuji, S. Nakayama and H. Suzuki, *Open string amplitudes in various gauges*, *JHEP* **01** (2007) 011 [hep-th/0609047].

[32] L. Rastelli and B. Zwiebach, *The off-shell Veneziano amplitude in Schnabl gauge*, *JHEP* **01** (2008) 018 [arXiv:0708.2591].

[33] S.B. Giddings, *The Veneziano amplitude from interacting string field theory*, *Nucl. Phys.* **B 278** (1986) 242.

JHEP07(2008)063

[34] M. Kiermaier, A. Sen and B. Zwiebach, *Linear b-gauges for open string fields*, *JHEP* **03** (2008) 050 [arXiv:0712.0627].

[35] L. Rastelli and B. Zwiebach, *Tachyon potentials, star products and universality*, *JHEP* **09** (2001) 038 [hep-th/0006240].

[36] M. Schnabl, *Wedge states in string field theory*, *JHEP* **01** (2003) 004 [hep-th/0201095].

[37] G. Zemba and B. Zwiebach, *Tadpole graph in covariant closed string field theory*, *J. Math. Phys.* **30** (1989) 2388.

[38] M. Bochicchio, *Gauge fixing for the field theory of the bosonic string*, *Phys. Lett.* **B 193** (1987) 31;
C.B. Thorn, *Perturbation theory for quantized string fields*, *Nucl. Phys.* **B 287** (1987) 61.

[39] C.B. Thorn, *String field theory*, *Phys. Rept.* **175** (1989) 1.

[40] C.R. Preitschopf, C.B. Thorn and S.A. Yost, *Superstring field theory*, *Nucl. Phys.* **B 337** (1990) 363.

[41] L.V. Ahlfors, *Conformal Invariants: topics in geometric function theory*, McGraw-Hill series in higher mathematics, McGraw-Hill, New York U.S.A. (1973).

[42] F.P. Gardiner, *Teichmuller theory and quadratic differentials*, John Wiley and Sons, New York U.S.A. (1987).

[43] D.J. Gross and W. Taylor, *Split string field theory. II*, *JHEP* **08** (2001) 010 [hep-th/0106036]; *Split string field theory. I*, *JHEP* **08** (2001) 009 [hep-th/0105059].

[44] E. Witten, *Some remarks about string field theory*, *Phys. Scripta* **T15** (1987) 70.

[45] A. Hashimoto and N. Itzhaki, *Observables of string field theory*, *JHEP* **01** (2002) 028 [hep-th/0111092].

[46] D. Gaiotto, L. Rastelli, A. Sen and B. Zwiebach, *Ghost structure and closed strings in vacuum string field theory*, *Adv. Theor. Math. Phys.* **6** (2003) 403 [hep-th/0111129].

[47] A. Sen, *Tachyon dynamics in open string theory*, *Int. J. Mod. Phys.* **A 20** (2005) 5513 [hep-th/0410103].

[48] N.D. Lambert, H. Liu and J.M. Maldacena, *Closed strings from decaying D-branes*, *JHEP* **03** (2007) 014 [hep-th/0303139].

JHEP07(2008)063